Final Technical Report

Pseudomorphic Semiconducting Heterostructures from Combinations of AlN, GaN and Selected SiC Polytypes: Theoretical Advancement and its Coordination with Experimental Studies of Nucleation, Growth, Characterization and Device Development

Supported under Grant #N00014-90-J-1427
Office of the Chief of Naval Research
Report for the period 7/1/95–12/31/95

DISTRIBUTION STATEMENT A
Approved for public release
Distribution Unlimited

R. F. Davis, S. Kern, K. Linthicum and W. Perry
Materials Science and Engineering Department
North Carolina State University
Campus Box 7907
Raleigh, NC 27695-7907

December, 1995

19960130 014

DISCLAIMER NOTICE

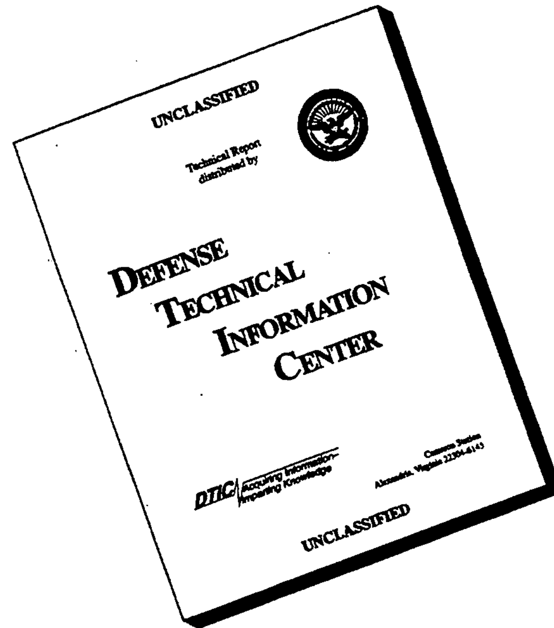

THIS DOCUMENT IS BEST QUALITY AVAILABLE. THE COPY FURNISHED TO DTIC CONTAINED A SIGNIFICANT NUMBER OF PAGES WHICH DO NOT REPRODUCE LEGIBLY.

REPORT DOCUMENTATION PAGE

Form Approved OMB No. 0704-0188

Public reporting burden for this collection of information is estimated to average 1 hour per response, including the time for reviewing instructions, searching existing data sources, gathering and maintaining the data needed, and completing and reviewing the collection of information. Send comments regarding this burden estimate or any other aspect of this collection of information, including suggestions for reducing this burden to Washington Headquarters Services, Directorate for Information Operations and Reports, 1215 Jefferson Davis Highway, Suite 1204, Arlington, VA 22202-4302, and to the Office of Management and Budget Paperwork Reduction Project (0704-0188), Washington, DC 20503.

1. AGENCY USE ONLY *(Leave blank)*

2. REPORT DATE
December, 1995

3. REPORT TYPE AND DATES COVERED
Final Technical 7/1/95–12/31/95

4. TITLE AND SUBTITLE
Pseudomorphic Semiconducting Heterostructures from Combinations of AlN, GaN and Selected SiC Polytypes: Theoretical Advancement and its Coordination with Experimental Studies of Nucleation, Growth, Characterization and Device Development

5. FUNDING NUMBERS
414s007---01
1114SS
N00179
N66005
4B855

6. AUTHOR(S)
Robert F. Davis

7. PERFORMING ORGANIZATION NAME(S) AND ADDRESS(ES)
North Carolina State University
Hillsborough Street
Raleigh, NC 27695

8. PERFORMING ORGANIZATION REPORT NUMBER
N00014-90-J-1427

9. SPONSORING/MONITORING AGENCY NAMES(S) AND ADDRESS(ES)
Sponsoring: ONR, Code 312, 800 N. Quincy, Arlington, VA 22217-5660
Monitoring: Administrative Contracting Officer, Regional Office Atlanta
Regional Office Atlanta, 101 Marietta Tower, Suite 2805
101 Marietta Street
Atlanta, GA 30323-0008

10. SPONSORING/MONITORING AGENCY REPORT NUMBER

11. SUPPLEMENTARY NOTES

12a. DISTRIBUTION/AVAILABILITY STATEMENT
Approved for Public Release; Distribution Unlimited

12b. DISTRIBUTION CODE

13. ABSTRACT *(Maximum 200 words)*

The effect of the C_2H_4/Si_2H_6 gas flow rate ratios on the growth mode of SiC thin films via gas source (GS) MBE was investigated via cross-sectional TEM. Step flow and step bunching occurred at the outset of deposition under any ratio. Subsequent deposition resulted in step flow and continued growth of 6H-SiC films or formation and coalescence of 3C-SiC islands using the gas flow ratio of one or C_2H_4-rich ratios, respectively. The growth of the 6H regions occurred via layer-by-layer mode; the nucleation and growth of the 3C regions occurred primarily on terraces between closely spaced steps. Double positioning boundaries were observed at the intersections of these latter regions. Using similar growth and characterization techniques, essentially atomically flat surfaces of AlN were grown on the surfaces of on-axis 6H-SiC wafers; coalesced island-like features separated by anti-phase boundaries at SiC steps were observed on the vicinal surfaces. The activated N was derived from an ECR plasma source. Pseudomorphic multilayer heterostructures containing 6H- and 3C-SiC separated by 2H-AlN as well as films of $(AN)_x(SiC)_{1-x}$ solid solutions have been grown. Metal-insulator-semiconductor diodes (Al/AlN/6H-SiC) have also been fabricated using GSMBE and several insulator (AlN) thicknesses and subsequently characterized using C-V measurements between 10 kHz and 1 MHz. The diodes could be accumulated and depleted over the entire frequency range studied with no frequency dispersion observed. Inversion was not achieved at room temperature. Thin layers (<1000Å) of AlN exhibited moderate leakage currents; these currents were reduced in thicker layers. The dielectric constant was calculated and matched well with other measured values. The use of NH_3 thermally cracked on the 6H-SiC surface as an alternative to ECR has resulted in marked improvement in the optical properties of the AlN and subsequently deposited GaN films as revealed by the sharp PL peak at 354 nm. An optically driven Philips thin film X-ray machine has also been purchased and commissioned as a part of this program.

14. SUBJECT TERMS
SiC, silicon carbide, AlN, aluminum nitride, gas source MBE, step bunching, layer-by-layer, double positioning boundaries, pseudomorphic, heterostructures, MIS diodes, accumulation, depletion, leakage current, dielectric constant, X-ray

15. NUMBER OF PAGES
68

16. PRICE CODE

17. SECURITY CLASSIFICATION OF REPORT	18. SECURITY CLASSIFICATION OF THIS PAGE	19. SECURITY CLASSIFICATION OF ABSTRACT	20. LIMITATION OF ABSTRACT
UNCLAS	UNCLAS	UNCLAS	SAR

Table of Contents

I. Introduction 1

II. Effects of Gas Flow Ratio on Silicon Carbide Thin Film Growth Mode and Polytype Formation During Gas-source Molecular Beam Epitaxy 2
S. Tanaka, R. S. Kern, and R. F. Davis

III. Gas-source Molecular Beam Epitaxy of Monocrystalline β-SiC on Vicinal α(6H)-SiC 5
L. B. Rowland, R. S. Kern, S. Tanaka, and R. F. Davis

IV. Initial Stage of Aluminum Nitride Film Growth on 6H-Silicon Carbide by Plasma-assisted, Gas-source Molecular Beam Epitaxy 9
S. Tanaka, R. S. Kern, and R. F. Davis

V. Epitaxial Growth of AlN by Plasma-assisted, Gas-source Molecular Beam Epitaxy 22
L. B. Rowland, R. S. Kern, S. Tanaka, and R. F. Davis

VI. Aluminum Nitride/Silicon Carbide Multilayer Heterostructure Produced by Plasma-assisted, Gas-source Molecular Beam Epitaxy 27
L. B. Rowland, R. S. Kern, S. Tanaka, and R. F. Davis

VII. Solid Solutions of AlN and SiC Grown by Plasma-assisted, Gas-source Molecular Beam Epitaxy 30
R. S. Kern, L. B. Rowland, S. Tanaka, and R. F. Davis

VIII. Fabrication and Characterization of Al/AlN/SiC MIS Diodes Grown by Gas-source Molecular Beam Epitaxy 34
R. S. Kern

IX. Design and Development of Multiple Quantum Well Vertical Cavity Surface Emitting Laser Structures Via Molecular Beam Epitaxy of III-N Layers 42
K. Linthicum

X. Chemistry, Microstructure, and Electrical Properties at Interfaces Between Thin Films of Titanium and Alpha (6H) Silicon Carbide (0001) 49
L. M. Porter and R. F. Davis

XI. Structural Characterization of GaN and AlGaN Films by X-Ray Diffraction 61
W. Perry

XII. Distribution List 68

I. Introduction

The advent of techniques for growing semiconductor multilayer structures with layer thicknesses approaching atomic dimensions has provided new systems for both basic physics studies and device applications. Most of the research involving these structures has been restricted to materials with lattice constants that are equal within $\simeq 0.1\%$. However, it is now recognized that interesting and useful pseudomorphic structures can also be grown from a much larger set of materials that have lattice-constant mismatches in the percent range. Moreover, advances in computer hardware and software as well as the development of theoretical structural and molecular models applicable for strained layer nucleation, growth and property prediction have occurred to the extent that the field is poised to expand rapidly. It is within this context that the research described in this report is being conducted. The materials systems of concern include combinations of the direct bandgap materials of AlN and GaN and selected, indirect bandgap SiC polytypes.

The extremes in thermal, mechanical, chemical and electronic properties of SiC allow the types and numbers of current and conceivable applications of this material to be substantial. However, a principal driving force for the current resurgence of interest in this material, as well as AlN and GaN, is their potential as hosts for high power, high temperature microelectronic and optoelectronic devices for use in extreme environments. The availability of thin film heterostructural combinations of these materials will substantially broaden the applications potential for these materials. The pseudomorphic structures produced from these materials will be unique because of their chemistry, their wide bandgaps, the availability of indirect/direct bandgap combinations, their occurrence in cubic and hexagonal forms and the ability to tailor the lattice parameters and, therefore, the amount of strain and the physical properties via solid solutions composed of the three components.

The research conducted within this program and described in the following sections has been concerned with (1) the determination of the effect of various C_2H_4/Si_2H_6 gas flow rate ratios on the growth mode and polytype of SiC thin films deposited via gas source MBE, (2) the deposition of AlN films, pseudomorphic multilayer heterostructures containing 6H- and 3C-SiC separated by 2H-AlN and films of $(AN)_x(SiC)_{1-x}$ solid solutions, (3) the fabrication by GSMBE and C-V characterization of Al/AlN/SiC MIS diodes, and (4) the purchase and commissioning of an optically-driven Philips thin film X-ray machine. These sections detail the procedures, results, discussions of these results, conclusions obtained in this program and suggested plans for future research. Each subsection is self-contained with its own figures, tables, and references.

II. Effects of gas flow ratio on silicon carbide thin film growth mode and polytype formation during gas-source molecular beam epitaxy

Satoru Tanaka, R. Scott Kern, and Robert F. Davis
Department of Materials Science and Engineering, North Carolina State University, P.O. Box 7907, Raleigh, North Carolina 27695-7907

(Received 16 June 1994; accepted for publication 27 September 1994)

Silicon carbide thin films have been grown on vicinal 6*H*-SiC(0001) substrates by gas-source molecular beam epitaxy at 1050 °C. The effect of gas flow ratios ($C_2H_4Si_2H_6$=1,2,10) on the growth mode was examined via cross-sectional high resolution transmission electron microscopy and *in situ* reflection high energy electron diffraction. Step flow, step bunching, and the deposition of 6*H*-SiC occurred at the outset of the exposure of the (1×1) surface to the reactants using any flow ratio. Subsequent deposition resulted in step flow and continued growth of 6*H* films or formation and coalescence of 3*C*-SiC islands using the gas flow ratio of one of the ethylene-rich ratios, respectively. The (3×3) surface reconstruction observed using the former ratio is believed to enhance the diffusion lengths of the adatoms which, in turn, promotes step flow growth. © *1994 American Institute of Physics.*

High purity, monocrystalline silicon carbide (SiC) is being extensively studied for high-temperature, -power, and -frequency electronic device applications.[1] More than 250 polytypes or stacking arrangements of the closest packed Si/C bilayers along the crystallographic axes of closest packing have been reported.[2] The 3*C* or *β*, 15*R*, 6*H*, and 4*H* polytypes are the most common; the numerals and the letters refer to the number of bilayers needed to form a unit cell and the cubic, or hexagonal nature of the cell, respectively. Single crystal 6*H* and 4*H* wafers are commercially available; thus, thin films of these polytypes can be homoepitaxially deposited via chemical vapor deposition (CVD),[3,4] if the growth mode is step flow.

Step flow can be achieved kinetically when the deposited adatoms reach surface step sites and retain the identical stacking sequence as the substrate. Thus, 6*H* films can be formed on 6*H*(0001) substrates with the availability of steps even at growth temperatures <1500 °C, i.e., in the temperature regime where 3*C* is found by experiment[2] to be the more commonly deposited phase (though quantum mechanical calculation[5] predicts 6*H* to be more stable than 3*C*). The steps serve as the primary surface template which forces replication of the substrate polytype in the growing film. Step flow has been achieved experimentally via CVD in the homoepitaxial growth of 6*H* and 4*H* films between 1200 and 1600 °C.[3,4,6] Kinetic[7] and microstructural[8] studies of the growth mechanisms of these films have explained the detailed mechanisms of step flow growth and the structural conditions which lead to the formation of the 3*C* polytype. By contrast, previous SiC film growth studies via molecular beam epitaxy (MBE) at lower growth temperatures (<1200 °C) on 6*H*-SiC substrates reportedly did not result in step flow and homoepitaxial reproduction of the 6*H* substrate. Yoshinobu *et al.* deposited 3*C* films via MBE on 6*H*-SiC(0001)[9] and 3*C*-SiC(001)[10] substrates at <1000 °C using an alternating supply of C_2H_2 and Si_2H_6. By contrast, using a simultaneous supply of each gas below 1100 °C resulted either in the absence of film growth or in polycrystalline island formation. Rowland *et al.*[11] reported the deposition of monocrystalline 3*C* on 6*H*-SiC(0001) at 1050 °C using a simultaneous supply of C_2H_4 and Si_2H_6 and the very slow growth rate of ≈100 Å/h. The research reported herein stems directly from this last effort.

In the present research, we have successfully grown 6*H*-SiC films on 6*H*-SiC substrates oriented 3–4° off (0001) toward ⟨11$\bar{2}$0⟩ using gas-source molecular beam epitaxy (GSMBE) (see Ref. 11 for a detailed description of the use of this technique), a simultaneous supply of source gases, and the conditions given in Table I. The effects of C_2H_4/Si_2H_6 gas flow ratios on growth mode have been investigated. Island formation occurred under ethylene-rich conditions; step flow growth was achieved using the gas flow ratio of 1. A growth model is proposed and discussed from the aspects of surface reconstruction, related adatom diffusivities, and based on observations of the initial stage of growth by high resolution transmission electron microscopy (HRTEM) and *in situ* reflection high energy electron diffraction (RHEED).

The as-received substrates contained a 6*H* epitaxial layer which had been thermally oxidized after deposition. They were dipped in a 10% HF solution for 5 min to remove the protective surface oxide layer (typically ≈750 Å), immediately loaded into the MBE system and annealed at 1050 °C under $\approx 1\times10^{-9}$ torr for 30 min to remove any residual hydrocarbon and surface oxide. During subsequent depositions, RHEED patterns were monitored by the use of a digital camera and a video recorder. Each of the resulting substrate/film couples was cut and glued face-to-face to make a cross-sectional TEM sample and thinned to electron transparency using standard sample preparation techniques.[12] Each sample

TABLE I. Range of growth conditions for the SiC films.

Substrate	6*H*-SiC(0001)
Temperature	1050 °C
Si_2H_6 flow rate	0.1 sccm
C_2H_4 flow rates	0.1–1.0 sccm
C_2H_4/Si_2H_6 flow rate ratios	1.0,2.0,10.0
Growth rates and time	≈50–100 Å/h, 1 h

© 1994 American Institute of Physics

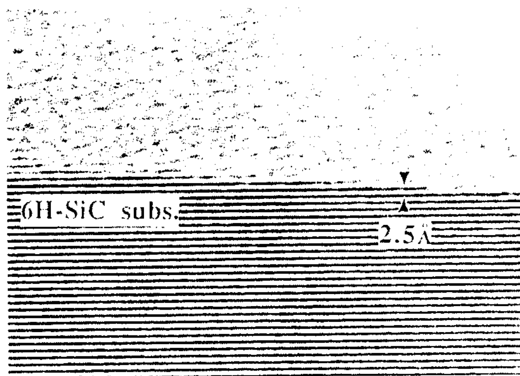

FIG. 1. Cross-sectional HRTEM image of the as-received $6H$-SiC epitaxial layer.

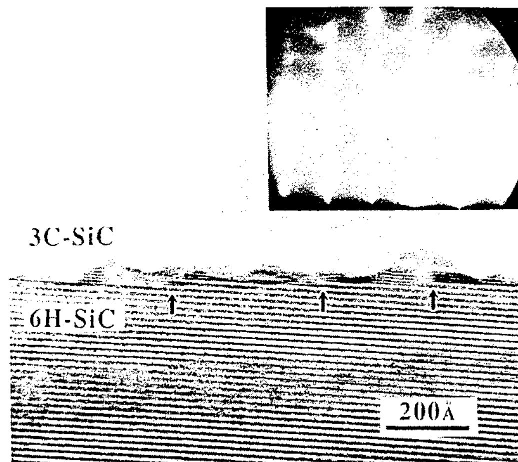

FIG. 2. Cross-sectional HRTEM image of $3C$ island growth at $C_2H_4/Si_2H_6=2$. Inset shows the RHEED pattern indicative of $3C$ island formation and double positioning boundaries (DPBs).

was examined along either $\langle\bar{1}100\rangle$ or $\langle\bar{2}110\rangle$ zone axes to observe the structure of the substrate surface or the deposited films, respectively, using a Topcon EM-OO2B operated at 200 kV.

Figure 1 shows the microstructure of the vicinal surface of the as-received $6H$-SiC(0001) epitaxial layer along the $\langle\bar{1}100\rangle$ zone axis. Single bilayer steps consisting of one Si and one C layer are predominant on the surface and stable to migration, as indicated by the fact that the sample shown in Fig. 1 has been heated to 1200 °C for 30 min without any measurable change in terrace width ($\approx$60 Å). Additional evidence for the existence of single bilayer steps on the as-received $6H$-SiC(0001) epitaxial layer has been obtained recently in this research using scanning tunneling microscopy.[13] Initial exposure of the surface to the reactant gases caused increases in both the average terrace width and average step height. This indicates the occurrence of step bunching. At this early stage of growth where single steps are present and relatively closely spaced, the adatoms can migrate to the step sites and establish the step flow mechanism, because the diffusion lengths of the adatoms equal or exceed the average terrace width. It should, and we believe it does, result in the growth of a $6H$ layer. It should be emphasized that, in theory, substantial step bunching should be observed if the surface diffusivities on the various $(000n)$ planes ($n=1-6$) of $6H$-SiC are different. Calculations by Heine *et al.*[5] show that the surface energies of the various bilayer planes of SiC are different and that the lowest energy planes in $6H$ are (0001) and (0004) (A planes in the ABC notation). Coupling this difference with heating to elevated temperatures such that atom migration occurs is believed to provide sufficient impetus for step bunching. Evidence of the occurrence of this phenomenon can be observed in Fig. 2 by the fact that the average terrace width ($\approx$300 Å) and average step height (1/2–2 unit cell heights) at the surface of the newly deposited $6H$ material ($c=15$ Å) (see arrows at steps) are now markedly greater than on the as-received material. As the terrace width increases, sufficient adatoms eventually cannot reach the step sites to retain step flow due to the limited diffusion length at the growth temperature. The growth of the $6H$ film will cease and islands of material which may be of a new polytype will begin to nucleate on the terrace site. This is shown by the advent and growth of the $3C$ layer in Fig. 2 after several minutes of deposition using $C_2H_4/Si_2H_6=2$. Indeed, our research indicates that if nucleation occurs on the terrace sites, only $3C$ will form.

The undulating surface morphology of the $3C$ film in Fig. 2 is a result of the growth of islands and their subsequent coalescence. The use of the more ethylene-rich condition of $C_2H_4/Si_2H_6=10$ resulted in similar features; however, the deposition rate and the density of the islands decreased. This is believed to have been caused by the interaction be-

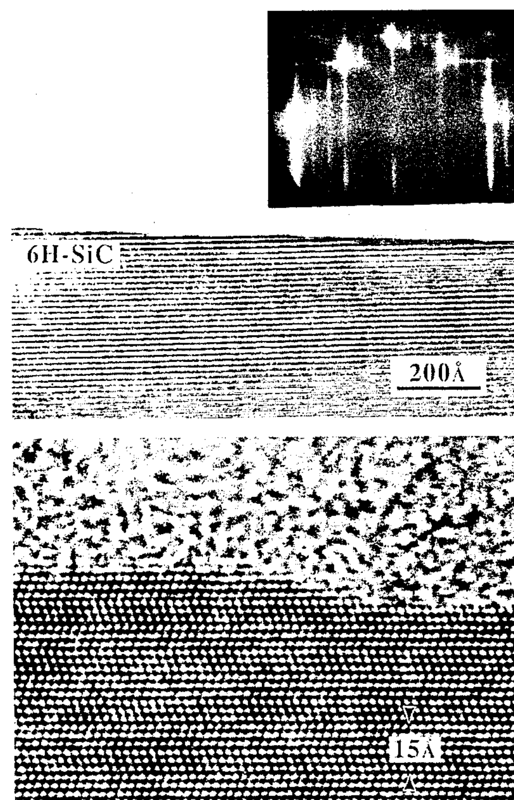

FIG. 3. (a) Cross-sectional HRTEM image of step flow growth at $C_2H_4/Si_2H_6=1$. Inset shows the (3×3) RHEED pattern. (b) A magnified image of the stepped surface shown in (a).

tween reactant gases on the surface which lowered the sticking probability of the Si_2H_6 molecules. During the growth of both films, RHEED initially showed a highly streaked (1×1) pattern indicative of *6H* deposition via step flow. This pattern changed to a (1×1) pattern of spots and streaks (see inset) indicative of *3C* island formation and evidence for double positioning boundaries (DPBs).[14] The details of the RHEED study will be reported in the near future.

Decreasing the C_2H_4 concentration to $C_2H_4/Si_2H_6=1$ caused a dramatic change in the film growth mode. Figure 3(a) shows only a *6H*-SiC film, grown for the time as the *6H/3C* combination shown in Fig. 2 and containing a stepped surface having an average terrace width of ≈250 Å. Figure 3(b) is a magnified image of this surface showing a step which is a half unit cell in height (3–4 bilayers). The *3C* polytype was not observed. The increased terrace width is again strong evidence for step flow. Under these growth conditions, the (1×1) RHEED pattern of the as-received substrate immediately reconstructed to (3×3) [see inset, Fig. 3(a)]. Kaplan[15] has proposed a model for this reconstruction which consists of an adsorbed Si bilayer. If true, our results indicate that the energy of the growing surface is reduced due to reconstruction by using $C_2H_4/Si_2H_6=1$ and that the surface mobilities of adatoms are enhanced on such a reconstructed surface which normally has a smaller number of dangling bonds for bonding to the adatoms. Thus, step flow can be enhanced and lead to step flow growth over a much larger period of time.

In summary, we have successfully grown *6H*-SiC films on *6H*-SiC substrates at 1050 °C by GSMBE using a simultaneous supply of source gases and $C_2H_4/Si_2H_6=1$. Surface reconstruction from (1×1) to (3×3) occurred at the outset of this growth which, in turn, is believed to have allowed an increase in the mobility of the adatoms and enhanced step flow growth. Using gas flow ratios of $C_2H_4/Si_2H_6=2$ and 10, the (1×1) RHEED pattern was retained and step bunching, as a result of an abbreviated period of step flow, was observed and followed by formation and coalescence of *3C* islands.

The authors express their appreciation to the Office of Naval Research for support of this research under Grant No. N00014-92-J-1500 and to Cree Research, Inc. for the *6H*-SiC wafers.

[1] R. F. Davis, Physica B **185**, 1 (1993).
[2] N. W. Jepps and T. F. Page, in *Progress in Crystal Growth and Characterization*, edited by P. Krishna (Pergamon, New York, 1983), Vol. 7, p. 259.
[3] H. S. Kong, J. T. Glass, and R. F. Davis, J. Appl. Phys. **64**, 2672 (1988).
[4] H. Matsunami, T. Ueda, and H. Nishino, Mater. Res. Soc. Symp. Proc. **162**, 397 (1990).
[5] V. Heine, C. Chen, and R. J. Needs, J. Am. Ceram. Soc. **74**, 2630 (1991).
[6] T. Kimoto, A. Yamashita, A. Itoh, and H. Matsunami, Jpn. J. Appl. Phys. **32**, 1045 (1993).
[7] T. Kimoto, H. Nishino, W. S. Yoo, and H. Matsunami, J. Appl. Phys. **73**, 726 (1993).
[8] F. R. Chien, S. R. Nutt, W. S. Yoo, T. Kimoto, and H. Matsunami, J. Mater. Res. **9**, 940 (1994).
[9] T. Yoshinobu, M. Nakayama, H. Shiomi, T. Fuyuki, and H. Matsunami, J. Cryst. Growth **99**, 520 (1990).
[10] T. Yoshinobu, H. Mitsui, I. Izumikawa, T. Fuyuki, and H. Matsunami, Appl. Phys. Lett. **60**, 824 (1992).
[11] L. B. Rowland, R. S. Kern, S. Tanaka, and R. F. Davis, J. Mater. Res. **8**, 2753 (1993).
[12] C. H. Carter, Jr., R. F. Davis, and S. R. Nutt, J. Mater. Res. **1**, 811 (1986).
[13] S. Tanaka, J. F. Wendelken, and R. F. Davis (unpublished).
[14] L. B. Rowland, R. S. Kern, S. Tanaka, and R. F. Davis, Appl. Phys. Lett. **62**, 3333 (1993).
[15] R. Kaplan, Surf. Sci. **215**, 111 (1989).

III. Gas-source molecular beam epitaxy of monocrystalline β–SiC on vicinal α(6H)–SiC

L. B. Rowland,[a] R. S. Kern, S. Tanaka, and Robert F. Davis
Department of Materials Science and Engineering, North Carolina State University, Box 7907, Raleigh, North Carolina 27695-7907

(Received 30 December 1992; accepted 20 July 1993)

Single-crystal epitaxial films of cubic β(3C)–SiC(111) have been deposited on hexagonal α(6H)–SiC(0001) substrates oriented 3–4° toward [11$\bar{2}$0] at 1050–1250 °C via gas-source molecular beam epitaxy using disilane (Si_2H_6) and ethylene (C_2H_4). High-resolution transmission electron microscopy revealed that the nucleation and growth of the β(3C)–SiC regions occurred primarily on terraces between closely spaced steps because of reduced rates of surface migration at the low growth temperatures. Double positioning boundaries were observed at the intersections of these regions.

Polytypes are special one-dimensional polymorphs which differ only in the stacking sequence along the closest-packed direction. Silicon carbide occurs in one cubic (zinc blende) polytype referred to as 3C– or β–SiC, where the 3 refers to the number of planes in the periodic sequence. The hexagonal (wurtzite) polytype also exists in this material. Both polytypes occur in more complex, intermixed forms yielding a wider range of ordered, larger period, hexagonal or rhombohedral structures of which 6H is the most common. All of these noncubic polytypes are known collectively as α–SiC.

The growth of 3C– and 6H–SiC thin films has been achieved primarily via chemical vapor deposition (CVD) (see Ref. 1 for a review of this research). Monocrystalline Si(100) wafers have been the principal substrate of choice for the deposition of 3C. It is now a common first step to transform the surface region of these wafers to β–SiC by reaction with a C-containing gas to reduce the effects of the large mismatches in lattice parameters ($\approx$20%) and coefficients of thermal expansion ($\approx$10%). The epitaxial growth of SiC films on α(6H)–SiC(0001) substrates via CVD has been reported for three decades.[1] Single phase β–SiC films result[2,3] when the [0001] direction of the 6H wafer is oriented off-axis $\leq$1°. The primary defects in these films are double positioning boundaries (DPB).[4] The use of vicinal 6H–SiC(0001) substrates cut 3–4° toward [11$\bar{2}$0] have resulted in high-quality monocrystalline 6H–SiC layers with low defect densities,[5,6] including the absence of DPB's.

Solid- and gas-source (GS) molecular beam epitaxy (MBE) techniques have also been employed for deposition of SiC films.[7,8] Kaneda *et al.*[7] used on-axis α(6H)–SiC{0001} substrates and electron-beam evaporated Si and C sources. Epitaxial 3C–SiC(111) films were obtained at particular Si-to-C flux ratios in the temperature range of 1150–1400 °C, as determined by reflection high-energy electron diffraction (RHEED). No information was given by these authors regarding either the microstructure or the type of defects present in these films. By contrast, Yoshinobu *et al.*[8] employed the periodic introduction of Si_2H_6 and C_2H_2 to achieve 3C–SiC growth on vicinal 6H–SiC(000$\bar{1}$) and 6H–SiC(0$\bar{1}$1$\bar{4}$) substrates at 850–1160 °C. Films grown on vicinal 6H–SiC(000$\bar{1}$) contained DPB's while those grown on 6H–SiC(0$\bar{1}$1$\bar{4}$) were free of these defects. Smooth films were obtained at the lowest growth rates used in the study (<0.01 μm/h).

In the present research, the 3C–SiC films were grown via GSMBE between 1050 and 1250 °C on α(6H)–SiC(0001) wafers oriented 3–4° off [0001] toward [11$\bar{2}$0] and produced by Cree Research, Inc. using a seeded Lely sublimation method. The MBE growth system (see Fig. 1) has been described previously.[9] Each wafer was sequentially cleaned prior to growth using a 10% HF etch at room temperature for 5 min, rinsed in DI water for 2 min, and heated in the MBE chamber for 5 min at the growth temperature to achieve the desorption and decomposition of any remaining hydrocarbon species and native oxide, respectively. The source gases of Si_2H_6 and C_2H_4 were used to deposit the SiC. The base and operating pressures were 10^{-9} Torr and 3×10^{-5}–3×10^{-6} Torr, respectively.

The surface morphology was determined using field-emission scanning electron microscopy (SEM) at an operating voltage of 2.0 kV. Reflection high-energy electron diffraction (RHEED) at 10 kV and high-resolution transmission electron microscopy (HRTEM) were used for structural and microstructural analyses. Samples were prepared for HRTEM using standard techniques.[10] An Akashi EM 002B high-resolution transmission electron microscope was used at 200 kV for the HRTEM analysis.

[a]Present address: Naval Research Laboratory, Code 6861, 4555 Overlook Avenue SW, Washington, DC 20375-5320.

 © 1993 Materials Research Society

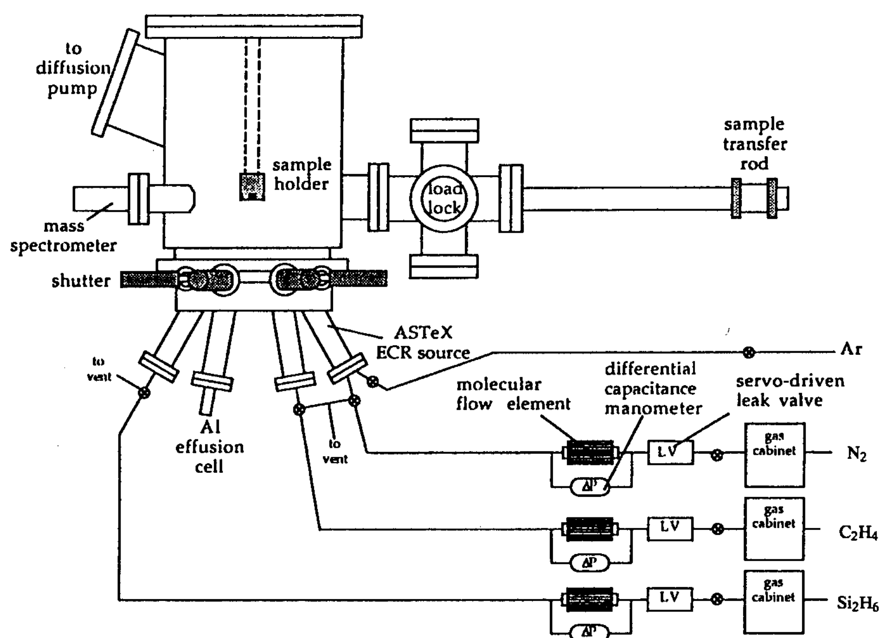

FIG. 1. Schematic of molecular beam epitaxy system.

The films grown in this study were single crystal SiC, as determined by HRTEM and/or RHEED. The surfaces of all films appeared smooth and specular to the naked eye. The surface morphologies of samples grown at 1250 °C using the Si : C flow rate ratio of 1 : 2 are shown in Fig. 2. The use of a total flow rate of 3.0 sccm resulted in a rough surface containing a high density of small (0.1–0.2 μm) triangular regions of different heights, as shown in Fig. 2(a). Reducing the total flow rate to 1.5 sccm produced a smoother top surface with regions of uniform height, as shown in Fig. 2(b). Further reduction to 0.30 sccm resulted in a significantly smoother surface with fewer, smaller regions [Fig. 2(c)]. The use of 0.06 sccm did not result in growth, as determined by HRTEM analysis.

Figure 3 is a cross-sectional HRTEM micrograph of the SiC film grown at 1250 °C using a total flow rate of 1.5 sccm. The lattice images of the film reveal it to be the β(3C) polytype in the (111) orientation. The micrograph and the corresponding selected-area diffraction pattern also show the epitaxial relationship between the substrate and the film. Stacking faults parallel to the interface can also be observed. Plan-view TEM on this sample (Fig. 4) shows that DPB's and stacking faults (denoted SF) are present in this sample. The same results were obtained at all growth temperatures using the C : Si flow rate ratio of 2 : 1.

The occurrence of 3C–SiC on vicinal α(6H)–SiC substrates is in contrast to the 6H films obtained by CVD, where step separation clearly defines the stacking sequence of the resulting films.[5,6] Initially, it was believed that a decrease in total flow rate at the same growth temperature would allow the 6H polytype to form, as the Si and C species would have more time to reach energetically favorable sites associated with steps. However, the 3C polytype formed regardless of the total flow rate. Growth at 1200 and 1050 °C under similar conditions also resulted in 3C–SiC. This appears to confirm the theoretical work proposed by Heine *et al.*[11] which proposed that metastable 3C–SiC would be the preferred polytype in thin film growth based on surface rather than bulk energetics, the idea being that adding a Si–C bilayer in the cubic stacking sequence is energetically more favorable than adding twinned bilayers (i.e., growth of an α–SiC polytype).

Films were also grown at 1050 °C using the flow rates of 2.0 sccm C_2H_4 and 0.50 sccm Si_2H_6. The decrease in temperature and the high flow rate were used to lower the reactivity and surface mobility and to increase the supply of precursor species, respectively, to enhance the nucleation density. An SEM micrograph of the surface of this film is shown in Fig. 5. The film appears much smoother than films grown at higher temperatures and/or at lower flow rates. However, individual regions are also observed with diameters of substantially less than 100 nm. The HRTEM microstructure of this film shown in Fig. 6 reveals a high density of steps (denoted by arrows) on the substrate surface and regions of 3C–SiC(111) which are centered on the terraces between the steps. Each terrace appears to have one individual region. In most areas, adjacent regions coalesce above the steps. The areas of coalescence were much more defective than the remainder of the film.

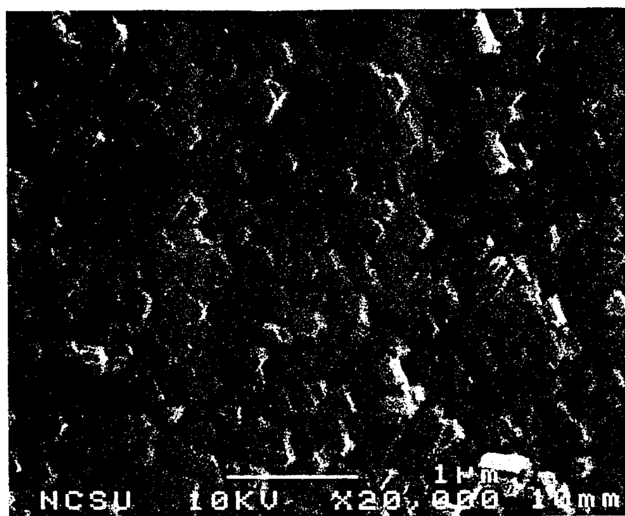

(a)

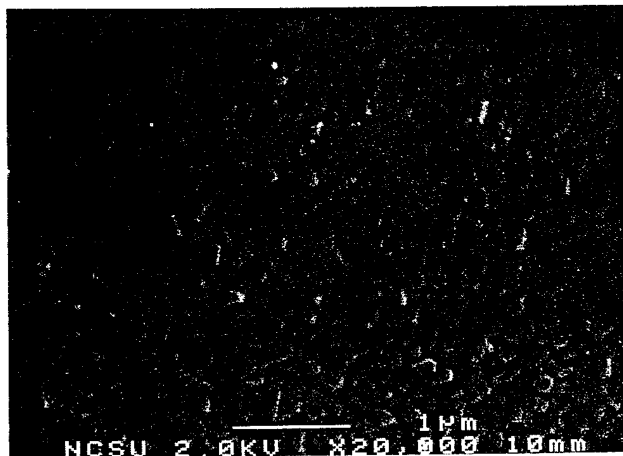

(b)

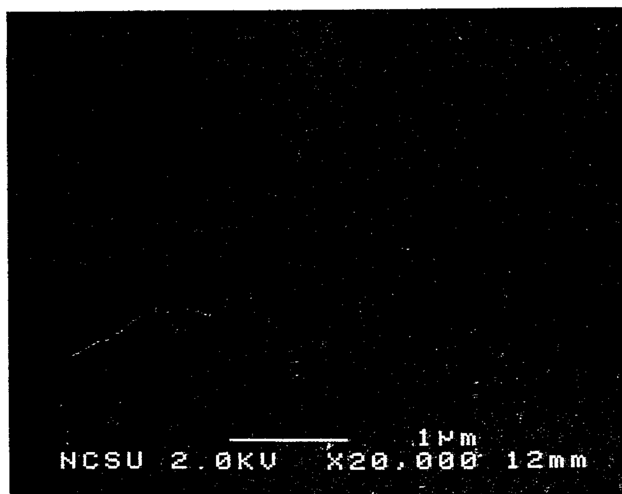

(c)

FIG. 2. Scanning electron micrograph of the surface of 3C–SiC films grown on 3–4° off-axis 6H–SiC substrates at 1250 °C using (a) 2.0 sccm C_2H_4 and 1.0 sccm Si_2H_6, (b) 1.0 sccm C_2H_4 and 0.5 sccm Si_2H_6, and (c) 0.2 sccm C_2H_4 and 0.1 sccm Si_2H_6.

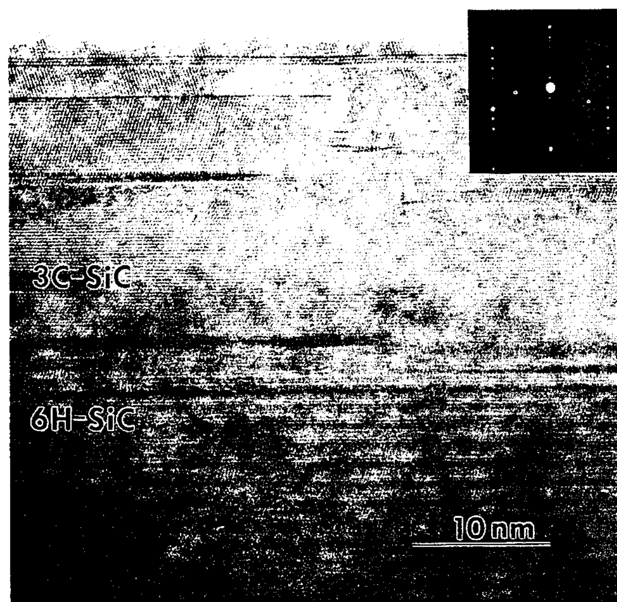

FIG. 3. Cross-sectional HRTEM micrograph of 3C–SiC(111) film on vicinal 6H–SiC(0001) substrate with inset of selected area diffraction pattern ([110] zone axis). Sample was grown at 1250 °C using 1.0 sccm C_2H_4 and 0.5 sccm Si_2H_6.

The evidence presented in Fig. 6 indicates that within the ranges of conditions employed in this study, nucleation on vicinal 6H–SiC substrates occurs on terraces between steps resulting in 3C–SiC(111). In the accepted model, independently proposed by Kong *et al.*[5] and Kuroda *et al.*,[6] the density and orientation of the surface steps determine the resultant SiC polytype. If few steps are present, as in the case of nominally

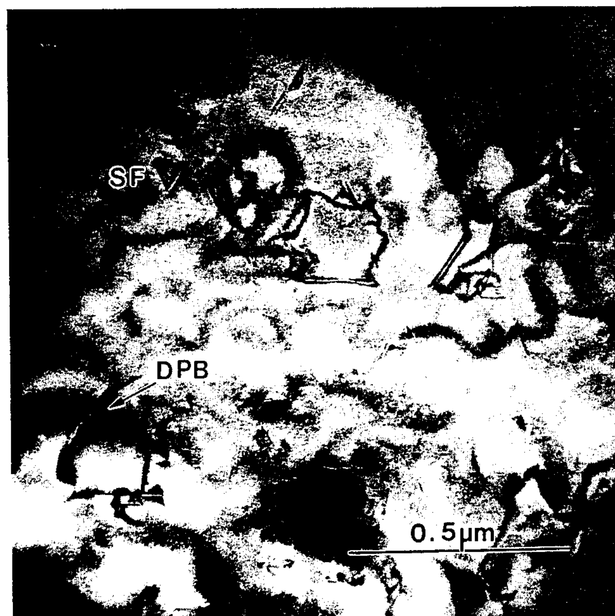

FIG. 4. Plan-view transmission electron micrograph of 3C–SiC film and 6H–SiC substrate shown in Fig. 3. Both stacking faults (denoted SF) and double positioning boundaries (denoted DPB) are visible.

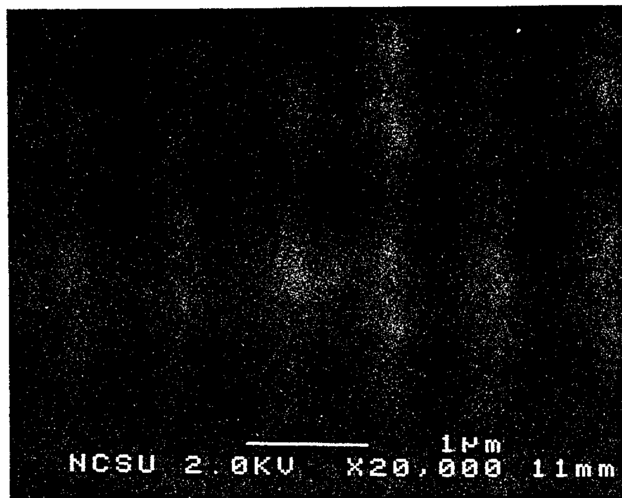

FIG. 5. Scanning electron micrograph of surface of 3C–SiC film grown on vicinal 6H–SiC at 1050 °C using 2.0 sccm C_2H_4 and 0.5 sccm Si_2H_6.

on-axis SiC, growth conditions determine the resultant polytype and 3C–SiC is usually formed. If there exists a high density of [11$\bar{2}$0] surface steps, then these steps serve as a template for SiC growth and the stacking sequence of the 6H polytype is preserved. However, in our studies, the kinetics of surface migration are sufficiently decreased as a result of the reduced substrate temperature that β–SiC nucleates on the terraces rather than at the surface steps. It is important to note that the terraces in Fig. 6 are longer than expected and the steps consist of multiple atom layers. It is not yet understood if this is a result of heat treatment or deposition; however, similar substrates have been examined prior to growth with no step bunching occurring.

The surface treatment prior to growth also differed between our MBE and the previous CVD studies. These differences may have affected the resultant SiC polytype and the density of defects, such as DPB's. Two groups of researchers have observed that variation in surface treatment prior to growth can reduce or virtually eliminate DPB's formed in the resultant film.[12,13] This difference in surface treatment may also cause the resultant polytype to be 3C rather than 6H. Studies concerned with this topic are ongoing in the authors' laboratory.

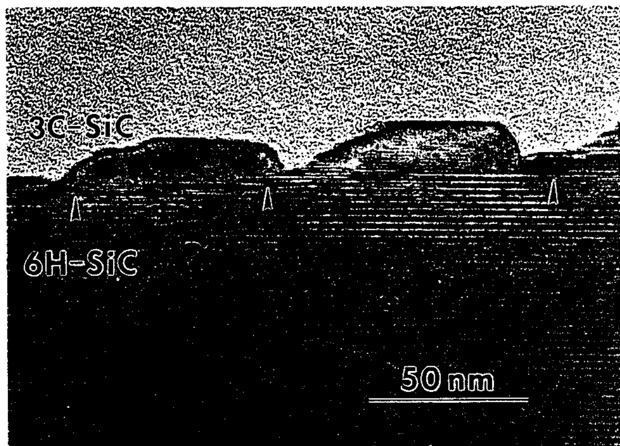

FIG. 6. High-resolution TEM micrograph of 3C–SiC regions and vicinal 6H–SiC(0001) substrate. Sample was grown at 1050 °C using 2.0 sccm C_2H_4 and 0.5 sccm Si_2H_6. Steps on the 6H–SiC substrate surface are denoted by arrows.

In summary, monocrystalline films of β(3C)–SiC(111) were grown on 3–4° off-axis α(6H)–SiC(0001) substrates at 1050–1250 °C by GSMBE using C_2H_4 and Si_2H_6 at a flow rate ratio of 2:1. High-resolution TEM showed that nucleation and growth occurred on the terraces between closely spaced substrate steps as a result of the reduction in the kinetics of surface migration of the reactive species relative to that found in CVD processes where α(6H)–SiC is normally deposited.

ACKNOWLEDGMENTS

The authors acknowledge the support of this research by the Office of Naval Research under Grant No. N00014-88-K-0341. We also express our appreciation to Applied Science and Technology, Inc., Woburn, MA, for the ECR source, and to Cree Research, Inc., Durham, NC, for the vicinal 6H–SiC substrates.

REFERENCES

1. R.F. Davis, J.W. Palmour, and J.A. Edmond, Diamond and Related Materials **1**, 109 (1992).
2. H.S. Kong, J.T. Glass, and R.F. Davis, Appl. Phys. Lett. **49**, 1074 (1986).
3. K. Shibahara, N. Kuroda, S. Nishino, and H. Matsunami, Jpn. J. Appl. Phys. **26**, L1815 (1987).
4. H.S. Kong, B.L. Jiang, J.T. Glass, G.A. Rozgonyi, and K.L. More, J. Appl. Phys. **63**, 2645 (1988).
5. H.S. Kong, J.T. Glass, and R.F. Davis, J. Appl. Phys. **64**, 2672 (1988).
6. N. Kuroda, K. Shibahara, W. Yoo, S. Nishino, and H. Matsunami, in *Extended Abstracts 19th Conf. on Solid State Devices and Materials* (Business Center for Academic Societies, Tokyo, 1987), p. 227.
7. S. Kaneda, Y. Sakamoto, T. Mihara, and T. Tanaka, J. Cryst. Growth **81**, 536 (1987).
8. T. Yoshinobu, H. Mitsui, I. Izumikawa, T. Fuyuki, and H. Matsunami, Appl. Phys. Lett. **60**, 824 (1992).
9. L.B. Rowland, R.S. Kern, S. Tanaka, and R.F. Davis, in *Proc. 4th Int. Conf. Amorphous and Crystalline Silicon Carbide and Related Materials,* edited by C.Y. Yang, M.M. Rahman, and G.L. Harris (Springer-Verlag, Berlin, 1992), p. 84.
10. J.C. Bravman and R. Sinclair, J. Electron Microsc. Technol. **1**, 53 (1987).
11. V. Heine, C. Cheng, and R.J. Needs, J. Am. Ceram. Soc. **74**, 2630 (1991).
12. J.A. Powell, D.J. Larkin, L.G. Matus, W.J. Choyke, J.L. Bradshaw, L. Henderson, M. Yoganathan, J. Yang, and P. Pirouz, Appl. Phys. Lett. **56**, 1353 (1990).
13. Y.C. Wang, M.S. Thesis, North Carolina State University, 1991.

IV. Initial Stage of Aluminum Nitride Film Growth on 6H-Silicon Carbide by Plasma-assisted, Gas-source Molecular Beam Epitaxy

Submitted for Consideration for Publication

to

Applied Physics Letters

By

Satoru Tanaka

R. Scott Kern

Robert F. Davis

Department of Materials Science and Engineering

North Carolina State University

Box 7907

Raleigh, North Carolina 27695-7907

July 1994

Abstract

The initial stage of AlN film growth on 6H-SiC(0001) substrates by plasma-assisted, gas source molecular beam epitaxy (PAGSMBE) has been investigated in terms of growth mode and interface defects. Cross-sectional high resolution transmission electron microscopy (HRTEM) was used to observe the microstructure of the deposited films and the AlN/SiC interfaces. Surface morphologies and interface atomic structures were compared between films grown on vicinal and on-axis surfaces. Essentially atomically flat AlN surfaces were obtained using on-axis substrates. This is indicative of two dimensional growth to a thickness of ~15Å. Island-like features were observed on the vicinal surface. The coalescence of these features at steps gave rise to anti-phase domain boundaries (APBs) as a result of the misalignment of the Si/C bilayer steps with the Al/N bilayers in the growing film. The quality of thicker AlN films is strongly influenced by the concentration of APBs formed at the outset of growth.

Monocrystalline, hexagonal (2H) AlN has a direct band gap of 6.28eV at 300K[1], a very approximate melting point ~3073K[2], and a room temperature thermal conductivity of 3.2W/cm·K[3]. It is a candidate material for high-power and high-temperature microelectronic and optoelectronic applications. GaN/AlN[4] and SiC/AlN[5] multilayer heterostructures and solid solutions[6,7] are also under study for some of the aforementioned applications. AlN is commonly deposited as a buffer layer on SiC and sapphire (Al_2O_3) substrates on which are grown thin films of GaN, InN and solid solutions of III-V nitrides. The a-axis lattice constant of AlN(3.112Å) differs from that of GaN(3.189Å) and 6H-SiC(3.08Å) by -2.4% and 1.0%, respectively; the a-axis thermal expansion coefficients of these three materials at 300K are also similar (AlN[8]: 4.36, GaN[9]: 5.59, 6H-SiC[10]: 4.2 ($10^{-6}\,K^{-1}$)). It is important to obtain very smooth and low defect density AlN films on which to deposit high quality GaN and related films. For the growth of multilayered structures such as GaN/AlN/SiC[11] and SiC/AlN/SiC[5], a smooth surface for each layer is especially desirable. The ability to achieve this objective is, in general, determined thermodynamically by the growth modes[12] of the various films, i.e. two-dimensional (Frank-van der Merwe[13]), three-dimensional (Volmer-Weber[14]) or a combination these modes (Stranski-Krastanov[15]). To obtain an atomically smooth surface for a given material under conditions where surface atomic migration occurs, the film growth mechanism should be either two-dimensional on the terraces or step flow. The occurrence of the latter mechanism is controlled by the kinetics of film growth and will pertain if the diffusion lengths of the adatoms are sufficient to allow them to reach the steps before nucleation or cluster formation on the terraces. In this study, the initial stage of AlN film growth on 6H-SiC substrates was investigated in terms of growth mechanism and its relationship to and the occurrence of defects at AlN/SiC interfaces using cross-sectional HRTEM.

The AlN films were grown via PAGSMBE on the Si(0001) surfaces of either vicinal (3-4° off from (0001) toward <11$\bar{2}$0>) or on-axis α(6H)-SiC substrates under the conditions given in Table I. Aluminum (99.999% pure) was evaporated from a standard effusion cell. Nitrogen (99.9995% pure) was decomposed using an electron cyclotron resonance (ECR)

plasma. A detailed description of the deposition technique has been published.[16] Each as-received substrate, consisting of a 6H epitaxial layer and a thermally grown oxide (typically ~750Å thick), was dipped in a 10% HF solution for 5 min. to remove the oxide layer. It was immediately loaded into the MBE system and annealed at 1050°C and $\approx 1\times10^{-9}$ torr for 5 min. to remove any residual hydrocarbons and silicon oxide. To observe the initial stage of AlN growth, the thickness of each film was controlled by varying the growth time. Following growth, each sample was cut and glued face-to-face and thinned to electron transparency using standard cross-sectional TEM preparation techniques.[17] Each sample was examined along the <$\bar{2}$110> zone axis using a Topcon EM-OO2B operated at a 200kV acceleration voltage.

Figures 1 (a) and (b) show the initial stage of growth of a 2H(wurtzite)-AlN(0001) film deposited simultaneously on both on-axis and vicinal 6H-SiC(0001) substrates, respectively. Both films were deposited at the same time. The ~15Å thick film on the on-axis substrate (Fig. 1(a)) possesses very smooth surface and excellent thickness uniformity, indicating two-dimensional growth. In contrast, a slightly rougher surface is observed in the AlN film grown on the vicinal surface (Fig. 1(b)). In each film the degree of surface roughness is directly related to the areal density of steps which is markedly higher in the vicinal surface, as indicated in Fig. 1(b). The average distance between monolayer steps on the vicinal SiC surface containing the AlN film is ~70Å. This is the same distance as that determined on the as-received substrate surface. This indicates that no step bunching occurred during deposition of AlN in contrast to that observed during SiC film growth.[18]

Higher magnification images of the films shown in Fig. 1 are presented in Figs. 2 (a) and (b). They more clearly reveal the surface topography, microstructure, and the abrupt nature of the 2H-AlN/6H-SiC interface for each sample. The on-axis AlN films consisted of 5-6 Al/N bilayers. However, island-like areas can be observed on each terrace site in the film deposited on the vicinal 6H-SiC substrate (Fig. 2(b)). The film thickness within these features varied from 3-4 to 7-8 Al/N bilayers. A 'valley' feature formed perpendicular to the substrate surface when the boundary of coalescence between island-like areas occurred at a step (see

arrows in Fig. 2(b)) due to the misalignment between the islands at this point. No other line or planar defects were observed in either film in this thickness range.

A more highly magnified HRTEM image is helpful in explaining this misalignment feature. Figure 3 (a) shows a micrograph of the AlN/SiC interface and a region of coalescence between two AlN island-like areas. The latter nucleated on the terrace sites which was observed[18] to be separated by one bilayer step. Figure 3 (b) shows a model of this structure which illustrates the formation of an anti-phase domain boundary (APB) at a step site. The APB was caused by the difference in the stacking sequence between the Si/C bilayers in the 6H-SiC (...ABCACB...) substrate and the Al/N bilayer in the 2H-AlN (...ABAB...) islands. In addition, an 'A' layer in each 2H-AlN (0001) crystal is rotated 60° from a 'B' layer position. The model is also based on the assumption that from the viewpoint of energetics the first AlN layer prefers to occupy the wurtzite position on the SiC surface, i.e., the N and Al atoms are sited above the Si and C atoms, respectively, on the final Si/C bilayer of the substrate. However, a detailed structural study using quantum mechanical calculations analogous to those used for the Si-$NiSi_2$ and Si-$CoSi_2$[19] systems should also be conducted to test this assumption.

As indicated by the arrows in Fig. 3 (b), the lattice can be elastically relaxed. The adatoms are affected by a potential energy barrier at the step sites[20], caused by the difference in c-axis crystallography and bonding characteristics between 6H-SiC and AlN, such that surface migration is hindered. This results in a variation in thickness from the area of coalescence to the center of the island features on the terrace sites. The majority of the nuclei on the different terrace sites fail to align with the neighboring nuclei (island) due to their anti-phase characteristics. Additional studies of the step configuration, however, indicate that some nuclei formed on different levels of the terraces can align with each other without any strain because of the step geometry of the 6H-SiC substrate.[21] It is clear that an ideal on-axis SiC surface which contains no steps should allow the nucleation and growth of a nearly perfect two dimensional AlN film for the first several monolayers. It has been found that continued

deposition of AlN films beyond a certain thickness of the film on the on-axis substrates resulted in the onset of three-dimensional growth. The critical thickness for the onset of this Stranski-Krastanov growth mode in the AlN/SiC system using the MBE deposition route will be determined in the near future.

In summary, the initial ~15Å of 2H-AlN film growth on both on-axis and vicinal 6H-SiC(0001) substrates has been investigated using cross-sectional HRTEM. The respective micrographs revealed very smooth and essentially defect free films on the former substrates, indicative of two-dimensional growth, and rough surfaces and APBs in the films deposited on the vicinal substrates. Highly magnified images and a corresponding structural model of the AlN/SiC interface and AlN film reveal the presence of APBs, due to the nature of the steps on the 6H-SiC substrate. It is suggested that essentially defect-free AlN films can be achieved using on-axis 6H-SiC substrates.

The authors express their appreciation to the Office of Naval Research for support of this research under Grant No. N00014-90-J-1427. Appreciation is also expressed to Cree Research, Inc. for the wafers of SiC and to Dr. T. Chikyow for fruitful discussions.

References

[1] W. M. Yim, E. J. Stofko, P. I. Pankove, M. Ettenberg, and S. L. Gilbert, J. Appl. Phys. **44**, 292 (1973).

[2] W. Class, NASA CR-1171 (U.S.A.), 1968.

[3] G. A. Slack, J. Phys. Chem. Solids **34**, 321 (1973).

[4] Z. Sitar, M. J. Paisley, B. Yan, J. Ruan, W. J. Choyke, and R. F. Davis, J. Vac. Sci. Technol. **B8**, 316 (1990).

[5] L. B. Rowland, R. S. Kern, S. Tanaka, and R. F. Davis, Appl. Phys. Lett. **62**, 3333 (1993).

[6] R. S. Kern, L. B. Rowland, S. Tanaka, and R. F. Davis, J. Mater. Res. **8**, 1477 (1993).

[7] Y. Koide, H. Itoh, M. R. Khan, H. Hiramatsu, N. Sawaki, and I. Akasaki, J. Appl. Phys. **61**, 4540 (1987).

[8] G. A. Slack and S. F. Bartram, J. Appl. Phys **46**, 89 (1975).

[9] H. P. Maruska and J. J. Tietjien, Appl. Phys. Lett. **15**, 327 (1969).

[10] A. Taylor and R. M. Jones, *in Silicon Carbide, A High Temperature Semiconductor*, edited by J. R. O'Conor and J. Smittens (Pergamon Press, NY, 1960), p.147.

[11] H. Amano, M. Kito, K. Hiramatsu, and I. Akasaki, Jpn. J. Appl. Phys. **28**, L2112 (1989).

[12] J. A. Venables, G. D. T. Spiller, and M. Hanbucken, Rep. Prog. Phys. **47**, 399 (1984).

[13] M. Volmer and A. Weber, Zeit. Phys. Chem. **119**, 277 (1926).

[14] F. C. Frank and J. H. van der Merwe, Proc. Royal Soc. **A198**, 205 (1949).

[15] I. N. Stranski and L. Krastanov, Sitzunsber. Akad., Wiss. Wien, Math-Naturewiss., K1 IIb **146**, 797 (1938).

[16] L. B. Rowland, R. S. Kern, S. Tanaka, and R. F. Davis, J. Mater. Res. **8**, 2310 (1993).

[17] C. H. Carter, Jr., R. F. Davis, and S. R. Nutt, J. Mater. Res. **1**, 811 (1986).

[18] S. Tanaka, R. S. Kern, and R. F. Davis, submitted to Appl. Phys. Lett.

[19] D. R. Hamann, Phys. Rev. Lett. **60**, 313 (1988).

[20] R. Ghez and S. S. Iyer, IBM J. Res. Develop. **32**, 804 (1988).

[21] S. Tanaka, R. S. Kern, and R. F. Davis, paper in progress.

Table and Figure Captions

Table I. Growth conditions for the AlN films.

Figure 1. Cross-sectional TEM images of AlN films grown on (a) on-axis and (b) vicinal α(6H)-SiC substrates. The arrows shown in Fig. (b) indicate step positions in the substrate.

Figure 2. High resolution TEM images of AlN films and AlN/SiC interfaces of (a) on-axis substrate and (b) vicinal substrate. The arrows shown in Fig. (b) indicate the step positions.

Figure 3. (a) High resolution TEM image at α(6H)-SiC step, showing the presence of an APB. The characters, BCA, and dots on the image present the stacking sequence of the 6H-SiC substrate. (b) The model of the APB based on the image in Fig. (a). The short arrows indicate the direction of lattice distortion.

Table I. Growth Conditions for the AlN films

Temperature	1050 °C
Al evaporation temperature	1260 °C
Nitrogen flow rate	3.5 sccm
Microwave power	100 W
Growth rate	~17 Å/min

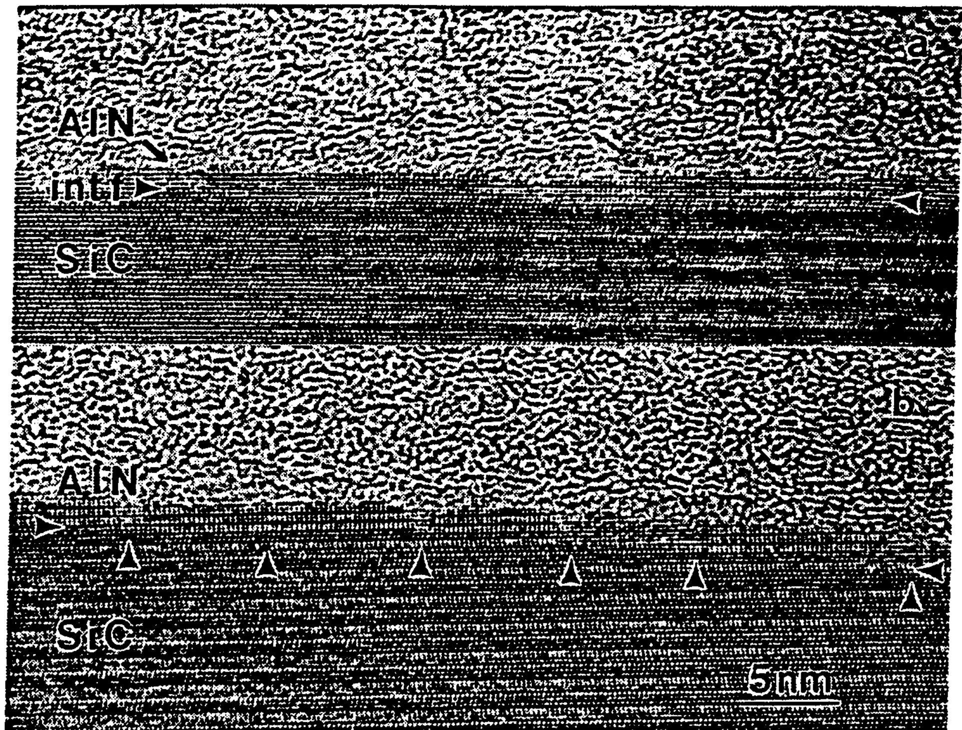

Figure 1. Cross-sectional TEM images of AlN films grown on (a) on-axis and (b) vicinal α(6H)-SiC substrates. The arrows shown in Fig. (b) indicate step positions in the substrate.

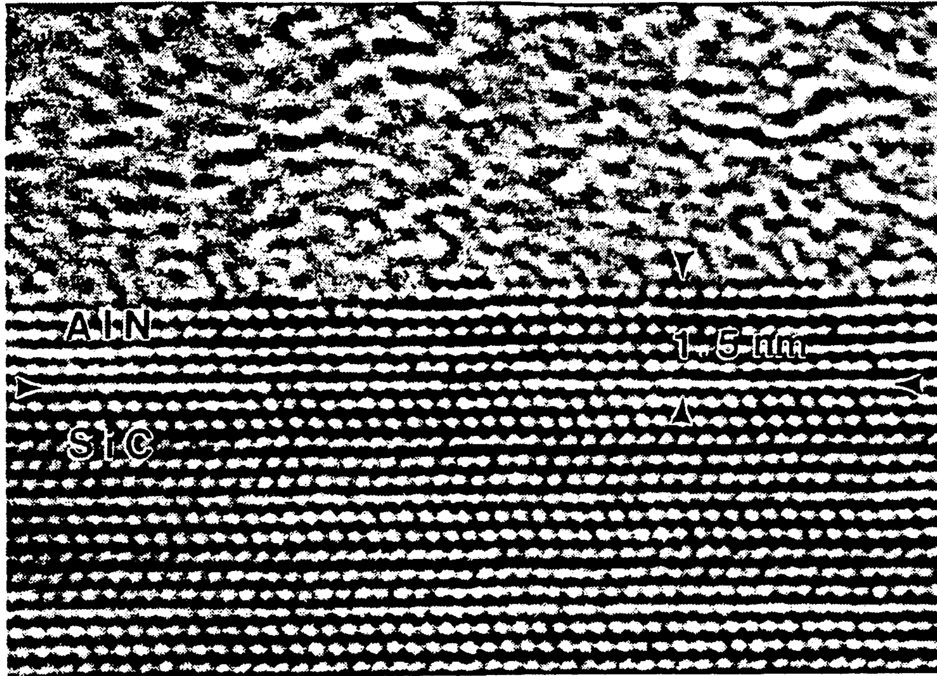

(a)

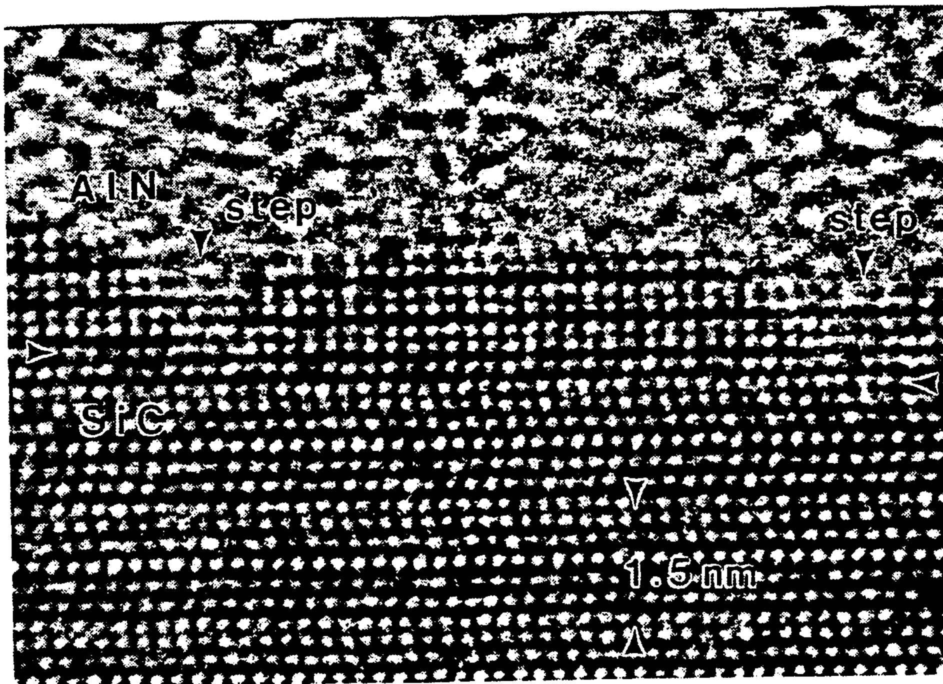

(b)

Figure 2. High resolution TEM images of AlN films and AlN/SiC interfaces of (a) on-axis substrate and (b) vicinal substrate. The arrows shown in Fig. (b) indicate the step positions.

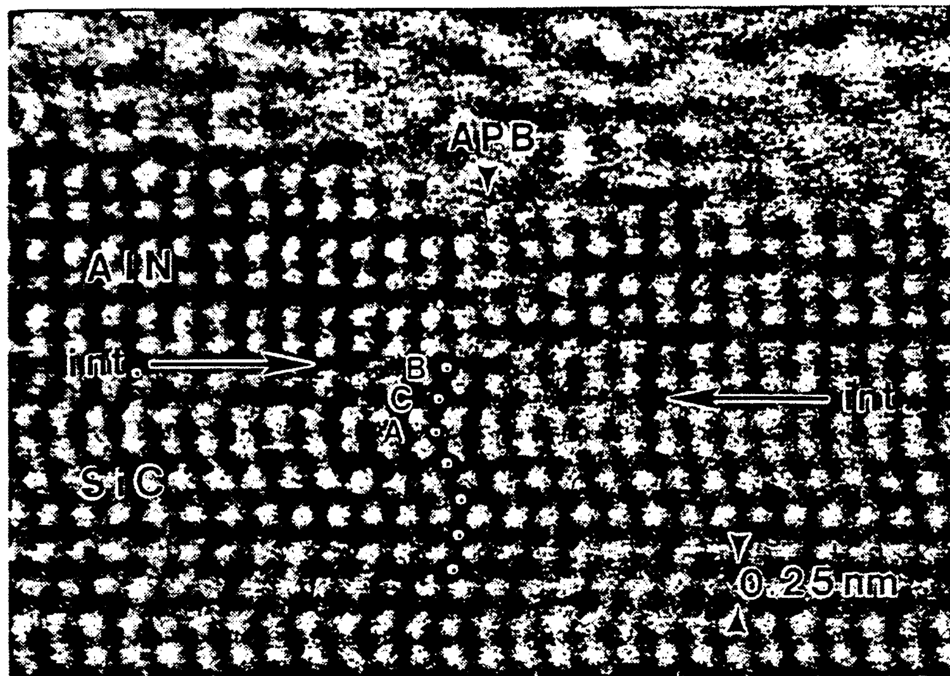

(a)

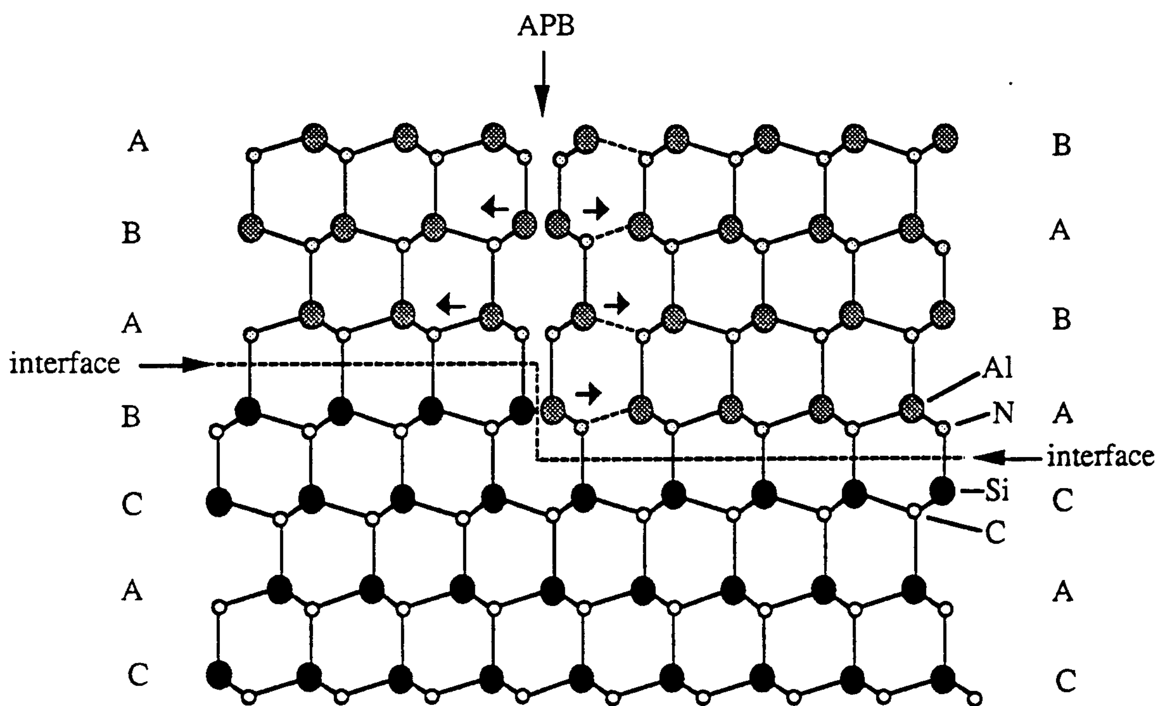

(b)

Figure 3. (a) High resolution TEM image at α(6H)-SiC step, showing the presence of an APB. The characters, BCA, and dots on the image present the stacking sequence of the 6H-SiC substrate. (b) The model of the APB based on the image in Fig. (a). The short arrows indicate the direction of lattice distortion.

V. Epitaxial growth of AlN by plasma-assisted, gas-source molecular beam epitaxy

L. B. Rowland,[a] R. S. Kern, S. Tanaka, and Robert F. Davis
Department of Materials Science and Engineering, North Carolina State University, Box 7907, Raleigh, North Carolina 27695-7907

(Received 15 December 1992; accepted 17 May 1993)

Monocrystalline AlN(0001) films with few defects were deposited on vicinal α(6H)–SiC(0001) wafers via plasma-assisted, gas-source molecular beam epitaxy within the temperature range of 1050–1200 °C. The Al was thermally evaporated from an effusion cell. An electron cyclotron resonance plasma source was used to produce activated nitrogen species. Growth on vicinal Si(100) at 900–1050 °C resulted in smooth, highly oriented AlN(0001) films.

I. INTRODUCTION

Aluminum nitride possesses a direct band gap of 6.28 eV at 300 K,[1] a melting point in excess of 2275 K,[2] and a thermal conductivity of 3.2 W/cm · K.[3] As such, it is a candidate material for high-power and high-temperature microelectronic and optoelectronic applications with the latter employment being particularly important in the ultraviolet region of the spectrum.[1] This material also has the highest reported surface acoustic wave velocity (Raleigh $V_R = 6–6.2$ km/s, $V_L = 11–12$ km/s[4–6]) for any material and a substantial electromechanical coupling coefficient (to 1%[7]). These properties strongly indicate that superior surface acoustic wave devices, operational in aggressive media and under extreme conditions both as sensors for high temperatures and pressures and as acousto-optic devices, can be developed.[8–10] However, progress regarding these (and other) applications is hampered by the lack of good single crystal material. The primary objective of the research reported below has been to address this issue via the fabrication of thin films of this material via molecular beam epitaxy (MBE) techniques.

In previous studies, mono- and polycrystalline films of AlN have been grown by chemical vapor deposition (CVD) using NH_3 and $Al(CH_3)_3$ or $AlCl_3$ on α(6H)–SiC,[11] sapphire,[1,9,12] and Si.[13–15] Chu *et al.*[11] obtained smooth monocrystalline AlN layers to a thickness of 25 μm on α(6H)–SiC{0001} substrates by CVD from 1200–1250 °C. A high density of defects in these AlN films was revealed by chemical etching. In general, films grown on sapphire and Si substrates possessed a much rougher morphology than those grown on α(6H)–SiC. This occurred very likely because the difference in lattice parameters between AlN and SiC is substantially less than between AlN and sapphire or AlN and Si.

Gas-source MBE using electron beam evaporated Al and NH_3 (Ref. 16) or thermally evaporated Al and plasma-derived activated nitrogen species[17] has also been used for single crystal AlN growth. Yoshida *et al.*[16] obtained single crystal AlN using an Al effusion cell and NH_3 at 1000–1200 °C on Si(111) and Al_2O_3(0001) and (01$\bar{1}$2) and obtained growth rates of up to 1 μm/h. They contended that their films were much smoother than CVD-grown material and rivaled bulk single crystal AlN. Sitar *et al.*[17] used an electron cyclotron resonance (ECR) plasma for decomposition of N_2 and Al and Ga effusion cells for growth of AlN/GaN superlattices by plasma-assisted, gas-source (PAGSMBE) on α(6H)–SiC(0001) and Al_2O_3(0001) at 600 °C. The thickness range of the AlN layers was 0.5–20 nm, as determined by cross-sectional transmission electron microscopy (TEM). However, the properties of the individual AlN layers were not examined.

II. EXPERIMENTAL

The approach taken in the present research has also been to use PAGSMBE to achieve surface reactions involving only Al and N in order to minimize the potential for unintentional impurity contamination from the p- and n-type dopants of C and O, respectively. The AlN films were grown on vicinal Si(100) wafers oriented 3.5 ± 0.5° toward [011] at 900–1050 °C and vicinal α(6H)–SiC(0001) oriented 3–4° toward [11$\bar{2}$0] at 1050–1200 °C in a PAGSMBE system described previously.[18] These temperatures are higher than necessary for the formation of single crystal AlN. However, they were employed to match the growth temperatures previously determined to be necessary to achieve single crystal films of SiC on Si(100)[18–20] and α(6H)–SiC(0001) substrates.[21,22]

[a]Present address: Naval Research Laboratory, Code 6861, 4555 Overlook Avenue, SW, Washington, DC 20375-5320.

 © 1993 Materials Research Society

Silicon(100) substrates were chemically cleaned using the following steps: (1) H_2SO_4 at 70 °C for 5 min, (2) de-ionized water for 1 min, (3) 1 : 1 solution (by volume) of NH_4OH and 50% H_2O_2 at 70 °C for 5 min, (4) de-ionized water for 1 min, (5) dip in 10% HF at room temperature, and (6) 2 min rinse in de-ionized water. Silicon carbide substrates were subjected only to cleaning steps (5) and (6) prior to introduction into the growth system. Thermal desorption of all substrates was also conducted at the growth temperature for 5 min prior to deposition to remove any remaining hydrocarbon and/or oxide contamination. An effusion cell was used for the evaporation of Al (99.999% pure). Reactive nitrogen species were produced via decomposition of N_2 (99.999% pure) in a compact electron cyclotron resonance (ECR) plasma source (Applied Science and Technology, Inc.). The pressure of the introduced N_2 was $1.2–1.5 \times 10^{-4}$ Torr. The microwave power supplied to the ECR was 100 W for all depositions.

The crystallography and surface character of the films were initially studied *in situ* using reflection high-energy electron diffraction (RHEED). The microstructure of the final growth surface was investigated using field-emission scanning electron microscopy (SEM). The orientation of the films grown on Si was determined via x-ray diffraction. A more in-depth examination of the crystallinity and the nature and distribution of the line and planar defects in films deposited on 6H–SiC was conducted using high-resolution transmission electron microscopy (HRTEM). The composition of the films, including any significant impurities, was determined using an Auger electron microprobe.

III. RESULTS AND DISCUSSION

Figure 1 shows the RHEED patterns ($[2\bar{1}\bar{1}0]$ azimuth) of AlN films grown on the 6H–SiC(0001) substrates at (a) 1200 °C, (b) 1100 °C, and (c) 1050 °C. These patterns indicate that all the films possess the wurtzite structure and are monocrystalline.

The growth rate versus temperature was essentially constant for a given Al flux. Conversely, changes in the AlN growth rate corresponded directly to changes in the Al flux. A constant Al source temperature and, consequently, a constant Al flux were used at the three temperatures of growth. An excess of activated nitrogen was present under all conditions. A constant growth rate of $\approx$0.40 nm/min was obtained at these temperatures.

Scanning Auger analysis of these films detected only Al and N except in a 2 nm surface region where the native oxide (and very likely the hydroxide) had formed during exposure to air. The stoichiometry of these films

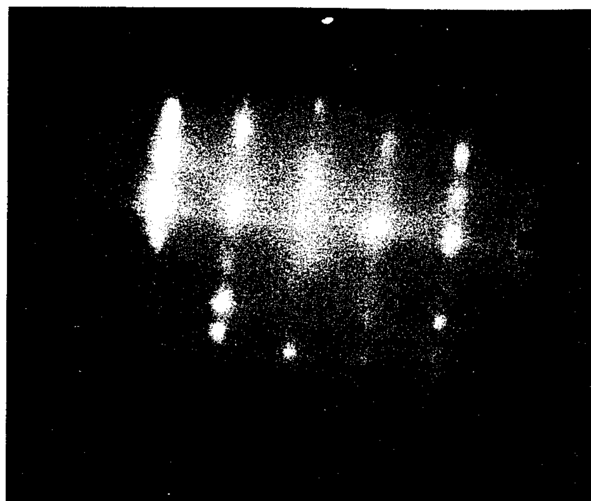

(a)

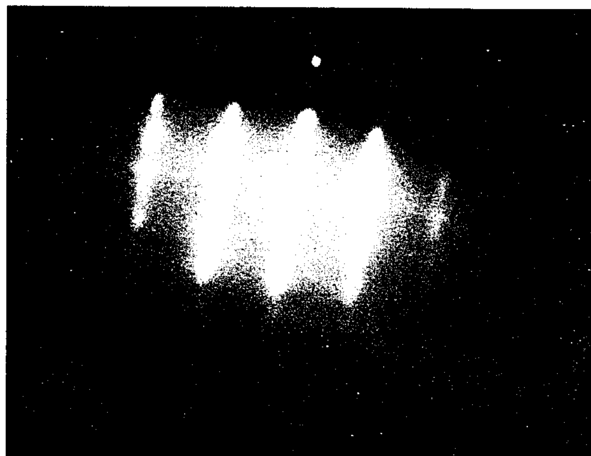

(b)

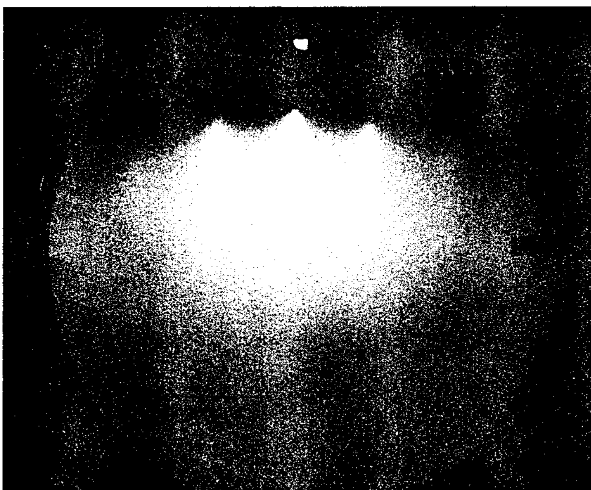

(c)

FIG. 1. RHEED patterns ($[11\bar{2}0]$ azimuth) of AlN grown on vicinal 6H–SiC(0001) at (a) 1200 °C, (b) 1100 °C, and (c) 1050 °C.

was very close to that obtained from analysis of high-purity, hot-pressed polycrystalline AlN. Figure 2 shows a HRTEM image of a thin AlN layer deposited on the 6H–SiC at 1200 °C. The top surface of the AlN is rough. Few defects are visible away from the interface. At the 2H–AlN/6H–SiC interface, however, strain contrast as evidenced by distortion in the lattice fringes can be seen (denoted by arrows in Fig. 2).

A further reduction in temperature to 1050 °C also resulted in the deposition of single crystal AlN films [as indicated in Fig. 1(c)] having an abrupt interface with the SiC substrates, but with a much smoother final surface, as shown in the SEM micrograph of Fig. 3. This essentially featureless microstructure supports the RHEED results. The surface morphology was difficult to observe at much higher magnifications in the SEM due to the insulating nature of both AlN and the SiC substrate. Figure 4 shows a HRTEM image of a film grown at 1050 °C capped by a monocrystalline, cubic (zinc blende structure) β–SiC(111) film grown in the same experiment. The smooth AlN surface and the abrupt junction with the β–SiC are apparent. Dislocations in the AlN films occurred at surface steps in the 6H–SiC substrate and may be observed in Fig. 4 (see arrow). No other defects were observed in this material. The use of nominally on-axis 6H–SiC substrates with widely spaced steps will be studied in the near future to reduce the defects present in these films.

Figure 5 shows RHEED patterns of AlN layers deposited at 900 and 1050 °C on Si(100) substrates. These films have the wurtzite structure and are very well oriented. There is only a small amount of angular spread in the spots, which implies that the films have a small nonepitaxial component. An x-ray diffraction scan of the film grown at 1050 °C is shown in Fig. 6.

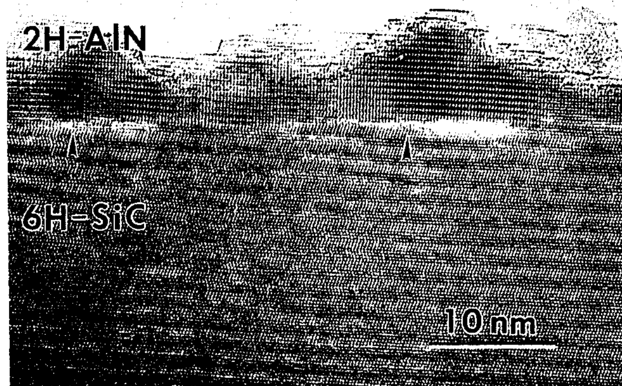

FIG. 2. HRTEM micrograph of AlN film grown at 1200 °C on vicinal 6H–SiC(0001). Arrows point to areas of lattice distortion in the lattice fringes of the AlN.

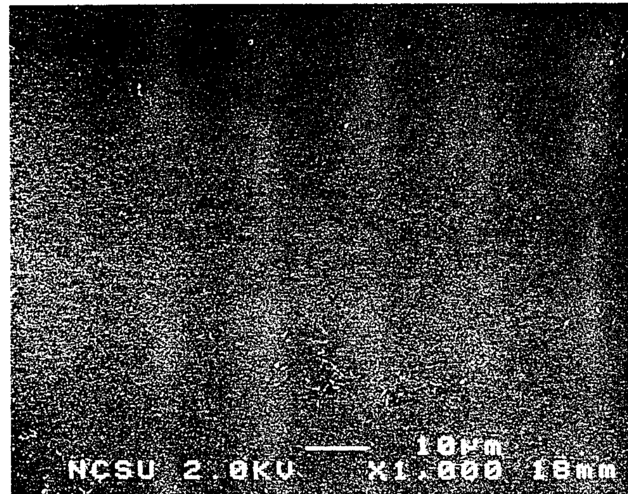

FIG. 3. SEM micrograph of the surface morphology of an AlN film grown on vicinal 6H–SiC(0001) at 1050 °C.

The single AlN(0002) peak supports the RHEED results regarding orientation. The AlN, therefore, grows with the closest packed plane parallel to the nonclosest packed (100) plane in the Si substrate. Figure 7 shows a SEM micrograph of the grown surface at 1050 °C.

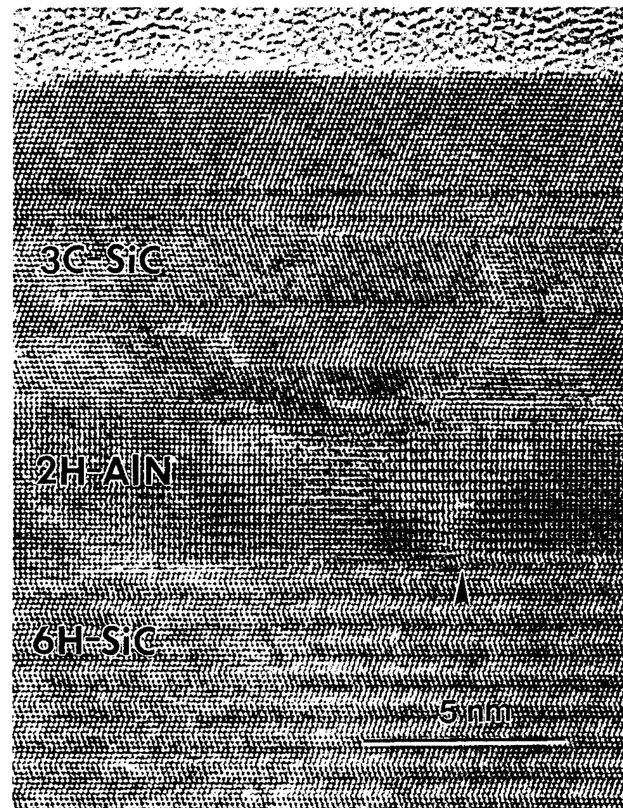

FIG. 4. HRTEM micrograph of AlN film grown at 1050 °C on vicinal 6H–SiC(0001). Layer above AlN layer is 3C–SiC also grown at 1050 °C using gas-source MBE. Arrow points to dislocation in the AlN film at a step on the 6H–SiC surface.

(a)

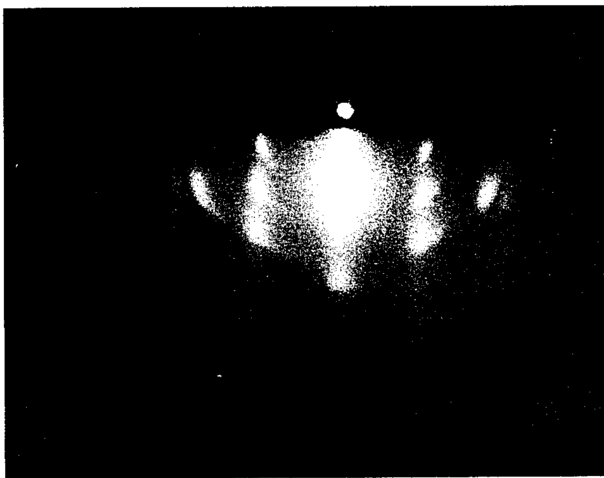

(b)

FIG. 5. RHEED patterns ([11$\bar{2}$0] azimuth) of AlN films grown on vicinal Si(100) at (a) 900 °C and (b) 1050 °C.

The film is smooth except for occasional small elongated depressions in the surface. The reason for these features has not been determined; however, they may be due to pitting of the Si surface before AlN growth. These films were extremely smooth when compared to those grown by CVD.[13–15]

An orientation of AlN, such as (10$\bar{1}$0), is more likely than (0001) on Si(100), based on crystallographic considerations. The latter orientation of AlN would be expected on Si(111), as the closest-packed (0001) planes of AlN contain the same general atomic arrangement. Previous reports of AlN on Si(100) are inconsistent with regard to orientational relationships. Several researchers have used trimethyaluminum and NH_3 in CVD growth on on-axis Si(100) substrates. Morita *et al.*[13] deposited single crystal AlN(0001) on Si(100) at 1260 °C. Yu

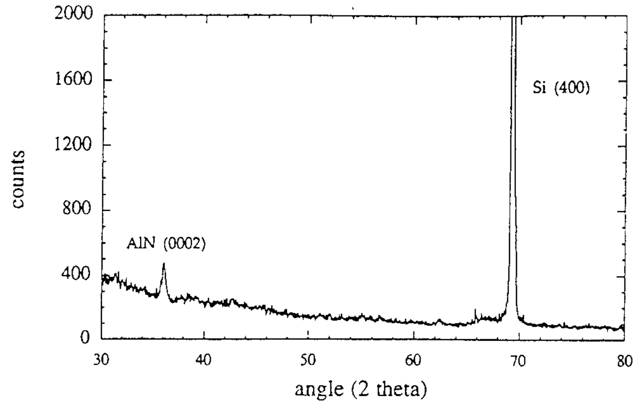

FIG. 6. X-ray diffraction spectrum (Cu K_α) of AlN film on vicinal Si(100) at 1050 °C.

et al.[14] grew epitaxial AlN(10$\bar{1}$0) on Si(100) at temperatures as low as 400 °C. Roughening and pitting of the Si surface has been observed at temperatures as low as 800 °C.[23] Thus, the roughness of the Si surface is likely to be more severe at 1260 °C than at 400 °C due to the evaporation of the oxide and the greater surface mobility at the higher temperature. This degradation of the surface may also explain why the films grown as a part of this study were AlN(0001) rather than AlN(10$\bar{1}$0).

IV. CONCLUSIONS

In summary, monocrystalline AlN films were grown on vicinal α(6H)–SiC(0001) at 1050–1200 °C using thermally evaporated Al and ECR plasma decomposed N_2. The surfaces of the films formed at 1200 °C were rough. Films grown at 1050 °C were much smoother and formed an abrupt interface with the substrate. These latter films were of excellent microstructural quality when compared to those grown by CVD and reported

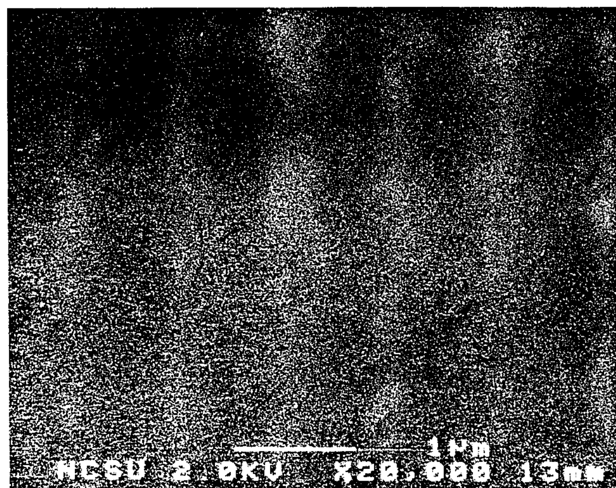

FIG. 7. Scanning electron micrograph of surface morphology of AlN grown on vicinal Si(100) at 1050 °C.

in the literature. Highly oriented AlN(0001) films with a very smooth surface morphology were also formed on vicinal Si(100) at 1050 °C. This c-axis alignment is believed to be caused by the roughness and pitting in the Si surface at the elevated growth temperatures. Doping with candidate n- and p-type impurities and the determination of the resultant properties of the AlN films will be investigated in the near future.

ACKNOWLEDGMENTS

The authors acknowledge the support of this research by the Office of Naval Research under Grant No. N00014-90-J-1427. We also express our appreciation to Applied Science and Technology (ASTeX), Inc., Woburn, MA, for the ECR source, to Cree Research, Inc., Durham, NC, for the vicinal α(6H)–SiC substrates, and to Ms. S. Rogers for the Auger analysis.

REFERENCES

1. W. M. Yim, E. J. Stofko, P. J. Zanzucchi, J. I. Pankove, M. Ettenberg, and S. L. Gilbert, J. Appl. Phys. **44**, 292 (1973).
2. M. G. Norton, B. C. H. Steele, and C. A. Leach, Science Ceram. **14**, 545 (1988).
3. G. A. Slack, J. Phys. Chem. Solids **34**, 321 (1973).
4. M. Kitayama, T. Fukui, T. Shiosaki, and A. Kawabata, Jpn. J. Appl. Phys. **22**, 139 (1982).
5. G. R. Kline and K. M. Lakin, Proc. IEEE Symp. Ultrasonics **14**, 495 (1983).
6. K. Tsubouchi, K. Sugai, and N. Mikoshiba, Proc. IEEE Symp. Ultrasonics **14**, 340 (1983).
7. M. Sano and M. Aoki, Oyo Butsuri **52**, 374 (1983).
8. J. K. Liu, K. M. Lakin, and K. L. Wang, J. Appl. Phys. **46**, 3703 (1975).
9. M. Morita, N. Uesugi, S. Isogai, K. Tsubouchi, and N. Mikoshiba, Jpn. J. Appl. Phys. **20**, 17 (1981).
10. G. D. O'Clock, Jr. and M. T. Duffy, Appl. Phys. Lett. **23**, 55 (1973).
11. T. L. Chu, D. W. Ing, and A. J. Noreika, Solid-State Electron. **10**, 1023 (1967).
12. H. M. Manasevit, F. M. Erdmann, and W. I. Simpson, J. Electrochem. Soc. **118**, 1864 (1971).
13. M. Morita, S. Isogai, N. Shimizu, K. Tsubouchi, and N. Mikoshiba, Jpn. J. Appl. Phys. **20**, L173 (1981).
14. Z. J. Yu, J. H. Edgar, A. U. Ahmed, and A. Rys, J. Electrochem. Soc. **138**, 196 (1991).
15. A. J. Noreika and D. W. Ing, J. Appl. Phys. **19**, 5578 (1968).
16. S. Yoshida, S. Mizawa, Y. Fujii, S. Takada, H. Hayakawa, S. Gonda, and A. Itoh, J. Vac. Sci. Technol. **16**, 990 (1979).
17. Z. Sitar, M. J. Paisley, B. Yan, R. F. Davis, J. Ruan, and J. W. Choyke, Thin Solid Films **200**, 311 (1991).
18. L. B. Rowland, R. S. Kern, S. Tanaka, and R. F. Davis, in *Proc. 4th Int. Conf. Amorphous and Crystalline Silicon Carbide,* edited by C. Y. Yang, M. M. Rahman, and G. L. Harris (Springer-Verlag, Berlin, 1992), p. 84.
19. S. Kaneda, Y. Sakamoto, C. Nishi, M. Kanaya, and S. Hannai, Jpn. J. Appl. Phys. **25**, 1307 (1986).
20. T. Sugii, T. Aoyama, and T. Ito, J. Electrochem. Soc. **137**, 989 (1990).
21. L. B. Rowland, R. S. Kern, S. Tanaka, and R. F. Davis (unpublished research).
22. T. Yoshinobu, H. Mitsui, I. Izumikawa, T. Fuyuki, and H. Matsunami, Appl. Phys. Lett. **60**, 824 (1992).
23. D. J. Robbins, A. J. Pidduck, A. G. Cullis, N. G. Chew, R. W. Hardeman, D. B. Gasson, C. Pickering, A. C. Daw, M. Johnson, and R. Jones, J. Cryst. Growth **81**, 421 (1987).

VI. Aluminum nitride/silicon carbide multilayer heterostructure produced by plasma-assisted, gas-source molecular beam epitaxy

L. B. Rowland,[a] R. S. Kern, S. Tanaka, and Robert F. Davis
Department of Materials Science and Engineering, North Carolina State University, Raleigh, North Carolina 27695-7907

(Received 9 December 1992; accepted for publication 2 April 1993)

Pseudomorphic structures containing β(3C)-SiC and 2H-AlN have been grown on vicinal α(6H)-SiC(0001) at 1050 °C by plasma-assisted, gas-source molecular beam epitaxy. Reflection-high energy electron diffraction and cross-sectional high-resolution transmission electron microscopy showed all layers to be monocrystalline. The AlN layers were uniform in thickness. Defects in these layers initiated at steps on the 6H-SiC film. The 3C-SiC layers contained a high density of stacking faults and microtwins caused primarily by the interfacial stresses generated by the mismatch in lattice parameters between AlN and β-SiC coupled with the very low stacking fault energy of SiC. This is the first report of the deposition of single crystal SiC/AlN/SiC thin film heterostructures on any substrate as well as the first report of the epitaxial growth of single crystal layers of binary materials with three different crystal structures.

Interest in wide band gap semiconductors for high-temperature and high-power electronic and short-wavelength optoelectronic applications has increased markedly within the past several years. Two materials which have generated much interest in this regard are SiC and AlN. The former occurs in over 250 polytypes, each of which possesses an indirect band gap. The most common of these polytypes are the cubic 3C (or β) and the hexagonal 6H, with band gaps of 2.28 and 3.0 eV at 25 °C, respectively.

Aluminum nitride has considerable potential for electronic and ultraviolet optoelectronic applications, particularly in severe environments, due to its large, direct band gap (6.28 eV at 25 °C), high melting point (in excess of 2000 °C), high thermal conductivity (3.2 W/cm K), and low dielectric constant ($\epsilon=9.0$). It typically forms in the wurtzite (2H) structure; however, the cubic, zincblende (3C) phase has been produced.[1,2]

Epitaxial AlN has been deposited previously on SiC substrates.[3-5] Chu *et al.*[3] obtained monocrystalline AlN up to 25 μm thick on hexagonal SiC {0001} substrates by chemical vapor deposition (CVD) from 1200 to 1250 °C. Sitar *et al.*[4] used an electron cyclotron resonance (ECR) plasma to decompose into N_2 and Al and Ga effusion cells to grow AlN/GaN superlattices by plasma-assisted, gas-source molecular beam epitaxy (MBE) (PAGSMBE) on α(6H)-SiC(0001) and Al_2O_3(0001) at 600 °C. Yoshida *et al.*[5] on Si(111) and Al_2O_3(0001) and (01$\bar{1}$2) at 1000–1200 °C were much smoother than CVD-grown material and rivaled bulk single crystal AlN. Conversely, Rutz and Cuomo[6] reported the deposition of monocrystalline SiC on a single crystal AlN film by pyrolysis of a SiC target at 1860 °C. The AlN substrate was formed at 1000 °C by reactive rf sputtering on a W(111) single crystal. However, thin-film growth of AlN/SiC/AlN or SiC/AlN/SiC heterostructures has not been reported to date.

Stable pseudomorphic heterostructures of AlN and SiC are feasible because of their similar crystal structure, lattice parameter, and thermal expansion behavior. Theory regarding the electronic structure and bonding at SiC/AlN interfaces has been developed.[7] Critical layer thicknesses prior to misfit dislocation formation at pseudomorphic interfaces of cubic AlN and cubic SiC have been calculated.[8] Superlattices would have a different band structure than either constituent because the Brillouin zone is reduced in the direction normal to the interfaces, and certain superlattice states occur at different points in k space than the corresponding bulk material.[9]

In the present research multiple layers of AlN and SiC were grown using a specially designed PAGSMBE system.[10] The precursors used for Si and C were Si_2H_6 and C_2H_4 (both 99.99% pure). Solid Al (99.999% pure) was evaporated from a standard effusion cell. Nitrogen was obtained by ECR plasma decomposition of N_2 (99.9995% pure). The system base and working pressures were 10^{-9} and 3×10^{-5} Torr, respectively. Vicinal 6H-SiC(0001) wafers oriented 3°–4° towards [11$\bar{2}$0] and containing a 0.8 μm epitaxial 6H-SiC layer deposited via CVD and thermally oxidized to a depth of 50 nm to aid in wafer cleaning were obtained from Cree Research, Inc. and used as substrates in this research. These substrates were chemically cleaned in 10% HF solution for 5 min to remove the oxide, rinsed in de-ionized H_2O, immediately loaded into the growth system and heated for 5 min at the growth temperature of 1050 °C. Additional growth conditions are listed in Table I. Figure 1 shows a typical plot of composition versus depth for a SiC/AlN multilayer heterostructure.

Reflection high-energy electron diffraction (RHEED) was used as an indicator of the quality and crystal structure of the resultant films. Figure 2 shows representative RHEED patterns for (a) the final growth surfaces of the films of AlN ([10$\bar{1}$0] azimuth) and (b) SiC ([110] azimuth). These patterns also show that both films were monocrystalline with the AlN having the 2H structure and

[a]Present address: Naval Research Laboratory, Code 6861, 4555 Overlook Ave., SW, Washington, DC 20375-5320.

 © 1993 American Institute of Physics

TABLE I. Growth conditions for the AlN and SiC layers.

AlN	
Nitrogen flow rate	8 sccm
Microwave power	100 W
Growth rate	26 nm/h
SiC	
Disilane flow rate	0.10 sccm
Ethylene flow rate	0.20 sccm
Growth rate	6.2 nm/h

the SiC the 3C modification, as indicated by the azimuthal assignments. The RHEED pattern in Fig. 2(b) of the top SiC layer also contains additional spots and is fully indexed in Fig. 3. It is probable that these extra spots arise from double positioning boundaries (DPBs). These incoherent twin boundaries occur when 3C-SiC(111) is grown on Si(111)[11] or on-axis 6H-SiC[12] because two different orientations, rotated 60° from each other, are present which have close-packed directions aligned in the interface. These different orientations differ in the cubic stacking sequence. One orientation has an ···ABCABC··· stacking sequence; the other, ···ACBACB··· . Extra reflections in the [110] RHEED pattern due to double positioning twins would either coincide with those of the film or be displaced by 1/3[111]. The extra spots are shown in Fig. 3.

An equivalent interpretation of the RHEED pattern shown in Fig. 2(b) is of two interpenetrating [110] RHEED patterns with a misorientation of 180°. This misorientation is caused by reflections from regions with both stacking sequences. The effect is shown in Fig. 4.

Figure 5 shows a representative high-resolution transmission electron microscopy (HRTEM) image of the off-axis 6H-SiC(0001) substrate, the 2H-AlN layer, and the 3C-SiC layer. The AlN film has an abrupt interface with the SiC substrate and a smooth, uniform surface. The 2H-AlN and 6H-SiC films are identically orientated in all directions, and the alignment of the atom columns is continuous across the interface. Thus, the AlN film is both epitaxial and pseudomorphic with respect to the substrate. Strain contrast, as evidenced by distortion in the lattice fringes, can be seen near steps in the SiC substrate surface,

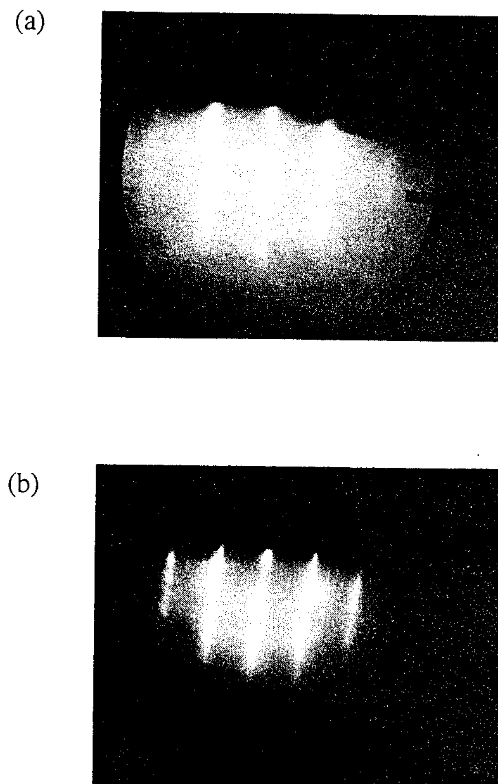

FIG. 2. (a) RHEED pattern ([10$\bar{1}$0] azimuth) of the final surface of a monocrystalline 2H-AlN layer grown on α(6H)-SiC epitaxial layer. (b) RHEED pattern ([110] azimuth) of the final surface of a monocrystalline 3C-SiC layer grown on 2H-AlN film.

as denoted by arrows in Fig. 5. Dislocations running parallel to the surface which arise from this strain can also be observed at or near each step.

The interface between the AlN and the top 3C-SiC layer is also abrupt, though some regions exist for which

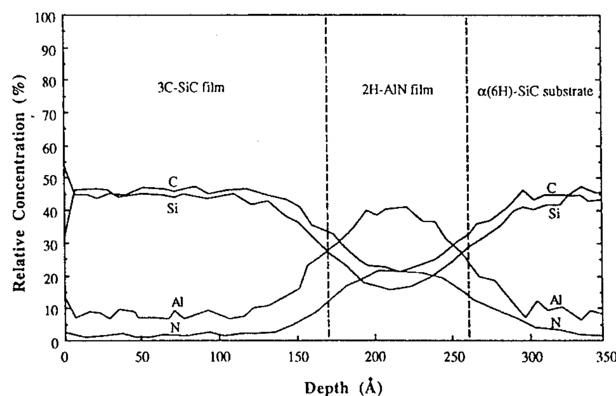

FIG. 1. Auger depth profile of representative SiC/AlN/SiC multilayer heterostructure.

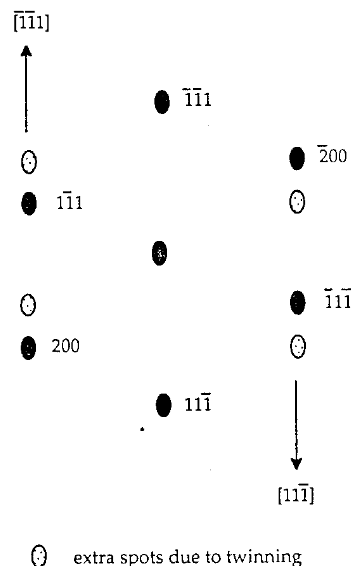

FIG. 3. Indexed RHEED pattern ([110] azimuth) of 3C-SiC layer shown in Fig. 2(b). Lighter spots are twin spots caused by DPBs.

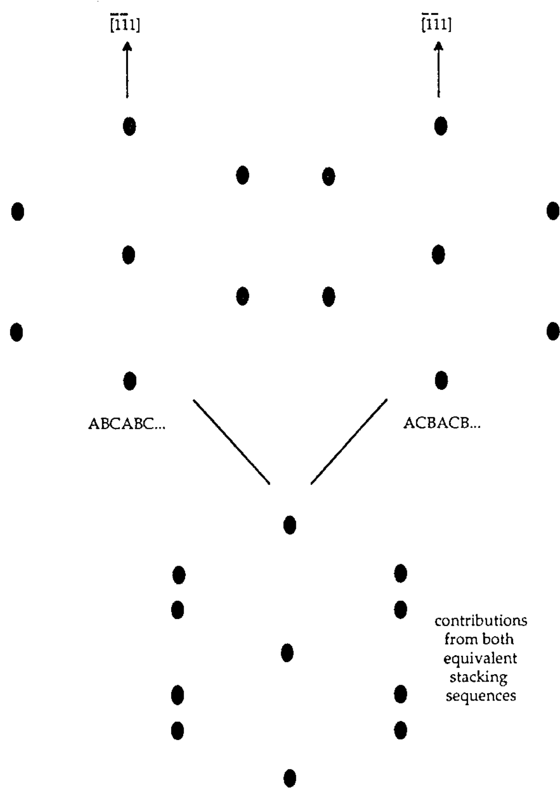

FIG. 4. Effect of two equivalent stacking sequences of 3C-SiC(111) on [110] azimuth RHEED pattern.

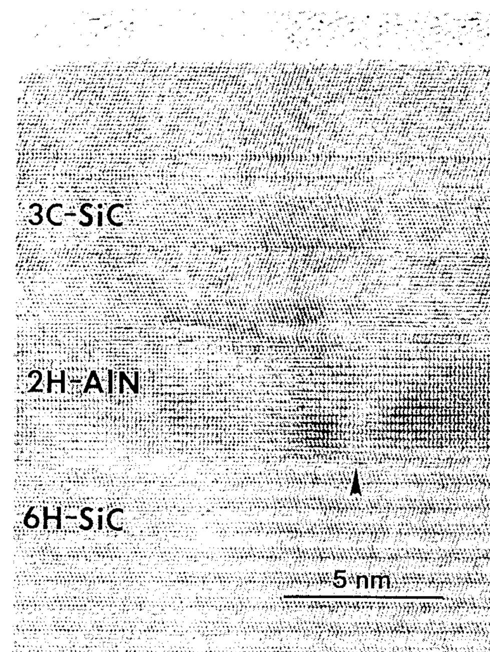

FIG. 5. High-resolution transmission electron micrograph of epitaxial, pseudomorphic SiC/AlN/SiC multilayer heterostructure. Arrow shows a position of lattice distortion in the AlN associated with steps contained in and dislocations running parallel to the SiC surface.

the transition between AlN and SiC becomes indiscernible. The lattice images show that the SiC layer is cubic as well as epitaxial and pseudomorphic with the AlN. Several ⟨111⟩ stacking faults can be seen in this layer.

Previous PAGSMBE growth in this research of SiC on similar substrates at 1000–1050 °C also resulted in 3C-SiC(111). This result, combined with those noted above, suggest that the cubic polytype forms preferentially at these temperatures under the conditions used in MBE. However, growth of SiC/AlN heterostructures at higher temperatures may result in hexagonal SiC layers, as atomic mobility on the AlN surface increases and the steps rather than the terraces become the templates for layer-by-layer growth. A trend towards the deposition of hexagonal SiC films at higher temperatures has been reported by several investigators.[12–14] It is also under study in the authors' laboratory and will be reported in the near future.

In summary, thin-film heterostructures composed of 3C-SiC, 2H-AlN, and 6H-SiC have been achieved. The 3C-SiC and the AlN layers were grown at 1050 °C using PAGSMBE. RHEED and cross-sectional HRTEM showed both of these layers to exist in an epitaxial and pseudomorphic relationship with each other and with the 6H-SiC homoepitaxial layer deposited by CVD. To the authors' knowledge, this is the first report and direct observation of a single crystal SiC/AlN/SiC heterostructure on any substrate. It is also the first known report of the single-crystal growth of layers of binary materials in three different crystal structures (the 6H-SiC epilayer on the SiC wafer is counted in this case). These unique structures, composed of direct (AlN) and indirect (SiC) wide band gap semiconductor materials undoubtedly possess important electronic, mechanical and thermal properties which are under investigation by the authors at this time.

The authors express their appreciation to the Office of Naval Research for support of this research under Grant No. N00014-90-J-1427, to Cree Research, Inc. for the vicinal 6H-SiC wafers and epilayers and to Applied Science and Technology, Inc. for supplying the ECR plasma source. Appreciation is also expressed to S. Rogers for the Auger chemical analysis.

[1] Z. Sitar, Ph.D dissertation, North Carolina State University, 1990.
[2] S. Strite and H. Morkoç (private communication).
[3] T. L. Chu, D. W. Ing, and A. J. Norieka, Solid-State Electron. **10**, 1023 (1967).
[4] Z. Sitar, M. J. Paisley, B. Yan, R. F. Davis, J. Ruan, and J. W. Choyke, Thin Solid Films **200**, 311 (1991).
[5] S. Yoshida, S. Mizawa, Y. Fujii, S. Takada, H. Hayakawa, S. Gonda, and A. Itoh, J. Vac. Sci. Technol. **16**, 990 (1979).
[6] R. F. Rutz and J. J. Cuomo, in *Silicon Carbide-1973* (University of South Carolina Press, Columbia, 1974), p. 72.
[7] W. R. L. Lambrecht and B. Segall, Phys. Rev. B **43**, 7070 (1991).
[8] M. E. Sherwin and T. J. Drummond, J. Appl. Phys. **69**, 8423 (1991).
[9] G. C. Osbourn, J. Vac. Sci. Technol. B **1**, 379 (1983).
[10] L. B. Rowland, R. S. Kern, S. Tanaka, and R. F. Davis, in *Proceedings of the Fourth International Conference on Amorphous and Crystalline Silicon Carbide*, edited by C. Y. Yang, M. M. Rahman, and G. L. Harris (Springer, Berlin, 1992), p. 84.
[11] I. H. Khan and R. N. Summergrad, Appl. Phys. Lett. **11**, 12 (1967).
[12] H. S. Kong, B. L. Jiang, J. T. Glass, G. A. Rozgonyi, and K. L. More, J. Appl. Phys. **63**, 2645 (1988).
[13] R. B. Campbell and T. L. Chu, J. Electrochem. Soc. **113**, 825 (1966).
[14] V. J. Jennings, A. Sommer, and H. C. Chang, J. Electrochem. Soc. **113**, 728 (1966).

VII. Solid solutions of AlN and SiC grown by plasma-assisted, gas-source molecular beam epitaxy

R. S. Kern, L. B. Rowland,[a] S. Tanaka, and R. F. Davis
Department of Materials Science and Engineering, North Carolina State University, Box 7907, Raleigh, North Carolina 27695-7907

(Received 16 November 1992; accepted 26 February 1993)

Solid solutions of aluminum nitride (AlN) and silicon carbide (SiC), the only intermediate phases in their respective binary systems, have been grown at 1050 °C on α(6H)–SiC(0001) substrates cut 3–4° off-axis toward [11$\bar{2}$0] using plasma-assisted, gas-source molecular beam epitaxy. A film having the approximate composition of $(AlN)_{0.3}(SiC)_{0.7}$, as determined by Auger spectrometry, was selected for additional study and is the focus of this note. High resolution transmission electron microscopy (HRTEM) revealed that the film was monocrystalline with the wurtzite (2H) crystal structure.

Silicon carbide is a wide band gap material that exhibits polytypism, a one-dimensional polymorphism arising from the various possible stacking sequences of, e.g., the silicon and carbon layers along the directions of closest packing. The single cubic polytype, β–SiC, crystallizes in the zinc blende structure, has a room temperature band gap of 2.3 eV, and is commonly referred to as 3C–SiC. In the Ramsdell notation, the three (3) refers to the number of Si and C bilayers necessary to produce a unit cell and the C indicates its cubic symmetry. There are approximately 250 other rhombohedral and hexagonal polytypes[1] that are classed under the heading of α–SiC. The most common of these latter polytypes is 6H–SiC, with a room temperature band gap of ≈3.0 eV.

Aluminum nitride normally occurs in the wurtzite (2H) structure; however, the cubic, zinc blende phase has been produced.[2,3] The 2H polytype possesses a direct band gap[4] and a thermal conductivity[5] of 6.28 eV and 3.2 W/cm · K, respectively. As such, this material is of particular interest for high power and optoelectronic devices, the latter of which would emit and absorb ultraviolet radiation.

Solid solutions of AlN and SiC have been achieved by two primary routes: reactive sintering of mixtures of powders of a variety of sources and thin film deposition from the vapor phase. Matignon[6] first reported the synthesis of an $(AlN)_x(SiC)_{1-x}$ material in 1924 formed by heating Al_2O_3, SiO_2, and coke in the presence of flowing N_2 at an unspecified temperature. Related hot pressing and annealing research coupled with x-ray diffraction and optical and electron microscopy by Rafaniello *et al.*[7,8] reportedly resulted in single phase, 2H material at all compositions hot pressed at 2300 °C, but only within the ranges of 0–15 and 75–100 wt. % AlN for samples prepared at 2100 °C and below. This latter result indicated a miscibility gap, the existence of which was subsequently confirmed by Ruh and Zangvil,[9] Zangvil and Ruh,[10–12] Kuo and Vikar,[13] and Czekaj *et al.*[14] using a variety of heat-treatment schedules. The tentative phase diagram proposed by Zangvil and Ruh[11] shows a flat miscibility gap at 1900 °C between ≈20 and 80 wt. % AlN. Above this temperature a 2H solid solution was reported from ≈20–100 wt. % AlN. From 0–20 wt. % AlN, solutions and two-phase mixtures of 6H, 4H, and 2H were observed.

Thin film solid solutions have been produced in the Soviet Union[15] via sublimation of a sintered SiC/AlN compact at ⩾2100 °C and in the United States[16] using low pressure (10–76 Torr) metal-organic chemical vapor deposition (MOCVD) and the sources of SiH_4, C_3H_8, NH_3, and $Al(CH_3)_3$ carried in H_2. The former research also showed that at $T \geqslant 2100$ °C, solid solutions having the 2H structure could be produced at compositions of AlN ⩾ 20 wt. %. By contrast, Jenkins *et al.*[16] have reported the MOCVD growth of solid solutions over the entire pseudobinary phase diagram. The composition of these films, grown from 1200–1250 °C, was strongly dependent on the system pressure, which varied from 10–76 Torr. Electron channeling patterns on selected films indicated that the films were monocrystalline. Films having cubic symmetry were obtained on Si(100) substrates; hexagonal films were deposited on α(6H)–SiC(0001) wafers.

In the present research, a specially designed and previously described[17] plasma-assisted, gas-source molecular beam epitaxy system was employed to deposit $(AlN)_x(SiC)_{1-x}$ thin film solid solutions on α(6H)–SiC(0001) substrates obtained from Cree Research, Inc.

[a]Present address: Naval Research Laboratory, Code 6861, 4555 Overlook Avenue SW, Washington, DC 20375-5000.

 © 1993 Materials Research Society

TABLE I. Growth conditions for $(AlN)_{0.3}(SiC)_{0.7}$ thin films.

Chamber base pressure	10^{-9} Torr
Deposition pressure	10^{-4} Torr
Deposition temperature	1050 °C
Flow rate (Si_2H_6)	0.75 sccm
Flow rate (C_2H_4)	3.75 sccm
Ar : N_2 ratio	20 : 1
ECR power	100 W
Aluminum cell temperature	1260 °C
Deposition time	2 h

and oriented 3.5 ± 0.5° off (0001) toward [11$\bar{2}$0]. The substrates were chemically cleaned before growth in a 10% HF solution for 5 min, followed by a de-ionized water rinse for 2 min, and loaded immediately into the growth chamber. Sources of Si and C were disilane, Si_2H_6, and ethylene, C_2H_4, respectively. Aluminum (99.999% purity) was evaporated from a standard MBE effusion cell. A compact electron cyclotron resonance (ECR) plasma source supplied by ASTeX, Inc., was used to decompose N_2 (99.9995% purity) diluted with ultrahigh purity Ar to obtain sufficient electron-atom collisions to sustain a plasma. The growth conditions for the composition chosen for additional study are listed in Table I.

Reflection high-energy electron diffraction (RHEED) was used to determine the crystalline quality of the surface of the resulting films. The chemical composition as a function of film thickness was determined using a scanning Auger microprobe with Zalar rotation capability.[18] High-resolution transmission electron microscopy (HRTEM) was employed to observe the microstructure of the film as well as the film/substrate interfacial region.

Figure 1 shows an Auger depth profile of a selected solid solution film. Use of pure AlN and SiC standards and appropriate Auger sensitivity factors for each element showed the composition to be approximately $(AlN)_{0.3}(SiC)_{0.7}$.

The RHEED pattern indicated that the film was monocrystalline. This was confirmed using HRTEM. A representative image of the film and substrate used to obtain the Auger profiles is shown in Fig. 2. The ...ABABAB... stacking sequence in the solid solution region shows that it possesses the wurtzite (2H) crystal structure. The micro-diffraction pattern shown in the inset is that of the [11$\bar{2}$0] azimuth for this structure. The random distribution of contrast is due to the elastic strain and slight buckling in the film. No second phase was observed within the film.

The resulting $(AlN)_x(SiC)_{1-x}$ thin films are, to the authors' knowledge, the first MBE grown alloys containing these components. The temperature of growth is also the lowest reported for these materials. This method of band gap engineering is particularly interesting from the standpoint of the materials involved. AlN is a direct transition material, while SiC is an indirect one. Solid solutions of the wurtzite crystal structure (2H) should have E_g from 3.33 eV to 6.28 eV. Experimental optical characterization by Nurmagomedov *et al.*[15] has indicated that the band gap is direct from 70–100 wt. % AlN. The band gap of cubic AlN has been theoretically estimated to be ≈5.11 eV at absolute zero and is believed to be indirect.[15] Therefore, cubic solid solutions should have E_g from 2.28 eV to roughly 5.11 eV and would probably be indirect at all compositions.

Epitaxial $(AlN)_x(SiC)_{1-x}$ alloys have been grown on α(6H)–SiC(0001) substrates by plasma-assisted gas-source molecular beam epitaxy at 1050 °C. The $(AlN)_{0.3}(SiC)_{0.7}$ composition was selected for additional study. Analyses by RHEED and HRTEM showed this film to be monocrystalline and to exhibit the wurtzite (2H) crystal structure. This is the first known report of a single crystal $(AlN)_x(SiC)_{1-x}$ alloy grown by MBE.

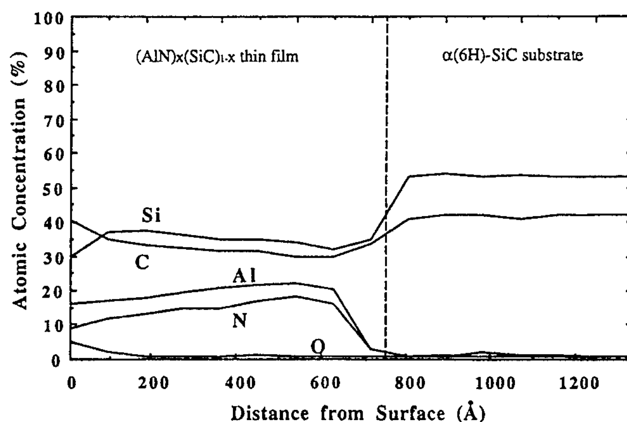

FIG. 1. Auger depth profile of an $(AlN)_x(SiC)_{1-x}$ thin film ($x \approx 0.3$) showing relative atomic concentration versus sputtering depth for each of the components. It is important to note that this film is ≈750 Å thick.

FIG. 2. High-resolution transmission electron micrograph of the 2H $(AlN)_x(SiC)_{1-x}$ thin film grown on an α(6H)–SiC(0001) substrate and used to obtain the Auger depth profile in Fig. 1. The inset shows the micro-diffraction pattern of this 2H film taken along the $[11\bar{2}0]$ zone axis.

ACKNOWLEDGMENTS

The authors acknowledge The Office of Naval Research for the sponsorship of this research under Contract No. N00014-88-K-0341, Cree Research, Inc. for the vicinal 6H–SiC substrates, Applied Science and Technology, Inc. for the ECR plasma source, R. L. Moore at Evans East for the AES analysis, and J. Bentley of Oak Ridge National Laboratories for helpful discussions. This research was also partially sponsored by the Division of Materials Sciences, United States Department of Energy, under contract DE-AC05-84OR21400 with Martin Marietta Energy Systems, Inc., and through the SHaRE Program under contract DE-AC05-76OR00033 with Oak Ridge Associated Universities.

REFERENCES

1. G. R. Fisher and P. Barnes, Philos. Mag. B **61**, 217 (1990).
2. Z. Sitar, M. J. Paisley, and R. F. Davis, Annual Progress Report, ONR Contract N00014-86-K-0686, June 1, 1989.
3. S. Strite and H. Makoç, private communication.
4. G. A. Slack, J. Phys. Chem. Solids **34**, 321 (1973).
5. W. M. Yim, E. J. Stofko, P. J. Zanzucci, J. I. Pankove, M. Ettenberg, and S. L. Gilbert, J. Appl. Phys. **44**, 292 (1973).
6. C. Matignon, C. R. Acad. Sci. **178**, 1615 (1924).
7. W. Rafaniello, K. Cho, and A. V. Vikar, J. Mater. Sci. **16**, 3479 (1981).
8. W. Rafaniello, M. R. Plinchta, and A. V. Vikar, J. Am. Ceram. Soc. **66**, 272 (1983).
9. R. Ruh and A. Zangvil, J. Am. Ceram. Soc. **65**, 260 (1982).
10. A. Zangvil and R. Ruh, Mater. Sci. Eng. **71**, 159 (1985).
11. A. Zangvil and R. Ruh, J. Am. Ceram. Soc. **71**, 884 (1988).

12. A. Zangvil and R. Ruh, in *Silicon Carbide '87* (The American Ceramic Society, Westerville, OH, 1989), pp. 63–82.
13. S. Kuo and A. V. Vikar, J. Am. Ceram. Soc. **73**, 2460 (1990).
14. C. L. Czekaj, M. L. J. Hackney, W. J. Hurley, Jr., L. V. Interrante, G. A. Sigel, P J. Schields, and G. A. Slack, J. Am. Ceram. Soc. **73**, 352 (1990).
15. Sh. A. Nurmagomedov, A. N. Pitkin, V. N. Razbegaev, G. K. Safaraliev, Yu. M. Tairov, and V. F. Tsvetkov, Sov. Phys. Semicond. **23**, 100 (1989).
16. I. Jenkins, K. G. Irvine, M. G. Spencer, V. Dmitriev, and N. Chen (in press).
17. L. B. Rowland, S. Tanaka, R. S. Kern, and R. F. Davis, in *Proceedings of the Fourth International Conference on Amorphous and Crystalline Silicon Carbide* (Springer-Verlag, Berlin, 1992), in press.
18. A. Zalar, Thin Solid Films **124**, 223 (1985).

VIII. Fabrication and Characterization of Al/AlN/SiC MIS Diodes Grown by Gas-source Molecular Beam Epitaxy

A. Introduction

Silicon carbide (SiC) is a wide bandgap material that is attractive for the fabrication of electronic devices that operate in a variety of harsh environments. Silicon carbide has a wide bandgap (≈3.0 eV at room temperature), excellent thermal stability [1-3], a high thermal conductivity (4.9 W $cm^{-1}K^{-1}$) [4], a high breakdown field (2×10^6 V cm^{-1}) [2] and a high saturated electron drift velocity (2×0^7 cm s^{-1}) [3]. In the last few years, blue light emitting diodes (LEDs), junction field effect transistors (JFETs) and metal-oxide-semiconductor field effect transistors (MOSFETs) have become commercially available. Excellent reviews of these devices have been published [5-11].

Since metal-insulator-semiconductors (MIS) structures are an important part of today's microelectronics industry, MIS diodes (using SiO_2, in particular, as the insulator) have been studied by a number of researchers. The majority of the studies have been done on 6H-SiC substrates. Although some work [12-16] has also been done on 3C-SiC, the defective nature of the material makes most of the measurements difficult to interpret since the resulting interface state densities and fixed oxide charge densities are very high. Most of this work has centered around the optimization of the oxidation both kinetically and electrically; however, the chemical character of the oxide has also been studied by Auger electron spectroscopy [17, 18] and secondary ion mass spectroscopy [16, 19, 20]. Nearly all reports (see, for example, [21]) show that the MOS diodes can be easily accumulated and depleted at room temperature; however, inversion cannot be obtained using typical testing procedures. The lowest reported values of fixed charge densities and interface state densities are 3×10^{11} cm^{-2} and 1.5×10^{11} cm^{-2} eV^{-1}, respectively. To date, there has only been one report [23] of a MIS diode made with an insulator other than SiO_2. In this case, Si_3N_4 was used, but had only minimal success due to very large density of defects and large leakage currents.

Aluminum nitride possesses a direct bandgap of 6.28 eV at 300 K [24], a melting point in excess of 2275 K [25], a thermal conductivity of 3.2 W cm^{-1} K^{-1} [26] and a low dielectric constant ($K_{AlN} = 8.5 \pm 0.2$) [27]. As such, it is a candidate material for high-power and high-temperature microelectronic and optoelectronic applications with the latter employment being particularly important in the ultraviolet region of the spectrum [24]. These properties strongly indicate that superior surface acoustic wave devices, operational in aggressive media and under extreme conditions both as sensors for high temperatures and pressures and as acousto-optic devices, can be developed [28-30]. However, progress regarding these (and other) applications is hampered by the lack of high-quality single crystal material.

Because of its thermal stability and wide bandgap, AlN has been investigated as a potential insulating material for Si [31-36], GaAs [35, 37-41] and InP [41, 42] based electronic device structures. Although Stevens *et al.* [43] have fabricated an operational Si-MISFET using AlN as the gate, only moderate success has been accomplished using AlN gates due to difficulties in growing high-quality films on these substrates. The purpose of this work was to study the feasibility of forming MISFET devices in SiC using AlN as the gate dielectric.

B. Experimental Procedure

Thin, epitaxial films of several thicknesses of AlN were grown on n-type (N_D-N_A $\approx 4\times10^{16}$ cm^{-3}) Si-face α(6H)-SiC(0001) substrates supplied by Cree Research, Inc. Each of the wafers contained a 0.8 μm epitaxial SiC layer deposited via CVD and a thermally oxidized 75 nm layer to aid in wafer cleaning. The surfaces were prepared by a 10% HF dip and a 10 minute anneal at 1050 °C in UHV, as well as a silane exposure and boil-off described in previous reports.

All growth experiments were carried out in the GSMBE system detailed in previous reports. Films of AlN were grown at 1100 °C. Source were aluminum (99.9999% purity), evaporated from a standard MBE effusion cell operated in all cases at 1150°C, and 7.0 sccm ammonia (99.999% pure). Typical base pressures of 10^{-9} Torr were used. Aluminum contacts (area = 4.558×10^{-3} cm^2) were deposited on the AlN by means of a standard evaporator and In-Sn solder was used as a backside contact to the SiC.

High frequency capacitance-voltage measurements were performed on samples ≈1000 Å thick using a HP 4284A LCR meter operating at 1 MHz. Samples could be tested in the dark and under illumination by a halogen lamp at temperatures up to 300 °C. The typical measurement sequence involved illuminating the sample while it is biased under depletion conditions until a stable capacitance is reached, switching the light off, sweeping the voltage from depletion into accumulation and sweeping from accumulation back to depletion. From the C-V curve and the knowledge of a few physical constants, several important parameters can be calculated.

From the C-V curve , the flat band voltage, V_{FB}, can be determined from the flat band capacitance, C_{FB}. The flat band capacitance is calculated by

$$C_{FB} = \frac{K_{AlN}\varepsilon_0}{d_{AlN} + \left(\frac{K_{AlN}}{K_{SiC}}\right)L_D} \tag{1}$$

where K_{AlN} (≈9) and K_{SiC} (≈10) are the dielectric constants of AlN and SiC, ε_0 is the permittivity of free space, d_{AlN} is the AlN thickness and L_D is the extrinsic Debye length in SiC. The Debye length can be calculated according to the relation

$$L_D^{SiC} = \sqrt{\frac{K_{SiC}\varepsilon_0 kT}{Nq^2}} \tag{2}$$

where k is Boltzmann's constant, T is temperature, N is the doping level in the SiC and q is the carrier charge.

Having determined the flat band capacitance, the flat band voltage can be read directly from the C-V curve. The deviation of this number from ideality (determined by the difference in the work functions of the Al metal and the SiC) can, in turn, be used to determine the interface charge trap density per unit area, N_t, which takes into account the density of interface states over the entire energy range of the bandgap. This density of interface charge traps can be calculated by

$$N_t = \frac{C_{AlN}^{max}}{qA}(V_{FB}-\phi_{ms}) \tag{3}$$

where C_{AlN}^{max} is the maximum capacitance of the AlN (read from the C-V curve), A is the contact area and ϕ_{ms} is the difference in the work functions of the metal (Al) and the semiconductor (SiC). Since the value of ϕ_{Al} is 4.28 V [44] and the value of ϕ_{SiC} is 4.5 V [45], ϕ_{ms} has a value of 0.22 V.

Another interesting consequence of these measurements is the ability to determine experimentally the value of the AlN dielectric constant. Knowing the thickness of the insulator, determined by HRTEM, profilometry, SEM or some other method, the AlN dielectric constant can be calculated by the following relation

$$K_{AlN} = \frac{d_{AlN}C_{AlN}^{max}}{\varepsilon_0 A}\ . \tag{4}$$

C. Results

In all cases, the diodes could be accumulated and depleted with the application of small gate voltages. However, deep depletion and inversion were not achieved in any case. Figure 1 shows a C-V curve for a typical 1000 Å sample measured at room temperature. In this particular case, where N_D-$N_A \approx 4\times10^{16}$ cm^{-3}, the Debye length can be calculated from Eq. 2 to be ≈190 Å.

Using the known data and others determined the from the graph, several other important points can be gleaned. First of all, the flat band capacitance and voltage are 310 pF and 0.7 V, respectively. Since only 0.22 V can be accounted for by the difference in the work functions of the metal (Al) and the semiconductor (SiC), the theoretical shift from flat band voltage is 0.48 V. Using Eq. 3, this translates to a density of (negatively charged) interface charge traps

of $\approx 2\times10^{11}$ cm^{-2}. From Eq. 4, the dielectric constant for AlN can be calculated to be 8.67 which fits other measured data [27] for AlN.

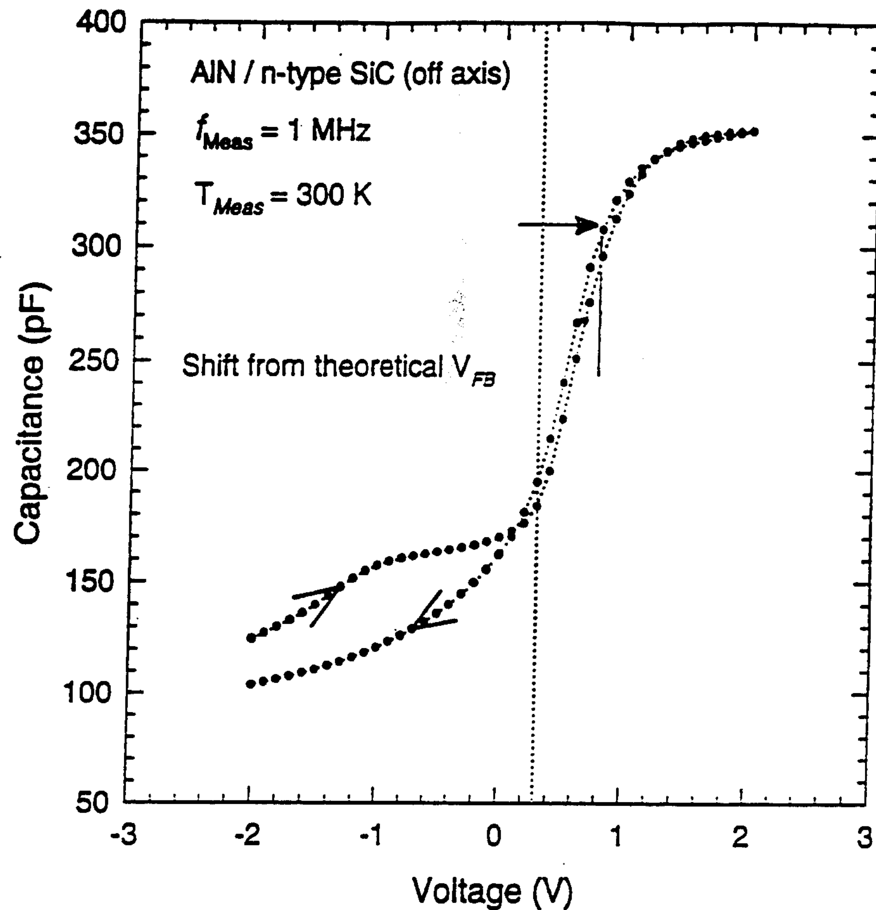

Figure 1. Room temperature C-V measurement of an Al/AlN/SiC MIS diode.

Figure 2 shows the side-by-side comparison of the same sample swept over the voltage range at room temperature while in the dark and while under illumination. The most significant features of this figure are the shift in the flat band voltage and the increased hysteresis observed under illumination.

Figure 3 displays the effect that temperature plays on the C-V measurements. The broadening of the curve (i.e., the hysteresis) is shown to occur with increasing temperature. In contrast to the effect shown by SiO_2/SiC interfaces, the flat band voltage shift *decreases* in the case of AlN insulators. As a result of this effect, the net interface trap density appears to be reduced as the temperature of the measurement is made.

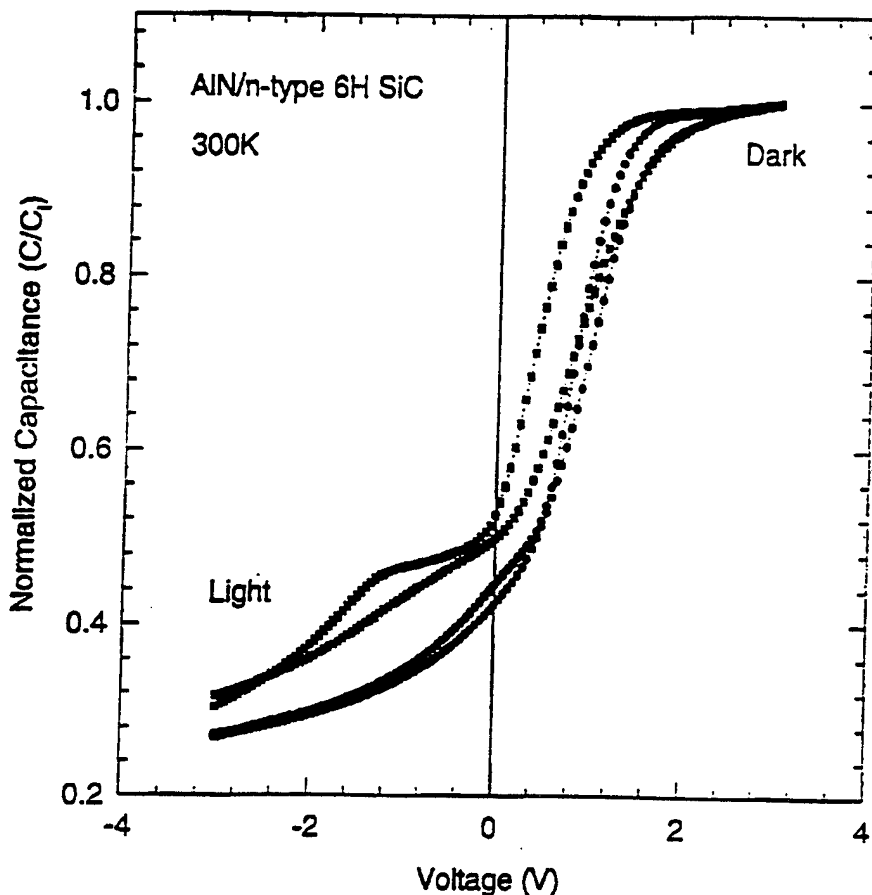

Figure 2. Room temperature C-V measurements of an Al/AlN/SiC MIS diode measured with and without illumination.

D. Discussion

Figure 1 shows the accumulation and depletion of a typical Al/AlN/SiC diode. Attempts to invert these samples at room temperature were unsuccessful. This is due to several factors. The extremely low intrinsic carrier concentration in SiC ($\approx 10^{-6}$ cm^{-3}) and the low carrier generation significantly reduce the number of minority carriers available in the SiC surface region. The low interface charge trap density and the very small amount of hysteresis make this insulator comparable to any reported thermally grown oxide layer. This curve is very similar to those done on SiO_2/Si MIS structures at very low temperatures ($\approx$150 K) which indicates that the traps present in this interface are very slow to react to the voltage and the frequency shift. In this case, the most likely origin of the traps is unsaturated bonds at the interface and, perhaps, a slight amount of intermixing at the interface creating a number of unsatisfied bonds. Since the interface is made up of a nonisovalent bonding configuration made up primarily of Si^{+4} and N^{-3} atoms which create a net positive charge in the vicinity of the interface, the interface traps are negatively charged in order to maintain charge neutrality.

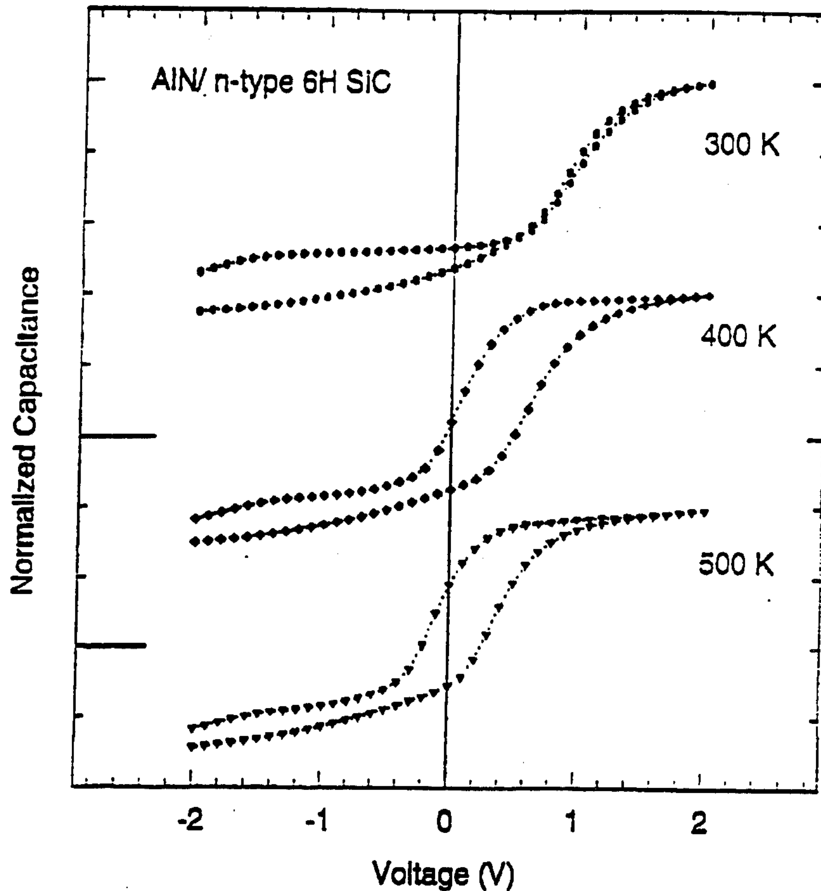

Figure 3. Temperature dependence of C-V measurements of an Al/AlN/SiC MIS diode.

The effects shown in Figs. 2 and 3 are particularly interesting in their relationship to the device physics associated with the AlN/SiC interface. Figure 2 shows that the charge contained in the traps can be modulated by the application of light. Though these traps are very slow when considering only a voltage bias, their electron population can be reduced and increased by the application and removal of light. Figure 3 shows the competition between the negatively charged (acceptor-like) traps and a donor-like trap of unknown origin. At higher temperatures, the latter trap begins to control the shift in V_{FB} and pushes it to smaller values. At this point, the nature of these traps is unknown, but is speculated to be associated with the relatively high level ($\approx 10^{20}$ cm^{-3}) of oxygen tied up at the interface of the AlN layer.

E. Conclusions

Thin AlN insulating layers on SiC have been used in MIS diode structures. The resulting diodes can be accumulated and depleted but cannot be inverted by high frequency C-V characterization. Layers thinner than 1000 Å are too leaky to measure, but 1000 Å thick layers

are sufficient. Very low interface trap densities ($\approx 2\times10^{11}$ cm^{-2}) and very accurate dielectric constant (8.67) values have been determined. The role of illumination and temperature have also been studied.

F. References

1. R. B. Campbell and H.-C. Chang, in *Semiconductors and Semimetals, Vol. 7B*, edited by R. K. Willardson and A. C. Beer (Academic Press, New York, 1971), p. 625.
2. W. von Muench and I. Pfaffeneder, J. Appl. Phys. **48**, 4831 (1977).
3. W. von Muench and E. Pettenpaul, J. Appl. Phys. **48**, 4823 (1977).
4. G. A. Slack, J. Appl. Phys. **35**, 3460 (1964).
5. R. F. Davis, J. W. Palmour and J. A. Edmond, Mater. Res. Soc. Symp. Proc. **162**, 463 (1990).
6. R. F. Davis, in *The Physics and Chemistry of Carbides; Nitrides and Borides*, edited by R. Freer (Kluwar Academic Publishers, The Netherlands, 1990), p. 589.
7. R. F. Davis, G. Kelner, M. Shur, J. W. Palmour and J. A. Edmond, Proc. IEEE **79**, 677 (1991).
8. R. F. Davis, J. W. Palmour and J. A. Edmond, Diam. Rel. Mater. **1**, 109 (1992).
9. R. F. Davis, Phys. B **185**, 1 (1993).
10. P. A. Ivanov and V. E. Chelnokov, Semicond. Sci. Technol. **7**, 863 (1992).
11. J. A. Powell, P. G. Neudeck, L. G. Matus and J. B. Petit, Mater. Res. Soc. Symp. Proc. **242**, 495 (1992).
12. K. Shibahara, S. Nishino and H. Matsunami, Jpn. J. Appl. Phys. **23**, L862 (1984).
13. R. E. Avila, J. J. Kopanski and C. D. Fung, Appl. Phys. Lett. **49**, 334 (1986).
14. S. M. Tang, W. B. Berry, R. Kwor, M. V. Zeller and L. G. Matus, J. Electrochem. Soc. **137**, 221 (1990).
15. M. Shinohara, M. Yamanaka, S. Misawa, H. Okumura and S. Yoshida, Jpn. J. Appl. Phys. **30**, 240 (1991).
16. C. Raynaud, J.-L. Autran, J.-B. Briot, B. Balland, N. Bécourt and C. Jaussaud, J. Electrochem. Soc. **142**, 282 (1995).
17. R. W. Kee, K. M. Geib, C. W. Wilmsen and D. K. Ferry, J. Vac. Sci. Technol. **15**, 1520 (1978).
18. R. Berjoan, J. Rodriguez and F. Sibieude, Surf. Sci. **271**, 237 (1992).
19. C. Raynaud, J.-L. Autran, B. Balland, G. Guillot, C. Jaussaud and T. Billon, J. Appl. Phys. **76**, 993 (1994).
20. C. Raynaud, J.-L. Autran, F. Seigneur, C. Jaussaud, T. Billon, G. Guillot and B. Balland, J. Phys. III **4**, 937 (1994).
21. A. Rys, N. Singh and M. Cameron, J. Electrochem. Soc. **142**, 1318 (1995).
22. J. N. Shenoy, G. L. Chindalore, M. R. Melloch, J. A. Cooper, Jr., J. W. Palmour and K. G. Irvine, J. Electron. Mater. **24**, 303 (1995).
23. G. E. Morgan, C. C. Tin, J. R. Williams and R. Ramesham, in *Silicon Carbide and Related Materials*, edited by M. G. Spencer, R. P. Devaty, J. A. Edmond, M. A. Khan, R. Kaplan, and M. Rahman (Institute of Physics, Bristol, 1994), p. 645.
24. W. M. Yim, E. J. Stofko, P. J. Zanzucchi, J. I. Pankove, M. Ettenberg and S. L. Gilbert, J. Appl. Phys. **44**, 292 (1973).
25. M. G. Norton, P. G. Kotula and C. B. Carter, J. Appl. Phys. **70**, 2871 (1991).
26. G. A. Slack, J. Phys. Chem. Solids **34**, 321 (1973).
27. S. Strite and H. Morkoc, J. Vac. Sci. Technol. B **10**, 1237 (1992).
28. J. K. Liu, K. M. Lakin and K. L. Wang, J. Appl. Phys. **46**, 3703 (1975).
29. M. Morita, N. Uesugi, S. Isogai, K. Tsubouchi and N. Mikoshiba, Jpn. J. Appl. Phys. **20**, 17 (1981).
30. G. D. O'Clock, Jr. and M. T. Duffy, Appl. Phys. Lett. **23**, 55 (1973).
31. S. Mirsh and H. Reimer, Phys. Stat. Sol. **11**, 631 (1972).
32. J. Bauer, L. Biste, D. Bolze and G. Eichorn, Phys. Stat. Sol. **399**, 173 (1977).

33. M. Morita, S. Isogai, K. Tsubouchi and N. Mikoshiba, Appl. Phys. Lett. **38**, 50 (1981).
34. M. Morita, K. Tsubouchi and N. Mikoshiba, Jpn. J. Appl. Phys. **21**, 728 (1982).
35. M. Koshinaka, H. Fujii, K. Nakanishi and Y. Shibuya, Vacuum **41**, 1971 (1990).
36. A. U. Ahmed, A. Rys, N. Singh, J. H. Edgar and Z. J. Yu, J. Electrochem. Soc. **139**, 1146 (1992).
37. F. Alexandre, J. M. Masson, G. Post and A. Scavennec, Thin Solid Films **98**, 75 (1982).
38. S. Fujieda, J. Mizuki and Y. Matsumoto, Jpn. J. Appl. Phys. **27**, L296 (1988).
39. S. Fujieda, Y. Mochizuki, K. Akimoto, I. Hirosawa, Y. Matsumoto and J. Matsui, Jpn. J. Appl. Phys. **29**, L364 (1990).
40. Y. Mochizuki, M. Mizuta, S. Fujieda and Y. Matsumoto, J. Appl. Phys. **67**, 2466 (1990).
41. P. Bhattacharya and D. N. Bose, Jpn. J. Appl. Phys. **30**, L1750 (1991).
42. S. Fujieda, K. Akimoto, I. Hirosawa, J. Mizuki, Y. Matsumoto and J. Matsui, Jpn. J. Appl. Phys. **28**, L16 (1989).
43. K. S. Stevens, M. Kinniburgh, A. F. Schwartzman, A. Ohtani and R. Beresford, Appl. Phys. Lett. **66**, 3179 (1995).
44. R. M. Eastment and C. H. B. Mee, J. Phys. F **3**, 1378 (1973).
45. J. A. Dillon, Jr., R. E. Schlier and H. E. Farnsworth, J. Appl. Phys. **30**, 675 (1959).

IX. Design and Development of Multiple Quantum Well Vertical Cavity Surface Emitting Laser Structures Via Molecular Beam Epitaxy of III-N Layers

A. Introduction

Recent research efforts in the wide bandgap, III-V nitride, semiconductor field have concentrated on the development of light-emitting diodes (LEDs) that emit in the blue spectral region. Nakamura recently developed an AlGaN/InGaN/AlGaN double heterostructure blue LED that is now commercially marketed by Nichia Chemical Industries Ltd. of Japan. The logical next step is the fabrication of blue and UV lasers. The III-V nitrides are most promising candidate materials for these devices because they possess three favorable characteristics: (1) they all have direct transition band structures, (2) their bandgap energies range from the deep UV (6.2 eV (AlN)) to the orange (2.8 eV (InN)) regions of the spectrum, and (3) they can be mixed to form solid solutions allowing for the tailoring of bandgap energies to specific wavelengths.

One of the promising optical devices ideally suited for fabrication using the III-V nitrides is the Vertical Cavity Surface Emitting Laser (VCSEL). VCSELs have significant advantages over edge-emitting lasers for optoelectronic communications. The laser beam emitted from the VCSEL propagates normal to the plane of the substrate, thereby making alignment for chip-to-chip communication much simpler. Additionally, the chip area occupied by a VCSEL is relatively small compared to one required by an edge-emitter [1]. One unique feature of these VCSELs is that both the central light-emitting active region and the outermost distributed Bragg reflectors (DBRs) which form the Fabry-Pérot cavity are all dimensionally defined in one integrated crystal growth sequence performed over the entire wafer using epitaxial techniques such as Molecular Beam Epitaxy (MBE), Gas Source Molecular Beam Epitaxy (GSMBE) and CBE [2]. Efficient performance of such a device requires both high-quality crystalline microstructures and precise control of layer thickness and alloy composition to obtain the highly reflective mirrors and to ensure that the Fabry-Pérot resonance is placed at the exact wavelength for lasing. A typical schematic of a VCSEL structure is shown in Fig. 1. By incorporating a strained MQW active region and by varying the compositional ratios of the group III elements (Al, Ga, and In), the emission wavelength can be tailored to emit in the UV, blue and blue-green spectra.

As an example of some of the design issues and dimensions involved in fabricating the DBRs for III-V laser use, the following schematic (Fig. 2) shows a DBR design which is designed to reflect light in the blue spectrum. The schematic shows the top DBR only and the active region for which the DBR is designed to operate.

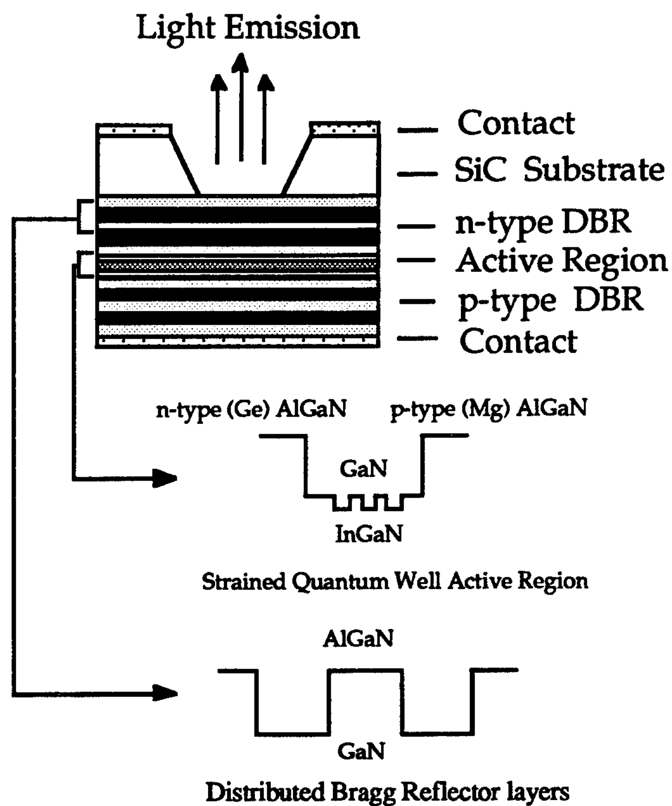

Figure 1. Schematic of a typical VCSEL structure.

Blue (450 nm) emission single quantum well

			Refractive Index *n*	Thickness *d*	Band *eV*	λ
Mirror stack		GaN	2.5	45 nm	3.4	1/4
		AlN	2.2	51 nm	6.2	1/4
	Dense	GaN	2.5	45 nm	3.4	1/4
	Rare	AlN	2.2	51 nm	6.2	1/4
In(.33)Ga(.67)N	p-type confinement/spacer		2.9	58 nm		3/8
	Active Layer		2.9	39 nm	2.93	1/4
	n-type confinement/spacer		2.9	58 nm		3/8

Laser Cavity: 155 nm
Each Mirror Stack: 1920 nm (assumes 20 periods)
Approximate Total: 3995 nm = 4 microns

Figure 2. Schematic of a DBR for blue spectral reflection.

Thin films of AlN, GaN and InN are presently grown by various techniques including metalorganic vapor phase epitaxy (MOVPE), RF sputtering, and molecular beam epitaxy (MBE). Additionally, researchers have successfully doped the III-V nitrides and their alloys creating n-type (Si, Ge) doped films [3-5] and more notably, p-type magnesium doped films [4,6,7]. Although these recent developments have provided all of the material ingredients necessary for the fabrication of efficient LEDs, further refinement in film quality, namely GaN and InN, is still needed for the GSMBE growth and fabrication of VCSEL structures.

Currently, MOVPE has played the dominate role in nitride based wide bandgap device development. MBE growth of the III-V nitrides has until recently predominately used nitrogen electron cyclotron resonance (ECR) plasma assisted GSMBE. One of the major consequences of using ECR plasmas is the resulting ion damage occurring during film growth. It is generally believed now that, as a result of the low bond strength of the surface and near-surface atoms of GaN and InN, there is an increased potential for point defect damage and resulting electrical compensation in these materials. This damage would arise from the interaction of high energy N species with the surface and near-surface regions of these materials during deposition [8-10]. This is especially true if the plasma power is increased to enhance the flux of the reactive species. Recent research has shown that GaN films grown at higher microwave powers exhibit degraded electrical and luminescent properties as compared to films grown at lower microwave power levels [11-14]. Therefore, an alternative method of producing atomic nitrogen that minimizes or eliminates the undesirable production of high energy ionic nitrogen is needed.

Currently, there are two alternative methods being researched to address this concern. The first method employs the use of a radio frequency (RF) plasma source [10, 15-17]. This source is found to emit a much larger fraction of atomic nitrogen and 1st-positive series excited molecular nitrogen than the ECR source [10]. The second method uses ammonia (NH_3) as the source of nitrogen [17, 18]. Methods of cracking the ammonia include precracking in cracker cells, cracking on the substrate surface and by employing reactive ion MBE (RIMBE) to produce low-energy NH_x^+ ions. This report presents the current research aimed at optimizing the microcrystalline and optical quality of GaN by employing thermally cracked NH_3 as the nitrogen source as an alternative to the ECR source in GSMBE.

B. Experimental Procedure

Thin films of GaN and AlN were grown on (0001) oriented α(6H)-SiC wafers provided by Cree Research, Inc. The films were grown by GSMBE using a commercial Perkin-Elmer 430 system. The Al and Ga fluxes were provided by standard Knudson effusion cells. Nitride grade ammonia is used as the source gas and is further purified by a Nanochem ammonia purifier. The gas enters the MBE chamber through an experimental ammonia cracker cell

manufactured by Effusion Science Inc. The cracker cell was designed with a Re filament and fits inside a standard effusion cell sleeve (2.25" diameter) [19]. All substrates were cleaned by a standard degreasing and RCA cleaning procedure prior to loading into the system. Additionally, the substrates were degassed at 700°C for 30 minutes prior to transferring to the deposition chamber.

Reflection high-energy electron diffraction (RHEED) was used to determine the crystalline quality of the films. Scanning electron microscopy (SEM) was used to analyze the films microstructures and photoluminescence analysis was performed on the GaN films.

C. Results and Discussion

Figure 3 shows the resulting surface morphologies of deposited GaN grown at 800°C using either ammonia cracked directly on the surface of the substrate or precracked in the ammonia cracker cell as well as the substrate surface.

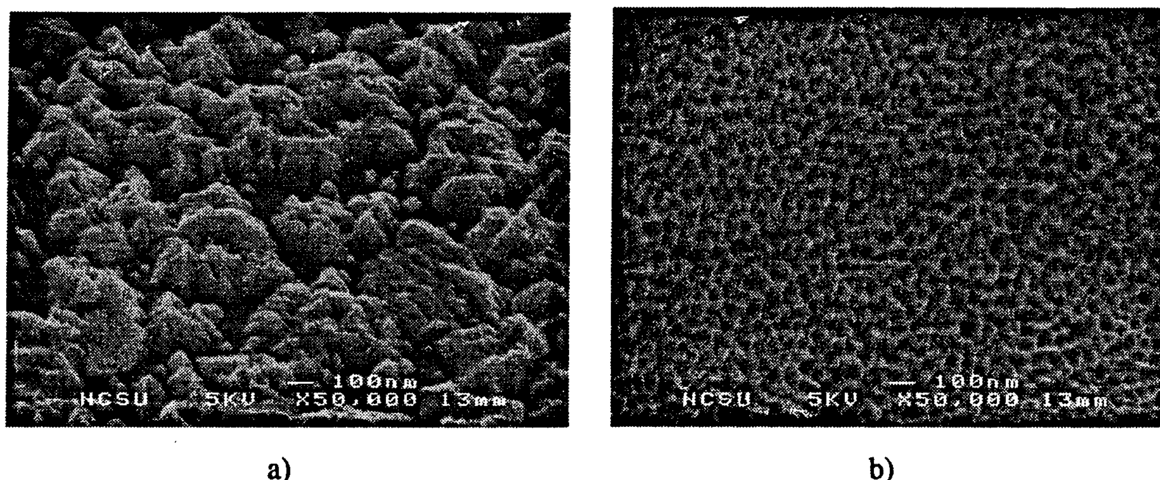

a) b)

Figure 3. Comparison of GaN grown a) with precracked NH_3 and b) without precracked NH_3.

Scanning electron microscopy image analysis of the GaN reveals smoother surface morphologies and enhanced growth rates were achieved when growth was performed without precracking the ammonia prior to cracking on the substrate. It is suspected that the reduced growth rate resulting from precracking occurs due to an effective reduction of NH radicals reaching the substrate surface. RGA characterization of the cracker cell revealed that the primary constituents of the cracked ammonia flux were N_2 and H_2, most likely resulting from recombination of NH molecules leaving the surface of the Re filament. N_2 and H_2 do not contribute to film growth, and thus the only relative source of NH radicals available are those produced from cracking on the substrate surface of any ammonia not previously cracked by the cracker cell.

Figure 4 shows the PL spectrum of GaN grown using ammonia as the nitrogen source. Prior PL of our GaN grown by ECR assisted GSMBE has resulted only in defect peaks and deep level emission. By switching over to ammonia as the nitrogen source, we have for the first time achieved PL emission near the band edge, 354 nm.

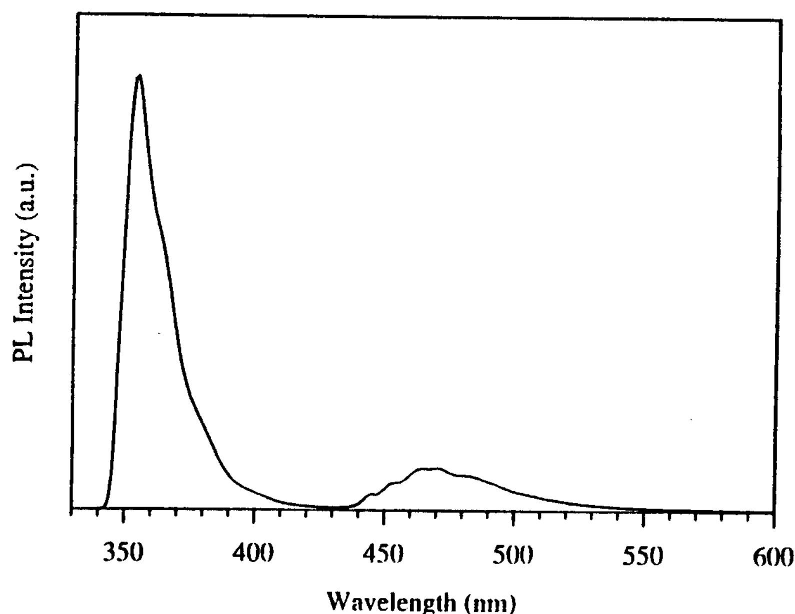

Figure 4. PL of GaN at 8K.

Figure 5 shows the results of SEM analysis performed on AlN grown using ammonia (with and without the assistance of precracking) as the source for nitrogen. In this case, no difference in either surface morphology or growth rate was found using the two methods.

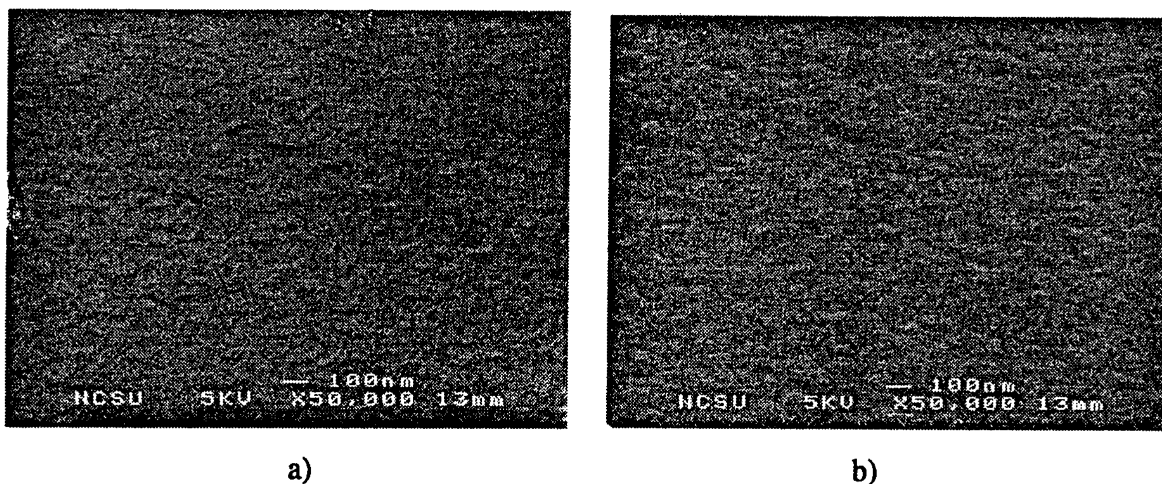

Figure 5. Comparison of AlN grown a) with precracked NH_3, and b) without precracked NH_3.

However, SIMS analysis of AlN grown using precracked NH_3 indicates Mn impurities have been incorporated into the film at atomic densities as high as 2×10^{20} cm^{-3}. The source of the Mn is thought to be from decomposition of the stainless steel cracker cell sleeve in the vicinity of the heated Re filament.

Figure 6 shows SEM results of GaN grown on an ALN buffer. These SEM results are typical of the GaN grown to date using AlN buffers without precracked NH_3. As can be seen from Figure 6(a), the surface morphology is still considerably rough compared to surfaces obtained by MOCVD growth techniques. However, Figure 6(b) shows a drastic reduction in columnar features commonly seen in ECR grown GaN. Typical growth conditions are listed in Table I.

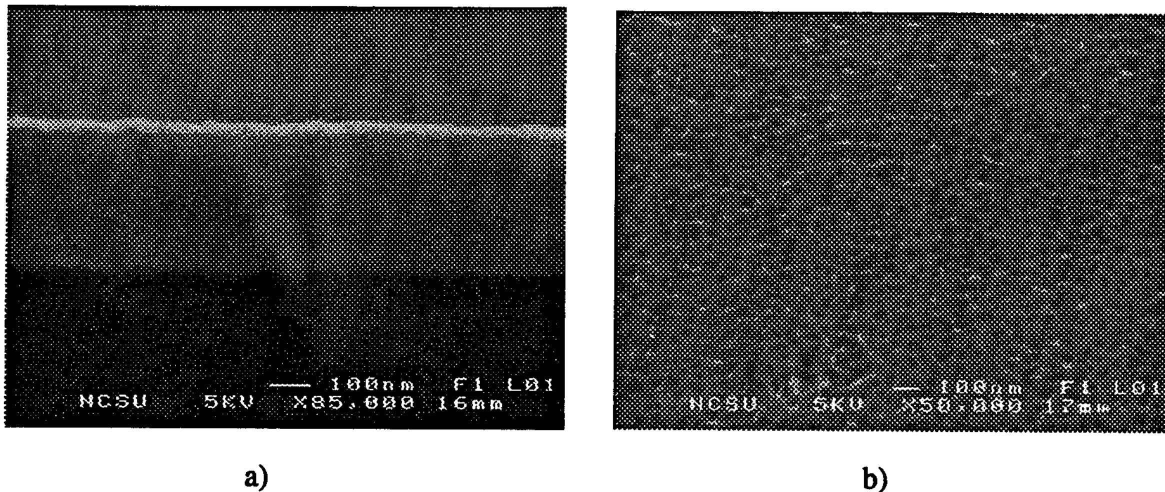

a) b)

Figure 6. Typical GaN grown on an AlN buffer layer.

Table I. Typical GaN Deposition Conditions

Substrate temperature	700-900°C
Ga cell temperature	800-950°C
Al cell temperature	1100-1150°C
Ammonia flow rate	2.00-10.00 SCCM
MBE chamber pressure during growth	2.00-8.50 E-5 Torr

D. Conclusions

The use of ammonia (NH_3) thermally cracked on the substrate surface (6H-SiC) has lead to a marked improvement in the optical properties of GSMBE grown GaN as characterized by the PL spectrum exhibiting a sharp peak at 354 nm in our films for the first time. Optimization of

the growth parameters for GaN deposition has not yet been achieved. The use of a high-temperature ammonia-cracking source to precrack the ammonia has resulted in the degradation of both the film morphology and growth rate for GaN. Additionally, there is some evidence that impurities from the cracker sleeve are being incorporated into the film when the cracker is used to precrack the ammonia. Analysis of RGA spectra reveal that molecular nitrogen and hydrogen are the primary constituents resulting from decomposition of the ammonia. Recombination of NH molecules leaving the Re filament surface are thought to be the source of the N_2 and H_2. This subsequently leads to a reduced growth rate for GaN films.

E. References

1. T. Miyamoto, T. Uchida, N. Yokouchi and K. Iga, J. Crystal Growth **136**, 210 (1994).
2. Y. M. Houng, M. R. T. Tan, B. W. Liang, S. Y. Wang, L. Yang and D. E. Mars, J. Crystal Growth **136**, 216 (1994).
3. S. Nakamura, P. Mukai and M. Senoh, Jpn. J. Appl. Phys. **31**, L139 (1992).
4. I. Akasaki, H. Amano, N. Koide, M. Kotaki and K. Manabe, Physica B **185**, 428 (1993).
5. N. Koide, H. Kato, M. Sassa, S. Yamasaki, K. Manabe, M. Hashimoto, H. Amano, K. Hiramatsu and I. Akasaki, J. Crystal Growth **115**, 639 (1991).
6. C. Wang and R. F. Davis, Appl. Phys. Lett. **63**, 990 (1993).
7. S. Nakamura, M. Senoh and T. Mukai, Jpn. J. Appl. Phys. **30**, L1708 (1991).
8. S. Strite, IBM Research Report #83986, March 28, 1994 and private discussions.
9. J. Smith, D. Chandrasekhar, B. Sverdlov, A. Botchkarev, A. Salvador and H. Morkoc, Appl. Phys. Lett. **67** (13), 1830 (1995).
10. W. C. Hughes, *et al.*, J. Vac. Sci. Technol. B **13**(4), 1571 (1995).
11. R. J. Molnar and T. D. Moustakas, J. Appl. Phys. **76**, (8) 4587 (1994).
12. R. C. Powell, N. E. Lee, Y. W. Kim and J. E. Greene, J. Appl. Phys. **73**, 189 (1993).
13. M. E. Lin, B. Sverdlov, G. L. Zhou and H. Morkoc, Appl. Phys. Lett. **62**, 3479 (1993).
14. R.Singh, R. J. Molnar, M. S. Unlu and T. D. Moustakas, Appl. Phys. Lett. **64**, 336 (1994).
15. W. Hoke, P. Lemonias and D. Weir, J. Cryst. Growth **111**, 1024 (1991).
16. R. Vaudo, J. Cook and J. Schetzina, J. Vac. Sci. Technol. B **12**(2), 232 (1994).
17. W. S. Wong, *et al.*, J. Cryst. Growth, in press.
18 N. Lee, R. Powell, Y. Kim and J. Green, J. Vac. Sci. Technol. A **13**(5), 2293 (1995).
19. Effusion Science Inc., 1994.

X. Chemistry, microstructure, and electrical properties at interfaces between thin films of titanium and alpha (6H) silicon carbide (0001)

L. M. Porter and R. F. Davis
Department of Materials Science and Engineering, North Carolina State University, Raleigh, North Carolina 27695-7907

J. S. Bow, M. J. Kim, and R. W. Carpenter
Center for Solid State Science, Arizona State University, Tempe, Arizona 85287-1704

R. C. Glass
Westinghouse Science and Technology Center, Westinghouse Corporation, Pittsburgh, Pennsylvania 15235

(Received 25 January 1994; accepted 15 November 1994)

Epitaxial thin films (4–1000 Å) of Ti contacts have been deposited via UHV electron beam evaporation at room temperature on monocrystalline, *n*-type, alpha (6H)–SiC(0001). The interfacial chemistry and microstructure, and the electrical properties, were investigated at room temperature and after annealing at 700 °C up to 60 min. High resolution TEM analyses revealed the formation during annealing of reaction zones consisting of Ti_5Si_3 and TiC. The corresponding electrical properties exhibited considerable stability except after an initial 20 min anneal. Current-voltage (*I-V*) measurements showed that the Ti contacts were rectifying with low ideality factors ($n < 1.09$) and typical leakage currents of 5×10^{-7} A/cm^2 at -10 V. The Schottky barrier heights calculated from x-ray photoelectron spectroscopy and *I-V* and *C-V* measurements were between 0.79 and 0.88 eV for the as-deposited contacts and between 0.86 and 1.04 eV for the annealed contacts.

I. INTRODUCTION

The extreme thermal, mechanical, and electronic properties of SiC have allowed its use for both structural applications and high-power, high-temperature, high-speed, and high-frequency electronic and optoelectronic devices. The chemistry at annealed Ti/SiC interfaces has been investigated for structural applications by many groups, as discussed below. However, no integrated study has been found that has examined the Ti/SiC interface in terms of the chemistry, microstructure, and electrical properties for the purpose of contacts in semiconductor devices.

The increased use of (6H)–SiC for many types of semiconductor devices is challenged by the difficulty of controlling the properties of the metal contact/SiC interface, including uniformity and thickness of the interfacial region, stability at high temperatures (~600 °C), and most importantly, the Schottky barrier height (SBH), or the energy barrier for electrons traversing the interface. It is important to understand the chemistry and microstructure at the interface between the metal contact and the SiC substrate before and after annealing at temperatures at or above which devices may be operated so that the resulting phases may be correlated with the electrical properties.

In this study, analytical techniques have been employed to investigate the interfacial chemistry and microstructure on both an atomic scale and a microscopic (<1 μm) scale between Ti and *n*-type 6H–SiC(0001) before and after annealing at 700 °C. In addition, the chemically cleaned SiC surface was characterized in terms of chemistry, structure, and amount of band bending. The results of these studies have been correlated with the electrical properties and SBH's of both the unannealed and annealed contacts.

II. EXPERIMENTAL PROCEDURE

A. SiC material and preparation

Vicinal, single-crystal, nitrogen-doped, *n*-type ($\approx 10^{18}$ cm^{-3}) wafers of 1 in. diameter 6H–SiC(0001) containing 0.5–1.5 μm thick, *n*-type ($\approx 10^{16}$–10^{17} cm^{-3}) homoepitaxial films thermally oxidized to a thickness of 500–1000 Å in dry oxygen at 1300 °C were provided by Cree Research, Inc. The epitaxial layers were unintentionally doped. The Si-terminated (0001) surface, tilted 3°–4° toward $[11\bar{2}0]$, was used for all depositions and analyses.

The substrates were simultaneously cleaned and the oxide layer etched from the surface using a 10 min dip in either an ethanol/hydrofluoric acid/water (10 : 1 : 1) or 10% hydrofluoric acid solution. This was followed by a quick rinse in de-ionized water. The substrates

 © 1995 Materials Research Society

were loaded immediately into a vacuum system transfer tube (base pressure $\approx 10^{-9}$ Torr), thermally desorbed at 700 °C for 15 min to remove any residual hydrocarbon contamination, and transferred to the metal deposition chamber.

B. Metal deposition

A UHV electron beam evaporation system was used to deposit various metal films having thicknesses ranging from 4–1000 Å onto the substrates described above. A substrate manipulator allowed for both heating and rotation and contained a manual shutter directly below the position of an inverted Mo substrate block located in the upper part of the chamber. The contact metals were evaporated using a dual source 270°, 10 cc electron beam evaporator made by Thermionics Corporation. A 330 l/s turbomolecular pump was used for roughing the system and during processing. A 500 l/s diode ion pump and a titanium sublimation pump were employed to achieve and maintain UHV base pressures of $<2 \times 10^{-10}$ Torr.

Prior to deposition, approximately 25–50 Å was typically evaporated from the source to liberate any foreign material which may have collected on its surface. Each substrate was covered by the shutter during this operation. To commence the deposition, the emission current was increased very slowly until a deposition rate of 10–12 Å/min was stabilized according to the XTC thickness monitor, and the shutter subsequently removed from in front of the sample. The pressure during the depositions was between 5×10^{-9} and 5×10^{-8} Torr. After $\approx$100 Å was deposited, the rate was typically increased to $\approx$20 Å/min. Throughout each deposition the substrates were rotated to ensure uniform thickness across the sample. The substrates were not intentionally heated.

C. Analysis techniques

Patterned structures consisting of 500 μm (0.02 in.) and 750 μm (0.03 in.) diameter circular contacts of 100 nm thickness were created for electrical characterization by depositing the metal through a Mo mask in contact with the SiC epitaxial layer. Silver paste served as the large area back contact. All subsequent annealing was conducted in UHV. Current-voltage (*I-V*) measurements were obtained with a Rucker & Kolls Model 260 probe station in tandem with an HP 4145A Semiconductor Parameter Analyzer. Capacitance-voltage (*C-V*) measurements were taken with a Keithley 590 CV Analyzer using a measurement frequency of 1 MHz.

Ti/SiC samples were prepared in cross section for analysis by transmission electron microscopy (TEM). High resolution (HR) images were obtained with an ISI EM 002B operating at 200 kV with an interpretable resolution limit of 0.18 nm. These images were typically recorded at an electron-optical magnification of 490,000 to 590,000. Some of the micrographs were digitized using a 512 × 512 CCD camera and the resulting images analyzed by using the SEMPER program.[1] Lattice spacings (*d*-spacings) and interplanar angles were measured from optical digital diffraction patterns and used to identify the reaction product phases. The values of the lattice spacings were calculated using the (0006) *d*-spacing in 6H–SiC, measured near the phase to be identified, as a baseline. Thus, the change in *d*-spacing due to different focusing conditions was negated. A database of *d*-spacings for each possible reaction product phase was compared to the experimentally determined *d*-spacings. The *d*-spacings from the database that were within 2% of the measured values were compared. An additional comparison of the interplanar angles from this selected list of phases were used for the final identification of phases. Most of the measured *d*-spacings and angles were within 1% of the theoretical values.

Analytical electron microscopy was performed using a Gatan 666 parallel electron energy loss spectrometer (PEELS) attached to a Philips 400 FEG operating at 100 kV. The spatial resolution of the PEELS was approximately 3 nm. Energy dispersive spectrometery (EDS) was performed using a JEOL 2000 FX operating at 200 kV with a probe size of approximately 40 nm. For fixed position PEELS and EDS, the probe position was adjusted in the diffraction mode by monitoring the shadow image in the Bragg disk of the transmitted beam. The image was created by defocusing the second condenser lens. A liquid nitrogen cooled double-tilted holder was used for all analytical experiments to minimize specimen contamination.

Surface chemistry was studied using a Riber x-ray photoelectron spectroscopy (XPS) system accessible by UHV transfer from the deposition chamber. This system consists of a Mg K_α (1253.6 eV) x-ray source operated at 14 kV with an emission-controlled current of 15 mA and a Mac2 semidispersive electron energy analyzer. Three different types of spectra were usually obtained. Survey scans, important for fingerprinting elements present at the surface, contained 2000 data points from 0 to 1000 eV and were obtained at a resolution, or band pass acceptance, of 2.0 eV and a counting rate of 100 ms. Scans of individual photoelectron peaks obtained at higher resolution (0.8 eV) contained 500–750 data points and a 20–30 eV binding energy range. Valence spectra contained 500 data points from 0 to 20 eV at a resolution of 0.8 eV. The results of this technique also allowed the calculation of the Schottky barrier height for thin films of Ti on SiC.

III. RESULTS AND DISCUSSION

A. Surface chemistry

Comparison of the XPS C 1*s* and Si 2*p* peak areas divided by their atomic sensitivity factors revealed that chemically cleaned, *non*thermally oxidized SiC substrates contained C-rich surfaces. Thermal oxidation and subsequent etching solved this problem. This indicates that the excess C was present only at the surface and occurred during the cessation of the growth process. As such, all as-received SiC substrates used for the Ti depositions in this research contained a thermally grown oxide.

In general, the cleaning procedures for these samples consisted of etching the oxide in a hydrofluoric acid solution followed by either a chemical or thermal process to remove hydrocarbon contamination. Figure 1 shows survey spectra obtained to determine the efficacy of three different procedures. The top spectrum represents a sample that was etched for 10 min in a 10% HF aqueous solution, quickly rinsed in de-ionized water, and heated to 700 °C for 15 min.

The spectrum shows that residual oxygen and, to a lesser extent, fluorine remained on the surface. The peaks marked with (A) are Auger peaks. The relative concentrations of the elements comprising the photoelectron signal can be estimated from the following expression[2]:

$$C_x = \frac{I_x/S_x}{\sum_i I_i/S_i}, \qquad (1)$$

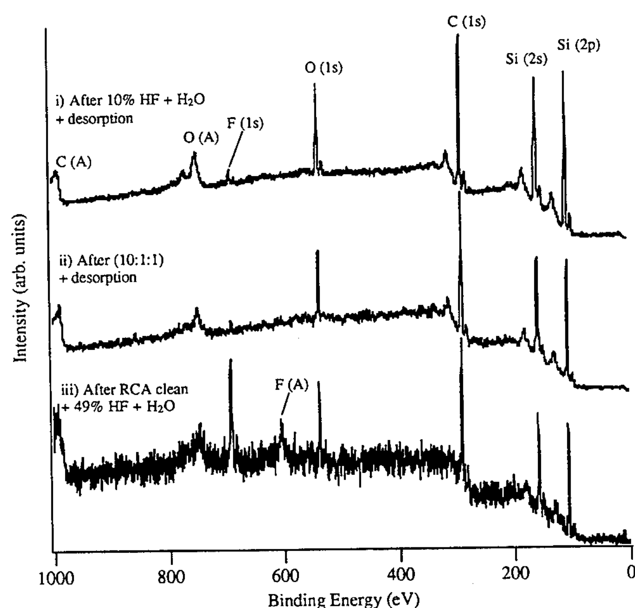

FIG. 1. XPS survey spectra of the (0001) SiC surface after (i) 10 min in 10% HF and a quick de-ionized water rinse, followed by a 15 min UHV desorption at 700 °C, (ii) 10 min in a (10 : 1 : 1) solution of ethanol/HF/de-ionized water, followed by a 15 min UHV desorption at 700 °C, and (iii) a modified RCA clean followed by 10 min in 49% HF and a 5 min rinse in de-ionized water.

where I is the integrated peak area and S is the atomic sensitivity factor. However, this expression does not take into account the fact that the top portion of a film contributes to more of the signal than the portion underneath. The concentrations are relative to the total signal and not to an actual volume at the surface. The atomic sensitivity factors are 0.205 for C 1*s*, 0.63 for O 1*s*, 1.00 for F 1*s*, and 0.17 for Si 2*p*.[2] The relative concentrations calculated using these sensitivity factors with their respective peak areas were (±1%) 49.7% Si, 40.0% C, 9.3% O, and 0.9% F. It is believed that the higher concentration of Si as compared to C is representative of a Si-terminated surface. Waldrop and Grant[3] calculated the amount of O on the same type of substrates to be ≈3/4 monolayer in addition to a trace amount of F ($F/O < 0.05$).

The middle spectrum represents a sample that was prepared by the same procedure as the previous sample except a (10 : 1 : 1) ethanol/hydrofluoric acid/de-ionized water solution was used in place of the 10% HF solution. Details regarding the use of the former solution for cleaning Si are presented in Ref. 4. The survey spectrum does not show any significant change in the amounts of O and F. The relative concentrations in this case were 45.8% Si, 44.8% C, 8.9% O, and 0.5% F. The C concentration is higher than in the case above because the sample was not thermally oxidized before surface treatment.

Results from a third cleaning procedure are shown in the bottom spectrum. This sample was first RCA cleaned, the sequence of which consisted of a 5 min dip in a (1 : 1 : 5) solution of $NH_4OH/H_2O_2/H_2O$ (70 °C), a 5 min rinse in de-ionized water, a 5 min dip in a (1 : 1 : 5) solution of $HCl/H_2O_2/H_2O$ (70 °C), and a 5 min rinse in de-ionized water. The sample was then etched in a 49% HF aqueous solution for 10 min and rinsed in de-ionized water for 5 min. The survey shows that the higher concentrated HF solution resulted in a substantial increase in the amount of F left on the surface. The relative concentrations were 41.2% Si, 42.9% C, 8.5% O, and 7.3% F. This sample also was not thermally oxidized before the surface treatment. It should also be mentioned that although this cleaning procedure did not consist of a thermal desorption, no significant changes in the amounts of O and F were found before and after the thermal desorptions for the preceding two procedures. Because of these results, the solutions containing lower HF concentrations were used for samples prior to metal deposition.

Figure 2 shows XPS Si 2*p* and C 1*s* spectra of a SiC surface that has been treated in 10% HF. The Si 2*p* peaks before and after desorption at 700 °C are virtually identical. Deconvolution of these peaks revealed both the main Si (bound to C) peak at 101.58 eV and a small peak at 102.98 eV, which is attributed to SiO_x.[5] The

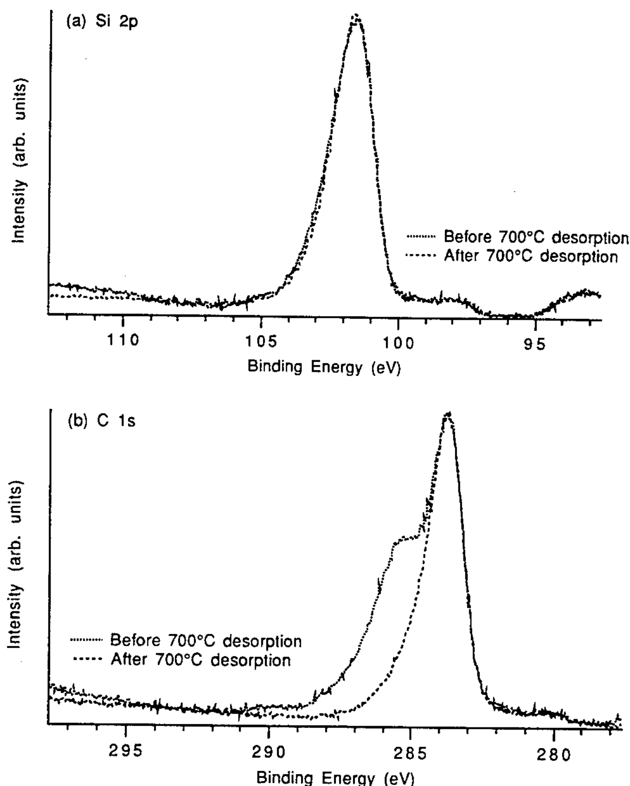

FIG. 2. XPS spectra of 6H–SiC(0001) after 10 min in 10% HF followed by a de-ionized water rinse. The (a) Si $2p$ and (b) C $1s$ peaks before and after a 700 °C desorption are shown.

C peak shows significant change after desorption. The main peak at 283.78 eV is due to C bound to Si in SiC.[6] Before desorption, a significant peak exists on the high binding energy side of the main peak and is attributed to adventitious carbon, which has a binding energy of 285.0 eV.[7]

B. Surface structure

The surface structure was monitored by low energy electron diffraction (LEED). A 1×1 unreconstructed surface was displayed for all samples treated by the various cleaning procedures noted above. This result is in agreement with that of Waldrop and Grant.[3] Kaplan[8] has noted that a 1×1 surface probably corresponds to a range of structures that do not have long-range order. The 1×1 patterns in this case are most likely due to adsorbed residual O and F.

C. Titanium/silicon carbide interfaces

1. Electrical properties

Current-voltage measurements of Ti contacts deposited at room temperature on n-type SiC(0001) were rectifying, as shown in Fig. 3, with low ideality factors ($n < 1.09$) and with typical leakage currents of 5×10^{-7} A/cm^2 at -10 V. The reverse bias characteristics

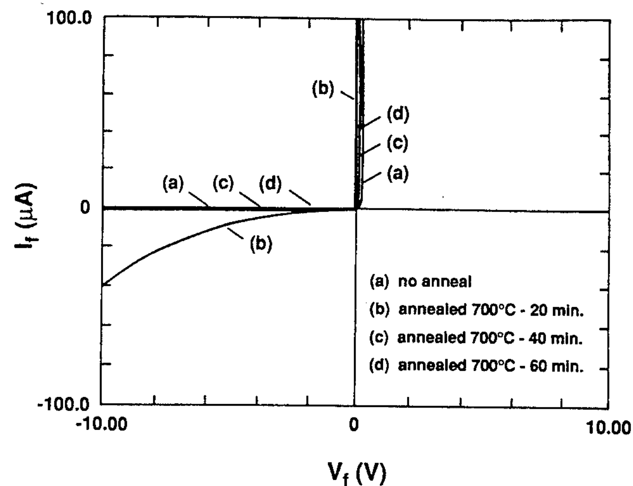

FIG. 3. Current-voltage characteristics of Ti/SiC after annealing at 700 °C (contact area = 2.0×10^{-3} cm^2).

did not show hard breakdown to 100 V, which is the voltage limit of the equipment. Instead, the leakage current steadily increased to ≈ 35 μA. This "soft breakdown" is expected from high fields at the contact edges due to the geometry of the contact structure. It is not believed that inhomogeneities in the interface structure are the cause of the increasing leakage[9] because of the atomic nature of this interface, which is described in the following section.

For values of applied voltage, V, greater than $3\ kT/q$, the current density can be expressed as

$$J = J_s \exp\left(\frac{qV}{nkT}\right), \tag{2}$$

where J_s is the extrapolated current density at zero voltage or saturation current density, and n is the ideality factor. Therefore, the ideality factor can be calculated from the linear region of a semilogarithmic plot of current versus voltage, shown in Fig. 4. The linear region in this case extends over approximately four decades of current. The reduced slope at higher voltages is due to the resistance of the substrate material. The low ideality factors were taken as evidence that thermionic emission theory may be applied for calculating the SBH.

Following Eq. (2) the SBH can then be determined from the equation

$$\Phi_B = \frac{kT}{q} \ln\left(\frac{A^* T^2}{J_s}\right), \tag{3}$$

where A^* is the effective Richardson constant. The value of A^* for 6H–SiC is 194.4 A/cm^2/K^2.[10] The accuracy of A^* is not usually critical, since, at room temperature, doubling its value only increases Φ_B by 0.018 eV.[11] Using this equation with $J_s = 2.0 \times 10^{-7}$ A/cm^2, a SBH of 0.83 eV was calculated for unannealed Ti contacts.

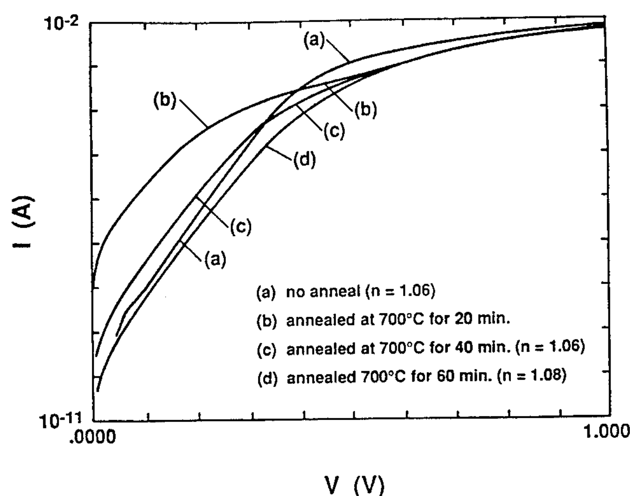

FIG. 4. Semilogarithmic *I-V* plot of Ti/SiC after annealing at 700 °C (contact area = 2.0×10^{-3} cm^2).

The barrier heights were also calculated from *C-V* measurements. Plotting $1/C^2$ vs V allows the barrier height to be determined from the equation:

$$\Phi_B = V_i + \xi + \frac{kT}{q} - \Delta\Phi\,, \qquad (4)$$

where V_i is the voltage intercept, ξ is the difference between the conduction band and the Fermi level in the bulk of the material and is a function of the carrier concentration, and $\Delta\Phi$ is the image force lowering. Figure 5 shows $1/C^2$ vs V of an as-deposited Ti/SiC contact biased from 0 to -5 V. Extrapolating the linear region gives an intercept of 0.67 V and a calculated value of the SBH of 0.88 V.

After annealing at 700 °C for 20 min, the leakage increased; however, after further annealing to a maximum time of 60 min the characteristics in terms of leakage and ideality factors again improved. The *I-V* characteristics through the annealing series are plotted in Fig. 3. It can be seen from the corresponding semilogarithmic plot (Fig. 4) that there was no linear region after annealing for 20 min. However, the ideality factors returned to low values ($n < 1.09$) after further annealing. The barrier heights after annealing for 40 and 60 min were 0.86 and 0.90 eV, respectively. The SBH after annealing for 60 min was calculated from *C-V* measurements to be 1.04 eV.

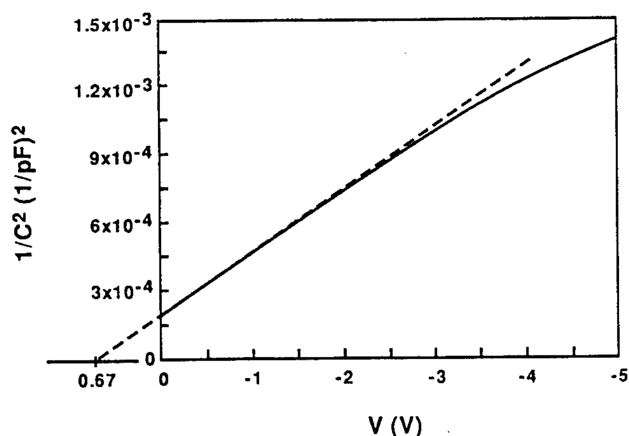

FIG. 5. $1/C^2$ vs V plot of as-deposited Ti/SiC (contact area = 2.0×10^{-3} cm^2).

The Schottky barrier height was also calculated from XPS spectra by careful comparison of core level peaks before and after deposition of very thin Ti films. Core level and valence band spectra were obtained of the SiC surface after chemical and thermal cleaning and prior to metal deposition. Immediately following the SiC surface analysis, a sequence of metal depositions was performed, which resulted in films of total thicknesses between 4 and 12 Å.

The binding energy (BE) of a photoelectron is related to its kinetic energy (KE) by the following relationship:

$$E_B = h\upsilon - E_K - \Phi_S\,, \qquad (5)$$

where $h\upsilon$ is the energy of the x-ray photons, E_K is the kinetic energy of the emitted electrons, and Φ_S is the work function of the spectrometer (analyzer). The value of binding energy which is obtained directly from an XPS scan is actually equal to the true binding energy, BE, plus Φ_S. Because binding energies are defined with respect to the Fermi level, it is important to use a known standard to define the Fermi level position. If the work function of the spectrometer tends to drift, a standard must also be used with each collection of data. Gold foil was used as the standard for both purposes. The Au $4f_{7/2}$ peak has a known binding energy of 84.00 eV. The measured value of the Au $4f_{7/2}$ peak is equal to 84.00 eV plus the work function of the spectrometer.

The relationship between the SBH and the values measured by XPS is shown in Fig. 6. This diagram shows energy bands in 6H–SiC which bend upward at the surface due either to surface states or to the metal contact. In nominally doped material, which was used in these experiments, the depth over which band bending occurs (>1000 Å) is much larger than the photoelectron escape death (≈20 Å); therefore, the XPS spectra effectively represent the position of energy bands at the surface.

Referring to Fig. 6, the SBH can be determined by the following expression:

$$\Phi_B = [(E_{C\,1s} - E_V) + E_g] - E_{C\,1s}\,, \qquad (6)$$

where $E_{C\,1s}$ is the C 1*s* binding energy originating at the SiC surface, $(E_{C\,1s} - E_V)$ is the C 1*s* to valence band maximum binding energy difference (constant for a given material), and E_g is the band gap. A value of

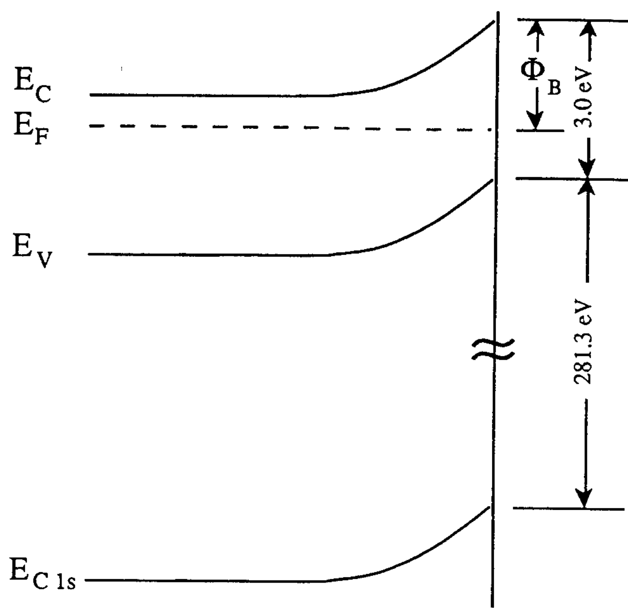

FIG. 6. Energy band diagram of 6H–SiC showing the relationship between Φ_B and binding energies measured by XPS.

$E_{C\ 1s} - E_V = 281.30$ eV was obtained from the SiC surface prior to metal deposition by extrapolating the leading edge of the valence band spectra to zero intensity. This value agrees very well with the 281.26 ± 0.1 eV value determined by Waldrop *et al.*[12] Substituting values into Eq. (6), the expression can be rewritten as

$$\Phi_B = 284.3 - E_{C\ 1s}\ (\text{eV}). \tag{7}$$

Therefore, the amount of band bending at the SiC surface prior to metal deposition is determined by the position of the C 1*s* peak. After deposition of the metal, shifts in core levels are used to calculate the SBH.

A deconvolution procedure was used to separate effects due to changes in chemical bonding and changes in band bending. One or more peaks, which typically were 20–30% Gaussian and 70–80% Laurentzian, were fit to the core levels of interest. The peaks were located by the midpoints of their full widths at half maximum (FWHM), which were 0.78–0.80 eV. The Si-bound-to-C part of the Si 2*p* peak and the C-bound-to-Si part of the C 1*s* peak were used to determine band shifting before and after the Ti depositions.

Table I lists the binding energies of the Si 2*p* (Si-bound-to-C) and C 1*s* (C-bound-to-Si) peaks after depositing, 0, 4, 8, and 12 Å of Ti. The total band bending at the SiC surface before deposition of Ti was determined by subtracting the C 1*s* binding energy from 284.30 eV [see Eq. (7)]. These results indicated that the energy difference between the conduction band minimum and Fermi level at the surface was 0.40 ± 0.1 eV.

TABLE I. Binding energies of Si 2*p* and C 1*s* peaks from SiC with various thicknesses of Ti. These binding energies have been corrected according to the Au $4f_{7/2}$ peak. Units are in electron-volts.

XPS peak	0 Å Ti	4 Å Ti	8 Å Ti	12 Å Ti
Si 2*p*	101.74	101.40	101.38	101.34
C 1*s*	283.90	283.62	283.56	283.52

Because these layers were so thin, it was important to make sure that complete coverage was achieved. Two-dimensional layer-by-layer growth, or Frank–van der Merwe growth, results in greater reduced intensities of the peaks originating from the substrate than three-dimensional island growth (a.k.a Volmer–Weber growth). An expression for the reduced intensities of the substrate peaks for layer-by-layer growth is expressed by the following relationship[13,14]:

$$I_{\text{red}} = (1 - \Theta)\exp\left[\frac{-(n-1)m}{\lambda}\right] + \Theta \exp\left(\frac{-nm}{\lambda}\right), \tag{8}$$

where Θ equals the covered monolayer fraction, n is the number of monolayers, m is the thickness of one monolayer, and λ is the attenuation length of the emitted electrons. The attenuation length is relatively independent of the particular material but is a function of the energy of the electrons. For C 1*s* and Si 2*p* peaks, λ is equal to approximately seven monolayers.[7] Between integer numbers of monolayer coverage (e.g., $n = 1$, $\Theta = 1$ to $n = 2$, $\Theta = 1$), the reduced intensity decreases linearly with Θ. At integer numbers of monolayer coverage, where $\Theta = 1$, Eq. (8) becomes

$$I_{\text{red}} = \exp\left(\frac{-nm}{\lambda}\right), \tag{9}$$

In comparison, three-dimensional island growth is expressed by

$$I_{\text{red}} = (1 - \Theta) + \Theta \exp\left(-\frac{nm}{\lambda}\right). \tag{10}$$

The reduced intensity (of either C 1*s* or Si 2*p* peaks) according to both the layer-by-layer and three-dimensional (assuming 50% coverage) growth models are plotted versus Ti thickness in Fig. 7. The thickness of one monolayer, m, was approximated to be $1/2c = 2.34$ Å for Ti, which has an hcp structure with $a = 2.95$ Å and $c = 4.68$ Å. The C 1*s* and Si 2*p* reduced intensities calculated and normalized from the peak areas are also plotted versus Ti thickness in Fig. 7. The data points follow the theoretical curve for two-dimensional growth very closely.

After depositing 4 Å of Ti, the Si 2*p* and C 1*s* binding energies (Table I) were reduced by 0.34 and

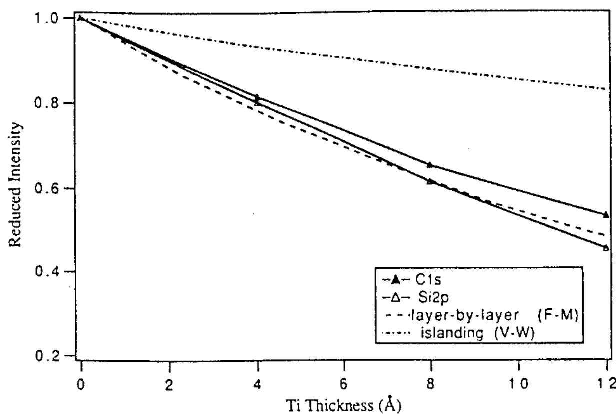

FIG. 7. Plot of the reduced intensities of the C 1*s* and Si 2*p* peaks vs Ti overlayer thickness as measured by the quartz deposition (film thickness) monitor. The theoretical curves represent layer-by-layer (Frank–van der Merwe) and three-dimensional island (Volmer–Weber) growth.

0.28 eV, respectively, which corresponds to an increase in band bending. Most of the band bending occurred within the first 4 Å of Ti. With 12 Å of Ti, the total reduction in binding energies of the Si 2*p* and C 1*s* peaks were 0.40 and 0.38 eV, respectively. The difference in binding energy shifts were within the experimental error estimated to 0.04 eV. The reduction in binding energies corresponded to an increase in the barrier height. Taking the average of the binding energy reductions and adding it to the initial amount of band bending gave a barrier height of 0.79 ± 0.1 eV.

The SBH's of Ti contacts on SiC calculated from *I-V*, *C-V*, and XPS measurements are summarized in Table II. The XPS analyses were performed only on as-deposited contacts, and *C-V* data were not obtained for samples annealed at 700 °C for 40 min. However, of the data collected, the agreement is good, within 0.15 eV, among the three measurement techniques.

2. Interface structure

The room temperature deposition of Ti on 6H–SiC(0001) resulted in epitaxial films. Both Ti (a = 2.95 Å, c = 4.68 Å) and 6H–SiC (a = 3.08 Å, c = 15.11 Å) have hexagonal crystal structures, corresponding to a −4% lattice mismatch between $(1\bar{1}00)_{Ti}$ and $(1\bar{1}00)_{SiC}$. The first indication of epitaxial growth was a 1 × 1 LEED pattern, similar to that of the SiC substrate, which was obtained from a deposited film of Ti (≈200 Å). Selected area cross-sectional TEM diffraction patterns of 6H–SiC and the Ti/6H–SiC interface are compared in Fig. 8. Figure 8(a) shows a diffraction pattern of the 6H–SiC substrate along the $[11\bar{2}0]$ zone axis, which is perpendicular to the [0001] direction. In Fig. 8(b) the diffraction pattern was obtained from an area which includes the interface of a Ti/SiC sample. The arrows mark spots from the Ti film. The other spots which are not present in (a) also

TABLE II. Barrier heights of unannealed and annealed Ti contacts on SiC measured by *I-V*, *C-V*, and XPS.

Anneal condition	$\Phi_B^{I\text{-}V}$ (eV)	$\Phi_B^{C\text{-}V}$ (eV)	Φ_B^{XPS} (eV)
Unannealed	0.83	0.88	0.79
700 °C/40 min	0.86	...	...
700 °C/60 min	0.90	1.04	...

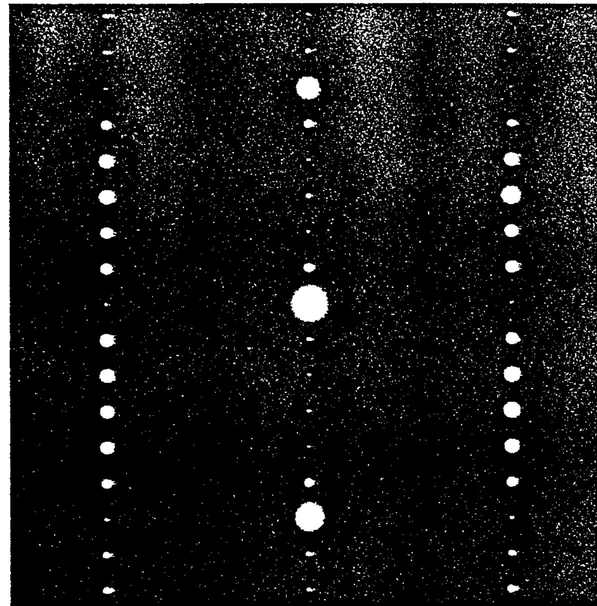

(a)

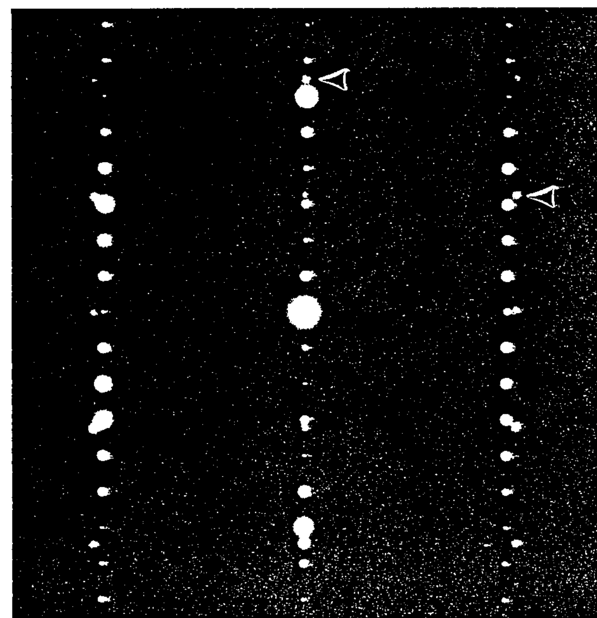

(b)

FIG. 8. Selected area TEM diffraction patterns of (a) 6H–SiC and (b) the Ti/SiC interface in cross-sectional view. Two of the spots due to the Ti film are marked with arrows in (b). $z = [11\bar{2}0]$.

originate from the Ti film. The fact that the Ti spots lie outside the SiC spots shows that the lattice parameter of the Ti film is smaller than that of the SiC substrate. The crystallographic relationships are $(0001)_{Ti} \parallel (0001)_{SiC}$ and $(\bar{1}100)_{Ti} \parallel (\bar{1}100)_{SiC}$.

The integrity of the interface structure is represented well by the HRTEM image shown in Fig. 9. The top part of the figure shows a high resolution image of the Ti/SiC interface region. The enclosed area is magnified in the bottom part of the figure. The image shows a nearly perfect interface. The arrow marks the location of a step in the SiC surface. Dislocations, which are also marked, were found in the film but did not extend to the interface. Therefore, it is believed that the films were pseudomorphic. These so-called "stand-off" dislocations have been observed by others.[15,16] It is believed that for strongly bound interfaces it is energetically favorable to have coherence for the first layer at the interface with the misfit dislocations being formed at a finite distance from the interface.

Also marked in the magnified image are the nearest plane spacings perpendicular to the interface. Titanium has a two-layer periodicity; thus, the nearest-neighbor planes are (0002) along the [0001] direction. The corresponding nearest-neighbor planes in 6H–SiC are (0006).

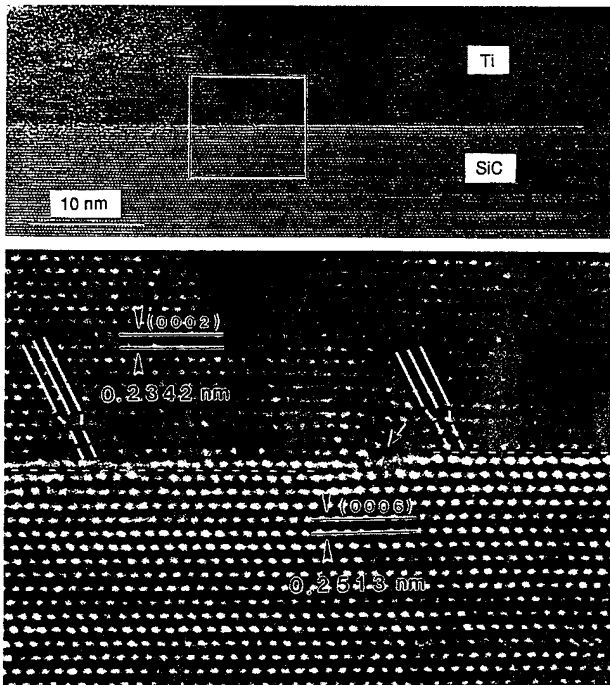

FIG. 9. High resolution TEM image of as-deposited Ti/SiC in cross section. The lower image is a magnification of the boxed-in region. The arrow at the interface marks the position of a step in the SiC surface. The misfit dislocations, as marked, did not extend to the interface.

3. Interface chemistry

After annealing at 700 °C for 20 min, the interface reaction zone (R.Z.) consisted of a 2 to 3 nm thick, continuous layer of cubic [B1 (NaCl structure)] TiC_{1-x} in contact with the SiC and a layer of orthorhombic Ti_5Si_3 containing discrete TiC_{1-x} particles at the Ti side of the interface (Fig. 10). The total width of the R.Z. was 10 to 15 nm. The size of the TiC_{1-x} particles was 5 ± 2 nm. The major product phase, Ti_5Si_3, was a continuous layer which contained low angle boundaries.

The width of the reaction zone did not change after annealing for 60 min. However, the TiC_{1-x} particles disappeared at the interface with Ti. The sequence of the layers comprising the interface was $SiC/TiC_{1-x}/Ti_5Si_3/Ti$. The lattice parameter of TiC_{1-x} varied by approximately 2% along the SiC interface. The crystallographic relationships are summarized by the following:

$$(0001)_{SiC} \parallel (11\bar{1})_{TiC_{1-x}} \parallel (0001)_{Ti_5Si_3} \parallel (0001)_{Ti}$$
$$[11\bar{2}0]_{SiC} \parallel [011]_{TiC_{1-x}} \parallel [4\bar{5}10]_{Ti_5Si_3} \parallel [11\bar{2}0]_{Ti} .$$

The contact properties of the annealed samples should now be associated with the TiC_{1-x} and Ti_5Si_3 phases rather than with Ti, which is no longer in contact with the SiC. Both TiC and Ti_5Si_3 would be expected to form low barrier contacts in the ideal case by virtue of their low work functions.[17,18] However, after annealing for 40–60 min, the calculated Schottky barrier height increased slightly. These results indicate that the formation of a reaction zone between the metal contact and the SiC substrate resulted in new interface states which pinned the Fermi level.

Concentration profiles obtained by PEELS perpendicular to the interface before annealing and for anneals

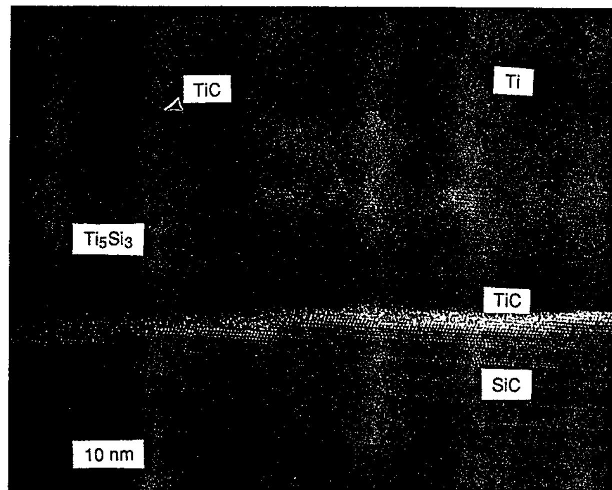

FIG. 10. High resolution TEM micrograph of the Ti/SiC interface after annealing for 20 min at 700 °C in UHV.

of 20 min and 60 min are shown in Fig. 11. The resolution is approximately 3 nm, as determined by the profile of the as-deposited Ti/SiC interface. After annealing for 20 min, the C concentration showed a high level near the SiC interface in addition to a peak near the interface with Ti. A peak in the Si concentration occurred in the reaction zone (R.Z.) closer to the SiC. This type of profile occurred because of the faster diffusivity of C than Si in all the reaction products. During the 60 min anneal, the C near the Ti interface diffused into the Ti, while more of the Si diffused through the reaction zone.

The α-Ti hcp phase is stable up to 882 °C[19]; therefore, there should be no polymorphic transformation of the Ti phase. At the annealing temperature of 700 °C,

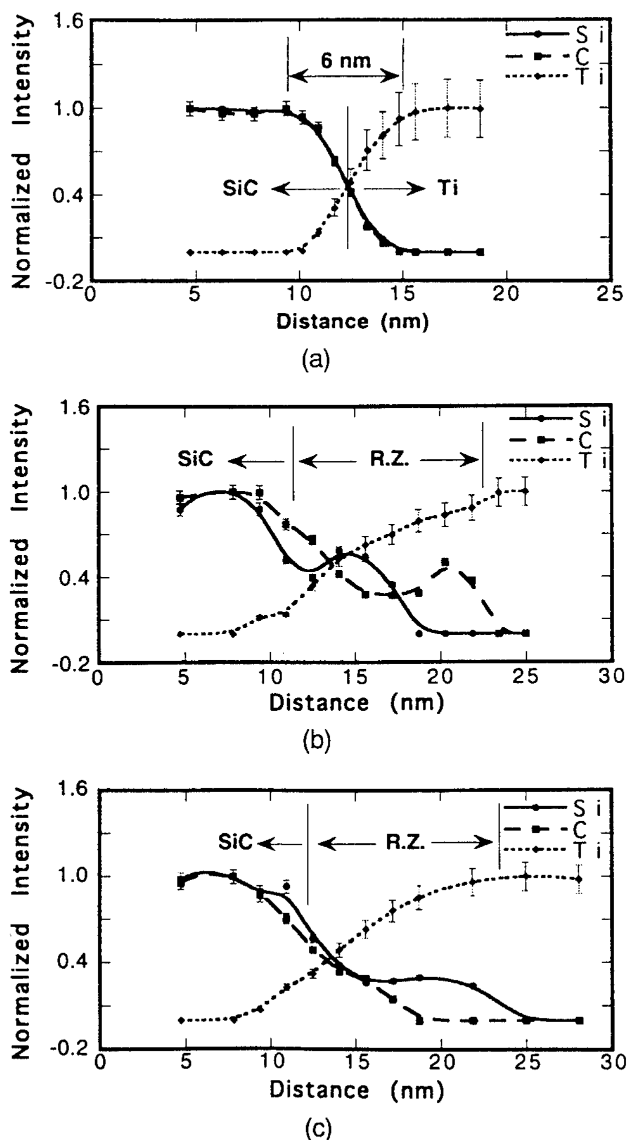

FIG. 11. Concentration profiles of Si, C, and Ti perpendicular to the Ti/SiC interface determined by parallel electron energy loss spectroscopy (PEELS) (a) before annealing and after annealing at 700 °C for (b) 20 min and (c) 60 min.

TiC_{1-x} is the only binary phase which exists between the two elements. At this temperature, TiC_{1-x} covers a range of stoichiometries from approximately 40.5 to 48.5 at. % C, while approximately 1.0% C and <0.5% Si are soluble in α-Ti. There are five titanium silicides at this temperature: Ti_3Si, Ti_5Si_3, Ti_5Si_4, TiSi, and $TiSi_2$.

The free energies of formation of the carbide and three of the silicides with Ti at 700 °C are listed in Table III. TiC has the lowest free energy of formation at this temperature, while the silicides have free energies of formation within 12.0 kJ/mol of each other. However, knowledge of all the thermodynamic data in a material system having three or more components is, in general, not sufficient to predict which product phases will form. These data (i.e., temperature, pressure, and free energies) can yield the equilibrium phase fields; however, the diffusion path is controlled by the diffusion coefficients of each component in the pertinent phases. It is the ratio of the diffusivities that determines the interface compositions, and accordingly the diffusion path.[22] Evidence has been reported in many metal/SiC systems that the reactions were limited by the dissociation of SiC, resulting in metal-rich silicides.[23–29]

There have been several extensive studies of the Ti–Si–C system at high temperatures. At temperatures between 570 °C and 1200 °C and at low or atmospheric pressures, the product phases in Ti/SiC diffusion couples were reported to be TiC,[30,31] Ti_5Si_3,[29] or both TiC_{1-x} and Ti_5Si_3.[28,32–34] At high pressures (10 to 20 kbars) and high temperatures (1200 °C to 1500 °C), $Ti_3SiC_{(1.78-2.00)}$ was identified along with TiC_{1-x} and Ti_5Si_3.[35] At the high end of this pressure range Ti_3Si formed, which exhibited a high solubility for carbon (up to 9 at. %).

Backhaus-Ricoult[28,33] heated diffusion couples between Ti and polycrystalline SiC to 1200 °C. By measuring the concentration profiles of each of the constituents and plotting them on the Ti–Si–C Gibbs phase triangle, the diffusion path was determined. It was stated that because the diffusion of C in Ti is ≈10 times faster than Si in Ti, the reaction runs from pure Ti to the Si-rich corner of the Ti phase field, which is connected to the Ti_5Si_3 phase field. The concentration of the slower diffusing Si quickly increases near the interface and reaches its solubility limit, at which point Ti_5Si_3 forms. The reaction path then passes through the phase field containing Ti_5Si_3, TiC_{1-x}, and Ti. Carbon reacts with Ti to form TiC within the Ti_5Si_3 phase. The morphology of the product layer showed the formation of TiC_{1-x} particles throughout a matrix of Ti_5Si_3, where the TiC particles contained more C closer to the SiC interface.

It is worthwhile to make some comparisons between our results and those described in the previous paragraph. The Ti/SiC samples in the present research were annealed at 700 °C; however, the same phases were formed in the reaction as those found at 1200 °C. The

TABLE III. Free energies of formation of binary Ti compounds with Si and C at 700 °C.

Compound	ΔG (kJ/mol)	Reference
Ti_5Si_3	−117.6	20
TiSi	−129.4	20
$TiSi_2$	−127.6	20
TiC	−172.6	21

diffusion paths are apparently very similar if not the same. The faster diffusivity of C in Ti would explain the formation of the TiC particles at the interface with Ti early in the annealing stage. An important difference is that a continuous TiC layer formed along the interface with SiC. It is believed that Backhaus-Ricoult[28,33] could not have seen this initial TiC layer without the use of high resolution TEM. It is also possible that the TiC layer formed to minimize the interface strain between the phases in the reaction zone and the monocrystalline 6H–SiC(0001) used in the present study. A large lattice misfit strain (~8.5%) exists between $(21\bar{3}0)_{Ti_5Si_3}$ and $(1\bar{1}00)_{6H\text{-}SiC}$, which were both normal to the $(0001)_{SiC}$ interface plane and parallel to each other. The resulting morphological sequence described above is more favorable in terms of strain. Between $(1\bar{1}1)_{TiC}$ and $(1\bar{1}02)_{SiC}$ there is only a 0.5% mismatch, while that between $(111)_{TiC}$ and $(21\bar{3}0)_{Ti_5Si_3}$ is 2.5%. These planes were chosen instead of the $(0001)_{SiC}$, $(1\bar{1}1)_{TiC}$, and $(0001)_{Ti_5Si_3}$ planes used to describe the crystallographic relationships because the former were almost parallel to each other while not parallel to the interface, while the latter were parallel to the interface and therefore could not be used to determine the mismatch.

Chemical bonding at the interface was studied by XPS after depositing a series of thin Ti films. Figure 12 shows the C 1*s* and Si 2*p* peaks after depositing 4, 8, and 12 Å Ti. Each of these peaks has been deconvoluted into a major and a minor peak.

After 4 Å of Ti was deposited, the C 1*s* peak was composed of a major peak at 283.62 eV and a minor peak at 282.04 eV. With thicker films of Ti, the minor peak grew; after 12 Å of Ti both peaks shifted to slightly lower binding energies of 283.52 eV and 281.94 eV, respectively. The major peak originates from C-bound-to-Si in SiC, and the minor peak is attributed to C-bound-to-Ti.[36] The increasing contribution of the minor peak at the greater film thicknesses is a result of the corresponding reduction in sensitivity to the underlying SiC. Titanium-carbon bonding is expected due to the highly negative free energy of formation of TiC.

Titanium silicide bonding was not detected. Because titanium has a lower electronegativity (1.54) than carbon (2.55), Si–Ti bonding should result in a peak at the low binding energy side of the Si 2*p* (Si-bound-to-C) peak. Instead, a minor peak at slightly higher binding energy was detected. After 4 Å Ti was deposited, the major and minor peaks were located at 101.40 eV and 102.56 eV, respectively. The minor peak is probably due to SiO_x, since the same binding energy difference existed prior to Ti deposition. Si 2*p* binding energies reported in the literature are ≈103.7 eV for SiO_2[37] and 102.7 eV for SiO.[5]

The combination of XPS and TEM analyses shows that interfacial TiC formation begins with an initial two-dimensional coverage of Ti at room temperature and is enhanced after annealing at 700 °C. On the other hand, there seems to be some oxygen which remains

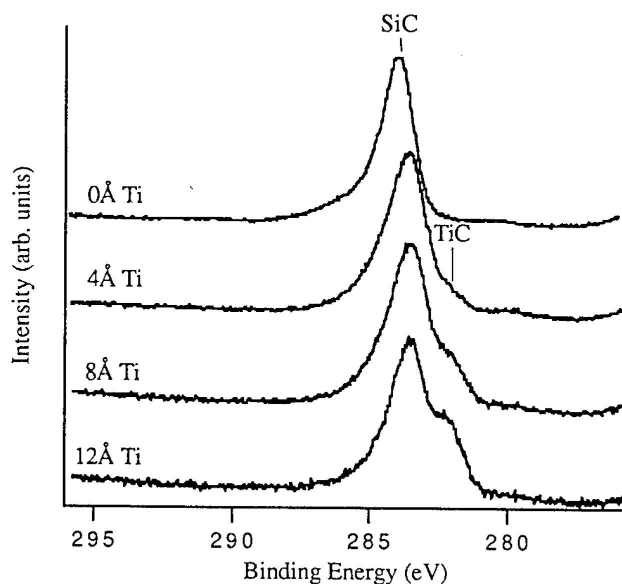

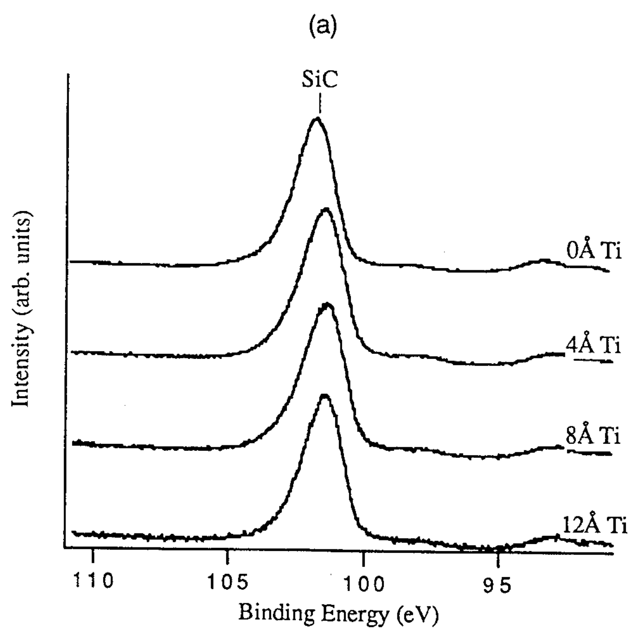

FIG. 12. XPS (a) C 1*s* and (b) Si 2*p* peaks from SiC after depositing 0, 4, 8, and 12 Å Ti.

at the interface bonded to Si. The amount of oxygen does not appear to be sufficiently high to interfere with creating a high quality interface, as indicated by high resolution TEM.

IV. CONCLUSIONS

A comprehensive study of the electrical properties, microstructure, and chemistry of both as-deposited and 700 °C annealed thin film Ti/6H–SiC(0001) interfaces was performed with specific regard to the application of contacts in semiconductor devices.

As received, thermally oxidized, *n*-type 6H–SiC (0001) substrates were simultaneously cleaned and etched in either an ethanol/hydrofluoric acid/water (10 : 1 : 1) or a 10% hydrofluoric acid solution followed by a 15 min thermal desorption at 700 °C in UHV. This procedure resulted in 1×1 unreconstructed surfaces which contained submonolayer residual O and trace amounts of F. X-ray photoelectron spectroscopy analyses revealed that the energy bands bent upward at the surface. This result indicates that surface states were present, which acted as acceptors and which are expected to prohibit an exact correlation between the Schottky barrier heights and metal work functions as predicted by the Schottky–Mott limit for ideal metal-semiconductor contacts.

The deposition of Ti onto these chemically treated, unheated SiC substrates resulted in epitaxial contacts, which exhibited rectifying behavior, low ideality factors ($n < 1.09$), and typical leakage currents of 5×10^{-7} A/cm^2 at -10 V. The SBH's calculated from *I-V*, *C-V*, and XPS measurements (0.79–0.88 eV) were somewhat lower than that predicted by the Schottky–Mott limit (1.03 eV). This result may be associated with surface states in the SiC substrates. On the other hand, other metal contacts would need to be examined to understand the relationship of the surface states to the resulting Schottky barrier heights.

The SBH's and electrical properties do not show substantial changes after annealing at 700 °C for up to 60 min, except after an initial 20 min anneal. However, interfacial chemical reactions resulted in the formation of Ti_5Si_3 and TiC_{1-x}, which is in agreement with several previous studies. The fact that the formation of Ti_5Si_3 and TiC, which are low work function metals,[17,18] did not result in a reduction of the SBH suggests that energy states were also present at the newly created interface between TiC and SiC.

ACKNOWLEDGMENTS

The authors would like to thank the Office of Naval Research under Contract Nos. N00014-92-J-1500 and N00014-92-J-1477 for funding the research performed at NCSU. The research performed at ASU was supported by DE-FG03-94ER45510. The microscopy was performed at the NSF/ASU HREM facility under NSF-DMR-9314326. A special thanks is also extended to J. R. Waldrop at Rockwell International Science Center for valuable discussions regarding XPS analyses.

REFERENCES

1. W. O. Saxton, T. J. Pitt, and M. Horner, Ultramicroscopy **4**, 343 (1979).
2. *Handbook of X-ray Photoelectron Spectroscopy*, edited by C. D. Wagner, W. M. Riggs, L. E. Davis, and J. F. Moulder (Perkin-Elmer Corp., Eden Prairie, MN, 1979).
3. J. R. Waldrop and R. W. Grant, Appl. Phys. Lett. **62**, 2685 (1993).
4. D. B. Fenner, D. K. Biegelsen, and R. D. Bringans, J. Appl. Phys. **66**, 419 (1989).
5. J. A. Taylor, G. M. Lancaster, A. Ignatiev, and J. W. Rabalais, J. Chem. Phys. **68**, 1776 (1978).
6. K. L. Smith and K. M. Black, J. Vac. Sci. Technol. A **2**, 744 (1984).
7. *Auger and X-ray Photoelectron Spectroscopy*, 2nd ed., *Practical Surface Analysis*, edited by D. Brigs and M. P. Seah (John Wiley & Sons, New York, 1990), Vol. 1.
8. R. Kaplan, Surf. Sci. **215**, 111 (1989).
9. R. T. Tung, Phys. Rev. B **45**, 13509 (1992).
10. J. W. Palmour, private communication (Cree Research, Inc., Research Triangle Park, NC, 1992).
11. S. M. Sze, *Physics of Semiconductor Devices*, 2nd ed. (John Wiley & Sons, Inc., New York, 1981).
12. J. R. Waldrop, R. W. Grant, Y. C. Wang, and R. F. Davis, J. Appl. Phys. **72**, 4757 (1992).
13. L. C. Feldman and J. W. Mayer, *Fundamentals of Surface and Thin Film Analysis* (North-Holland, New York, 1986).
14. Z. Sitar, L. L. S. Smith, and R. F. Davis, J. Cryst. Growth, **141**, 11 (1994).
15. W. Mader and G. Necker, in *Metal-Ceramic Interfaces*, edited by M. Ruhle, A. G. Evans, M. F. Ashby, and J. P. Hirth (Pergamon Press, New York, 1990).
16. K. L. Merkle, M. I. Buckett, and Y. Gao, Acta Metall. Mater. **40**, S249 (1992).
17. K. Senzaki and Y. Kumashiro, Bull. Electrotech. Lab. Jpn. **41**, 593 (1977).
18. G. V. Samsonov, L. N. Okhremchuk, N. F. Podgrushko, I. A. Podchernyaeva, and V. S. Fomenko, Inorg. Mater. **12**, 720 (1976).
19. *Phase Diagrams of Binary Titanium Alloys*, Monograph Series on Alloy Phase Diagrams, edited by J. L. Murray (ASM INTERNATIONAL, Metals Park, OH, 1987).
20. I. Barin, *Thermochemical Data of Pure Substances* (VCH, New York, 1989), Vol. 2.
21. *JANAF Thermochemical Tables*, J. Phys. Chem. Ref. Data, edited by M. W. Chase, Jr., C. A. Davies, J. R. Downey, Jr., D. J. Frurip, R. A. McDonald, and N. A. Syverud (The American Chemical Society and The National Institute of Physics for the National Bureau of Standards, Midland, MI, 1985), Vol. 14.
22. G. R. Purdy, D. H. Weidel, and J. S. Kirkaldy, Trans. Metall. Soc. **230**, 1025 (1964).
23. M. Nathan and J. S. Ahearn, J. Appl. Phys. **70**, 811 (1991).
24. I. Ohdomari, S. Sha, H. Aochi, and T. Chikyow, J. Appl. Phys. **62**, 3747 (1987).
25. C. S. Pai, C. M. Hanson, and S. S. Lau, J. Appl. Phys. **57**, 618 (1985).

26. T. C. Chou, A. Joshi, and J. Wadsworth, J. Mater. Res. **6**, 796 (1991).
27. T. C. Chou, A. Joshi, and J. Wadsworth, J. Vac. Sci. Technol. A **9**, 1525 (1991).
28. M. Backhaus-Ricoult, in *Metal-Ceramic Interfaces*, edited by M. Ruhle, A. G. Evans, M. F. Ashby, and J. P. Hirth (Pergamon Press, New York, 1990).
29. M. Nathan and J. S. Ahearn, Mater. Sci. Eng. **A126**, 225 (1990).
30. M. B. Chamberlain, Thin Solid Films **72**, 305 (1980).
31. J. J. Bellina, Jr. and M. V. Zeller, in *Novel Refractory Semiconductors*, edited by D. Emin, T. L. Aselage, and C. Wood (Mater. Res. Soc. Symp. Proc. **97**, Pittsburgh, PA, 1987), p. 265.
32. C. G. Rhodes and R. A. Spruling, in *Recent Advances in Composites in the United States and Japan*, edited by J. R. Vinson and M. Taya (American Society for Testing and Materials, Philadelphia, PA, 1985).
33. M. Backhaus-Ricoult, Ber. Bunsenges. Phys. Chem. **93**, 1277 (1989).
34. I. Gotman, E. Y. Gutmanas, and P. Mogilevsky, J. Mater. Res. **8**, 2725 (1993).
35. S. Sambasivan and W. T. Petuskey, J. Mater. Res. **7**, 1473 (1992).
36. L. Ramqvist, K. Hamrin, G. Johansson, A. Fahlman, and C. Nordling, J. Phys. Chem. Solids **30**, 1835 (1969).
37. T. L Barr, Appl. Surf. Sci. **15**, 1 (1983).

XI. Structural Characterization of GaN and AlGaN Films by X-Ray Diffraction

A. Introduction

X-ray diffraction is a powerful tool for analysis of material quality and composition. In this report a new system, the Philips X'Pert Materials Research Diffractometer (MRD), will be discussed and initial results for GaN, AlN and their solid solutions will be presented.

The X'Pert MRD is designed to study epitaxial layers and highly-oriented thin films. Applications include calculations of layer/substrate mismatch, layer and superlattice thickness and composition, layer perfection and strain and relaxation in single crystal films. The system's most notable features include pre-aligned optic modules that are easily interchanged. The MRD cradle gives precise X, Y and Z translation, and full 180° psi (Ψ) and 360° phi (φ) rotation. Computer control allows for incremental scans and precise control.

Gallium nitride forms a continuous solid solution with both InN and AlN. Potential applications include both semiconductors and optoelectronic devices. No commercially available lattice matched substrates exist for these materials; the common substrates include sapphire (Al_2O_3) and silicon carbide (SiC). The lattice parameters for GaN, AlN, Al_2O_3 and SiC are displayed in Table I [1]. GaN, AlN and InN crystallize in the hexagonal wurtzite structure with two formula units per unit cell.

Table I. Comparison of III-Nitride Material Properties with Various Substrate Materials

Crystal Properties		GaN	AlN	InN	SiC-6H	Al_2O_3
Lattice	a	3.189	3.112	3.54	3.081	4.758
Parameters (Å)	c	5.185	4.982	5.7	15.12	12.99
Thermal exp.	a	3.17	4.15		4.2	7.5
Coefficient (10^{-6}/K)	c	5.59	5.27		4.68	8.5

Al_2O_3 is the most common substrate used for GaN despite a significant (>12 %) lattice mismatch and difference in the coefficient of thermal expansion. Silicon carbide, with a 2.8 % lattice mismatch, has been the subject of much research recently.

This report will focus on GaN and AlGaN films grown on SiC with AlN used as the buffer layer for GaN growth. The primary diffraction tools used are rocking curves and diffraction space mapping. The FWHM of rocking curves is used as a gauge of film quality. There are two types of rocking curves, coupled 2theta-omega (2θ-ω) and omega (ω) scans. 2θ-ω scans measure the broadening due to microscopic tilts of the GaN layer, while ω scans measure the

broadening due to variations in the bragg plane spacing. Common symmetric rocking curves used in the literature are the (0002) and (0004) GaN reflections measured by 2θ-ω scans.

Recent work showed high-quality GaN on 6H-SiC exhibits a FWHM value of 66 arcsec for the GaN(0004) reflection. A high temperature (1100°C) buffer layer was used to improve film quality. The sample had a threading dislocation density of 10^9 cm^{-2} within the first .5 μm that decreased substantially with thickness. This is among the lowest ever reported for GaN. The photoluminescence FWHM of 4 meV was also very good.

There have been few reports of diffraction space maps for GaN and none for AlGaN. Recent work by Ponce, *et al.* presented a space map for the (0002) reflection of GaN and the (0006) reflection of SiC. They found negligible strain in the epilayer (FWHM of 17 arcsec) and long range variation in orientation (2.7 arcmin). The threading dislocation density of their films was 10^9 cm^{-2}.

Asymmetric rocking curves are often used to calculate the percentage of film relaxation. Two of the common asymmetric reflections for GaN are the {0015} and {0025} family of planes. The procedure used is provided by Philips.

B. Experimental Procedure

All X-ray experiments are performed on the Philips X'Pert MRD system. The primary (incident) optics for all measurements is a Ge 4-bounce [220] Bartel's monochromator. This monochromator filters out all x-ray radiation except the Cu $K_{\alpha 1}$ line. The secondary (defracted) optics for rocking curves is a simple slit assembly and for area scans, a triple-axis optics with a triple-bounce channel cut Ge [220] analyzer crystal is used. The minimum resolution for rocking curves and area scans is .0001°.

The MRD cradle has five motorized movements. The phi (Ψ) rotation range is 360° with a reproducibility of .01°. The psi (φ) tilt range is 180° with a reproducibility of .01°. The X/Y manipulator has a 100 mm range and a .01 mm step size for both directions. The Z-translation stage has a step size of .001 mm.

The X-ray tube is a ceramic tube that can be changed from point to line focus without realigning the systems. All rocking curves and area scans are performed with the point focus. The tube voltage is 40 keV and the current is 45 mA for all experiments.

For symmetric rocking curves psi optimization is performed to ensure the scan is through the reciprocal lattice points (rlp) of the materials. Often the substrate is off-axis SiC, with a misoriented-cut of 3-4°, and this must be accounted for. An ω scan is first executed to locate the SiC peak. A 2θ scan is then performed, followed by a φ scan. For further optimization, ω and φ are then repeated. After this, a 2θ-ω scan of both the SiC and GaN (or AlGaN) reflections can be performed.

For asymmetric scans Ψ optimization is performed. A 360° Ψ scan is first performed for the predicted SiC (0006) peak values. Silicon carbide ω and 2θ scans are then performed for optimization. Then the 2θ-ω scan of both the SiC and GaN (or AlGaN) reflections can be performed.

After optimization either ω or 2θ-ω rocking curves are performed with time steps ranging from 1 to 5 seconds and step width of .005 to .0005°. It is also possible to perform these scans as a function of distance along a sample with incremental steps of 1 mm or smaller.

For area scans, the same 2θ-ω values can be used, but further optimization is required The ω for each peak should be measured to set up the proper ω scan range. The ω step width may be larger than the 2θ-ω step widths since it is an offset and not as important.

C. Results

A series of symmetric and asymmetric rocking curves were performed on a 1.4 mm GaN grown on on-axis 6H-SiC (0001). The buffer layer was AlN. The GaN (0002) reflection is presented in Fig. 1. The FWHM is 100 Arcsec. The reflections for the SiC (0006) and AlN (0002) are also presented. The FWHM of the SiC substrate is 61 Arcsec; the shoulder in the peak may be due to additional phases that crystallize in the SiC epi-layer grown on the wafers after they are cut. The width of the AlN (0002) peak, 237 arcsec, is wider due to the high density of dislocations present in the buffer layer, as seen by cross-sectional TEM [1].

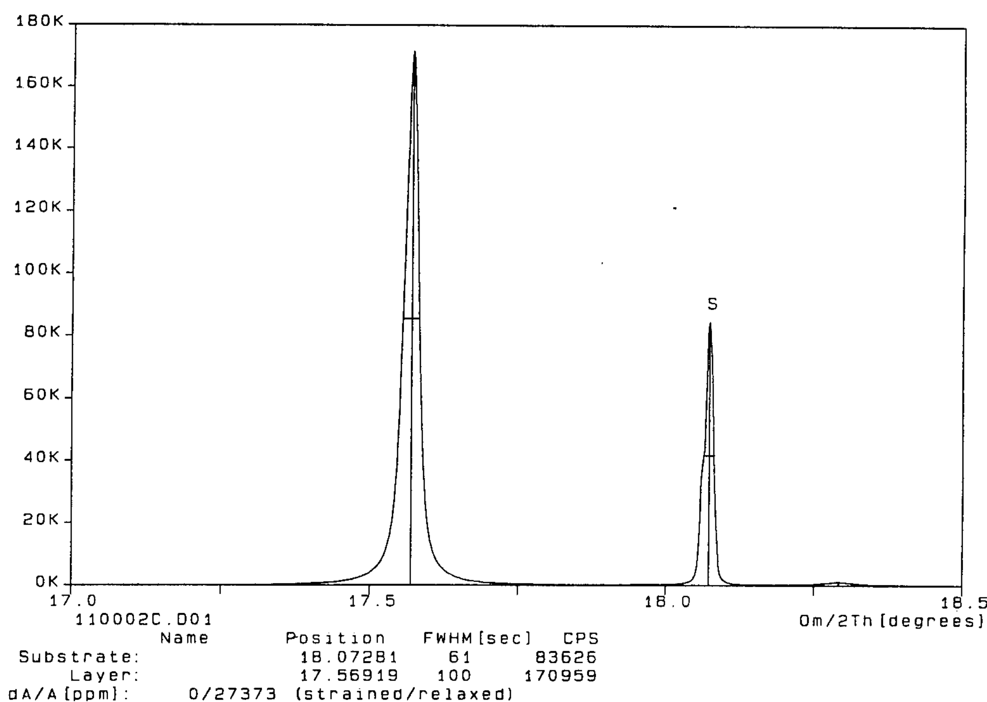

Figure 1. X-ray diffraction rocking curve for GaN (0002) on SiC (0006).

A high resolution reciprocal space map of the GaN (0002) and SiC (0006) reflections is presented in Fig. 2. The elongation of the GaN reciprocal lattice point in the direction perpendicular to the diffraction vector (ω scan) represents the broadening due to microscopic tilts of the GaN layer. The FWHM in this direction is 103 arcsec, and for the SiC (0006) reflection it is 96 arcsec. The FWHM for the GaN (0002) and SiC (0006) reflections in the direction parallel to the diffraction vector (2θ–ω scan) are 26 and 15 arcsec, respectively. The difference in these values from those obtained by the normal rocking curve procedure (100 and 61 arcsec) are due to the triple-bounce analyzer crystal. The X-ray beam that reflects from the sample diverges as it approaches the detector. The analyzer curve removes much of this divergence, while the normal slits used for rocking curve measurements do not. Thus, rocking values reported in the literature are dependent on the setup used. For example, Ponce *et al.* presented a reciprocal space map for GaN using a double-bounce analyzer crystal and report FWHM values for the GaN (0002) and SiC (0006) reflections. Caution must be taken in comparing these values to ours.

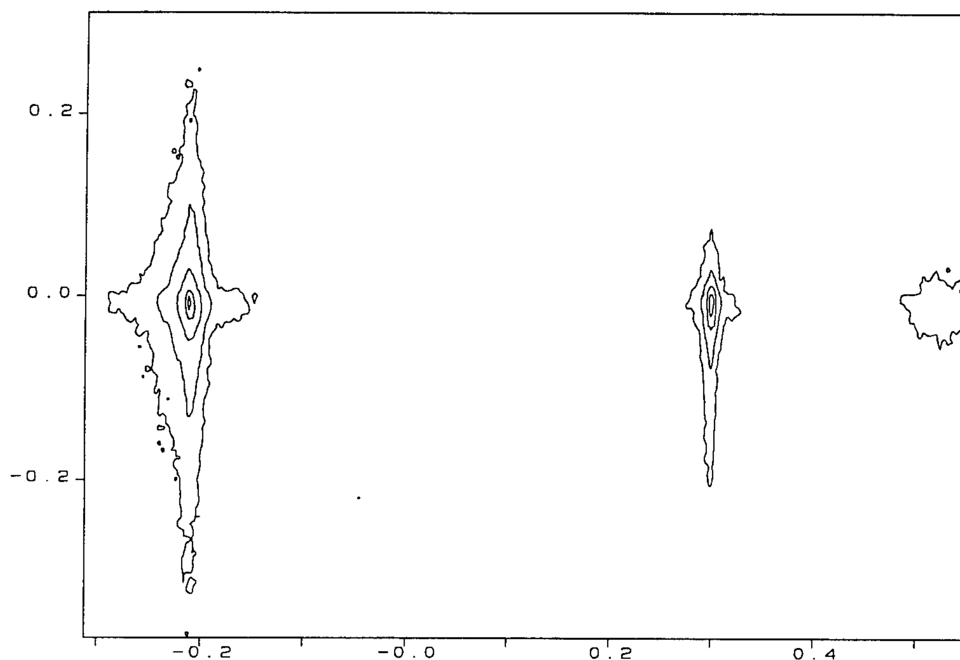

Figure 2. X-ray diffraction area map for GaN (0002) on SiC (0006). The horizontal axis corresponds to ω scans and the vertical axis corresponds to ω-2θ scans.

The rocking curve for the GaN (0004) and SiC (000 12) reflections is shown in Fig. 3. The FWHM for each peak is 99 and 66 arcsec, respectively. No reciprocal space maps were taken for these reflections.

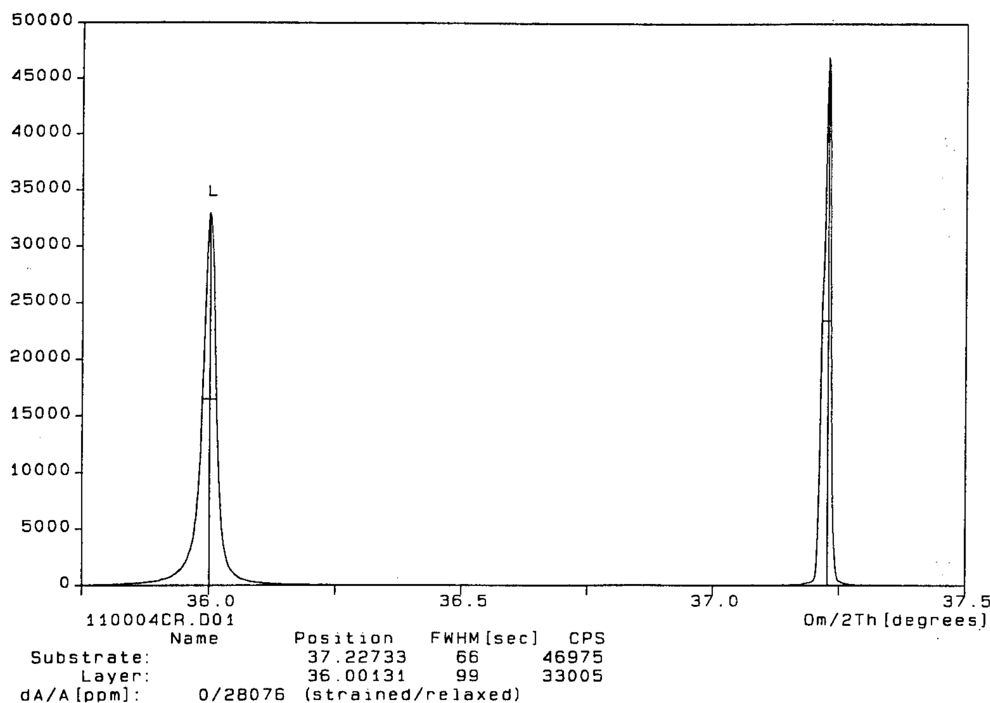

Figure 3. X-ray diffraction rocking curve for GaN (0004) on SiC (000 12).

The asymmetric reflections for GaN that have the highest peak intensities are the (015) and (025) family of planes. The rocking curve of the GaN (015) reflection is presented in Fig. 4. Using the peak separation between the GaN (015), (015), (025), and (025) reflections and the accompanying SiC reflections the percentage of film relaxation was calculated. Initial results show the film to be 93.8 % relaxed although further work will be done to verify these results.

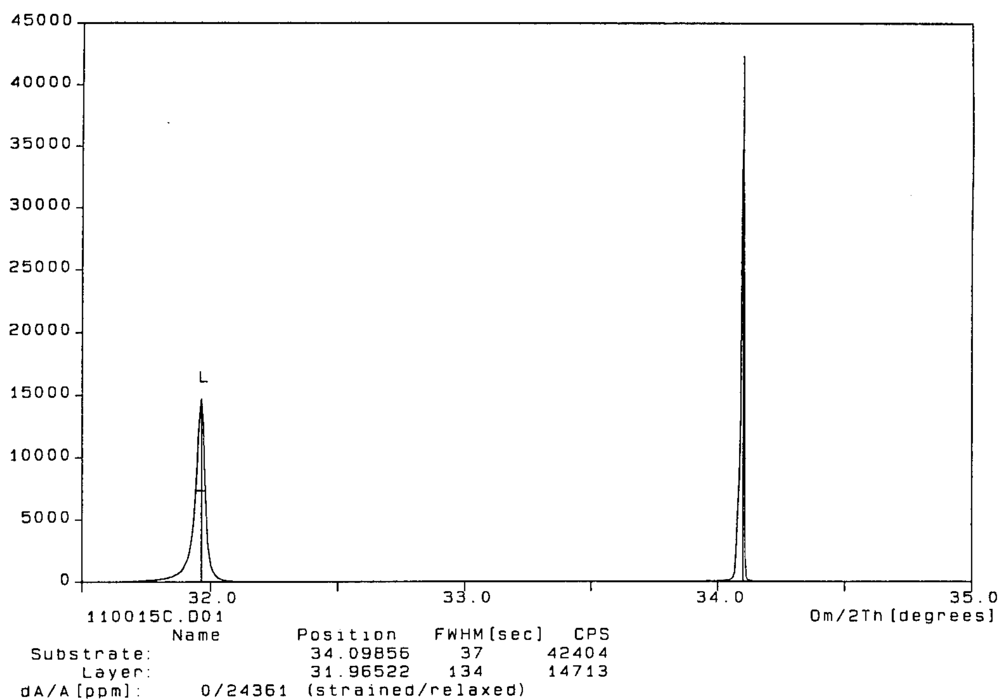

Figure 4. X-ray diffraction rocking curve for GaN (0015) on SiC (001 15).

A rocking curve for AlGaN grown directly on SiC is present in Fig. 5. The FWHM of the AlGaN (0002) peak is 341 arcsec and the SiC (0006) peak is 118 arcsec. The shoulders on the SiC peak are due to additional phases that crystallize in SiC epilayer. This, along with the peak width, indicates the relatively poor quality of this wafer. Two scans were performed at Ψ=0 and 180° to calculate an alloy composition of $Al_{.39}Ga_{.61}N$ assuming Vegard's law for lattice spacing. This composition of this sample as determined by an average of Auger electron spectroscopy (AES), Rutherford backscattering (RBS) and energy dispersive X-ray (EDX) analyses is $Al_{.41}Ga_{.59}N$. The discrepancy between this value and that obtained from rocking curves may be due in part to strain effects.

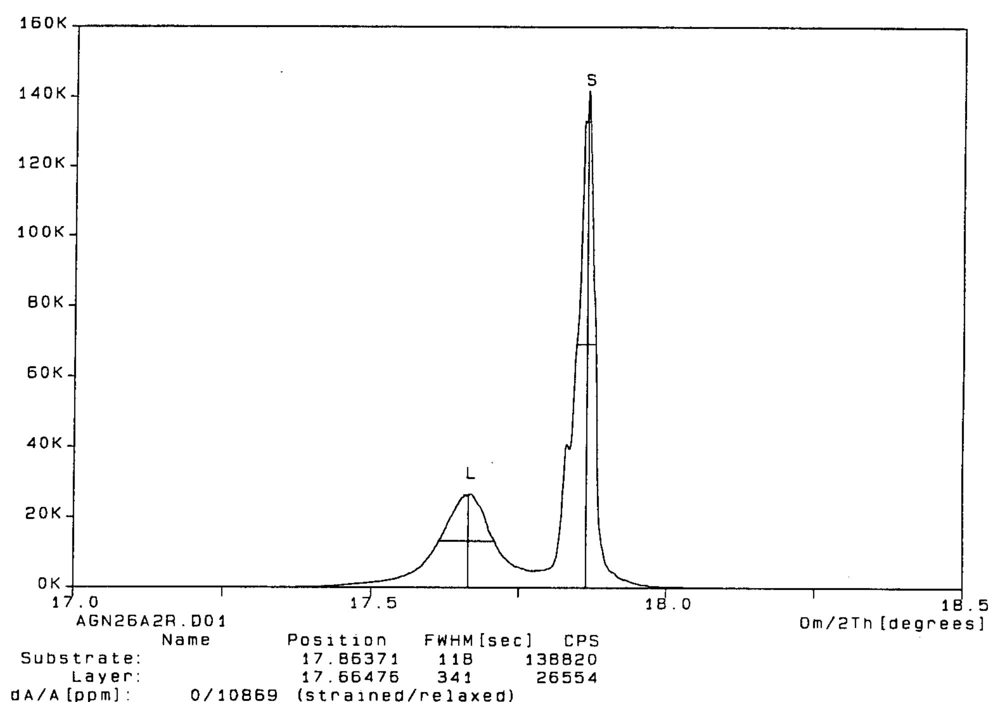

Figure 5. X-ray diffraction rocking curve for AlGaN (0002) on SiC (0006).

A reciprocal space map of the same sample is presented in Fig. 6. The FWHM for the AlGaN (0002) and SiC (0006) reflections in the direction parallel to the diffraction vector ($2\theta-\omega$ scan) are 113 and 24 arcsec, respectively.

D. Conclusions

A new Philips MRD was installed and used to characterize GaN and AlGaN. Rocking curves for the GaN (0002) and (0004) reflections of a 1.4 μm film on SiC were presented. A reciprocal space map of the GaN (0002) and SiC (0006) reflections were also presented. The

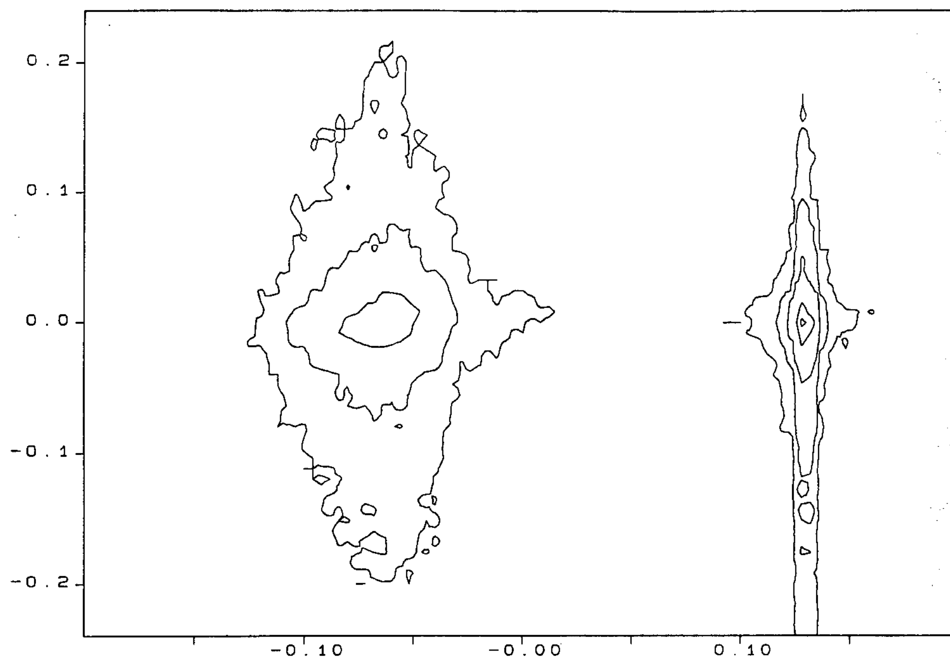

Figure 6. X-ray diffraction area map for AlGaN (0002) on SiC (0006). The horizontal axis corresponds to ω scans and the vertical axis corresponds to ω-2θ scans.

FWHM for the GaN (0002) and SiC (0006) reflections in the direction parallel to the diffraction vector (2θ–ω scan) are 26 and 15 arcsec, respectively. These are much lower than those calculated from the conventional rocking curves due to the triple-bounce analyzer crystal removing the divergence of the beam reflected from the sample.

An initial calculation of film relaxation for GaN was 93.8 %. This was done with rocking curves of asymmetric reflections using a method provided by Philips.

Rocking curves for AlGaN grown directly on SiC were used to estimate alloy composition. Assuming Vegard's law for lattice spacing the alloy composition was determined to be $Al_{.39}Ga_{.61}N$. This composition of the alloy as determined by an average of other characterization techniques was $Al_{.41}Ga_{.59}N$.

F. References

1. T. W. Weeks, Jr., M. D. Bremser, K. S. Ailey, E. Carlson, W. G. Perry and R. F. Davis, Appl. Phys. Lett. **67** (3) 17 July 1995
2. F. A. Ponce, B. S. krusor, J.S. Major, Jr., W. E. Plano, and D. F. Welch, Appl. Phys. Lett. **67** (3) 410 (1995)

XII. Distribution List

Mr. Max Yoder Office of Naval Research Electronics Division, Code: 312 Ballston Tower One 800 N. Quincy Street Arlington, VA 22217-5660	3
Administrative Contracting Officer Office of Naval Research Regional Office Atlanta 101 Marietta Tower, Suite 2805 101 Marietta Street Atlanta, GA 30323-0008	1
Director, Naval Research Laboratory ATTN: Code 2627 Washington, DC 20375	1
Defense Technical Information Center Bldg. 5, Cameron Station Alexandria, VA 22314	4